

Reversible Formation of Alkyl Radicals at $[\text{Fe}_4\text{S}_4]$ Clusters and Its Implications for Selectivity in Radical SAM Enzymes

*Alexandra C. Brown, Daniel L. M. Suess**

Department of Chemistry, Massachusetts Institute of Technology, Cambridge, Massachusetts
02139

Supporting Information

A.	Synthetic protocols	S2–S9
B.	NMR spectra of compounds.....	S10–S29
C.	Experimental details and NMR spectrum for radical reactions	S30–S38
D.	Discussion of the mechanism of the radical release reaction.....	S39–S41
E.	Kinetic simulations	S42–S52
F.	EPR spectra	S53–S56
G.	IR Spectra.....	S57–S62
H.	UV-Vis spectra	S63–S68
I.	Cyclic voltammetry	S69-70
J.	Crystallographic Details.....	S71
K.	References	S72

A. Synthetic protocols

General Considerations: Unless otherwise noted, all reactions were performed using standard Schlenk techniques or in an LC Technologies inert atmosphere glove box under an atmosphere of nitrogen (< 1 ppm O₂/H₂O). All compounds are air and water sensitive and were manipulated and stored to avoid exposure to air and water. Glassware was dried in an oven at 160 °C prior to use. Molecular sieves (3 Å), neutral alumina, and Celite® were activated by heating to 300 °C overnight under vacuum prior to storage under an atmosphere of nitrogen. Diethyl ether (Et₂O), benzene and pentane were degassed by sparging with argon, dried by passing through a column of activated alumina, and stored under an atmosphere of nitrogen over 3 Å molecular sieves. Tetrahydrofuran (THF) was distilled from sodium/benzophenone and stored under an atmosphere of nitrogen over 3 Å molecular sieves. Hexamethyldisiloxane (HMDSO) was degassed by sparging with nitrogen and stored under an atmosphere of nitrogen over 3 Å molecular sieves. C₆D₆ was degassed by three freeze–pump–thaw cycles and stored under an atmosphere of nitrogen over 3 Å activated molecular sieves. (IMes)₃Fe₄S₄Cl was prepared according to previously reported procedures.¹ 4-CF₃-pyridine, pyridine, and ⁿBu₃SnH were dried over CaH₂ and distilled under nitrogen. Grignard reagents (octylmagnesium bromide, 6-hexenylmagnesium bromide, and cyclopentylmethylmagnesium bromide) were prepared by addition of the halide to activated magnesium turnings in THF. Bromomethylcyclopentane was prepared by dropwise addition of elemental bromine to a solution of cyclopentylmethanol and PPh₃ in CH₂Cl₂.² NaBAR^F₄ (sodium tetrakis[(3,5-trifluoromethyl)phenyl]borate) was prepared according to literature procedure.³ [Cp₂Co][BAR^F₄] was synthesized by salt metathesis from [Cp₂Co][PF₆] using the procedure reported for [Cp₂Fe][BAR^F₄].⁴ All other reagents were purchased and used as received. NMR spectra were recorded on Bruker 400 and 500 MHz spectrometers. ¹H and ¹³C {¹H} chemical shifts

are given relative to residual solvent peaks, $^{119}\text{Sn}\{^1\text{H}\}$ shifts are relative to neat Me_4Sn (0 ppm). FT-IR samples were taken as thin films using a Bruker Alpha Platinum ATR spectrometer with OPUS software in a glovebox under an N_2 atmosphere. EPR spectra were recorded on a Bruker EMX spectrometer at 9.37 GHz as frozen glasses. Simulations were performed using EasySpin⁵ (5.2.21) in MATLAB (R2017b). UV-vis spectra were taken on a Cary 50 spectrometer. GC/MS experiments were carried out on an Agilent 5973N gas chromatograph/mass spectrometer using EI-MS ionization. X-ray structural determinations were performed at the MIT diffraction facility using a Bruker X8 diffractometer with an APEX II CCD detector or a Bruker D8 Venture diffractometer with a Photon2 CPAD detector. Diffraction data was collected, integrated, and corrected for absorption using Bruker APEX3 software and its associated modules (SAINT, SADABS, TWINABS). Structural solutions and refinements (on F^2) were carried out using SHELXT and SHELXL-2018 in ShelXle.⁶ Ellipsoid plots and figures were made using Mercury.

General preparation of alkylated clusters: $(\text{IMes})_3\text{Fe}_4\text{S}_4\text{Cl}$ (1 eq) was suspended in Et_2O (ca. 0.03 M). A solution of Grignard reagent (0.09–0.14 M in THF, 1.05 eq) was added dropwise. The dark red-brown solution was stirred for 5 min and filtered through Celite. The filtrate was added to a column of neutral alumina (2.5 g of alumina per 100 mg of $(\text{IMes})_3\text{Fe}_4\text{S}_4\text{Cl}$, packed as a suspension in Et_2O) to remove residual Mg salts. The product was eluted from the column with one column volume of Et_2O and the solvent was removed in vacuo.

$(\text{IMes})_3\text{Fe}_4\text{S}_4(\text{benzyl})$ (2): 500 mg of $(\text{IMes})_3\text{Fe}_4\text{S}_4\text{Cl}$, 0.14 M benzylmagnesium chloride. The resulting orange-brown solids were washed with pentane (3 x 2 mL). Yield: 334 mg (64%). ^1H NMR (500 MHz, C_6D_6 , 293 K) δ 224 (s, 2H, Fe- CH_2), 11.36 (s, 2H, benzyl *m*-CH), 6.98 (s, 12H,

Mes CH), 5.98 (s, 6H, backbone CH), 2.37 (s, 18H, Mes *p*-CH₃), 1.98 (s, 36H, Mes *o*-CH₃), –4.68 (s, 2H, benzyl *o*-CH), –6.50 (s, 1H, benzyl *p*-CH); ¹³C{¹H} NMR (125 MHz, C₆D₆): δ 193.8 (benzyl), 193.3 (benzyl), 143.4 (IMes), 139.1 (IMes), 132.9 (IMes), 131.4 (IMes), 126.4 (IMes), 71.9 (benzyl), 37.1 (IMes), 21.4 (IMes). EPR: *g* = [2.123 1.953 1.931] (toluene, 15 K, 9.37 GHz). X-ray quality crystals were grown by diffusion of pentane into Et₂O at room temperature.

(IMes)₃Fe₄S₄(octyl) (3): 100 mg of (IMes)₃Fe₄S₄Cl, 0.1 M octylmagnesium bromide. The resulting orange-brown solids were washed with pentane (2 x 1 mL) to give 57.9 mg of product. A second crop of crystals were collected by cooling the pentane washes to –40 °C for 16 h. Total yield: 70.2 mg (66%). ¹H NMR (400 MHz, C₆D₆, 293 K) δ 258 (s, 2H, Fe-CH₂), 21.81 (s, 2H, Fe-CH₂CH₂), 7.02 (s, 12H, Mes CH), 6.14 (s, 6H, backbone CH), 2.41 (s, 2H, Fe-(CH₂)₃CH₂), 2.33 (s, 18H, Mes *p*-CH₃), 2.07 (s, 36H, Mes *o*-CH₃), 1.66 (s, 2H, Fe-(CH₂)₄CH₂), 1.39 (m, 4H, Fe-(CH₂)₅CH₂CH₂), 0.93 (t, 3H, *J* = 5.94 Hz, Fe-(CH₂)₇CH₃), 0.67 (s, 2H, Fe-(CH₂)₂CH₂); ¹³C{¹H} NMR (125 MHz, C₆D₆): δ 145.7 (IMes), 138.6 (IMes), 132.9 (IMes), 130.9 (IMes), 127.7 (IMes), 41.1 (Fe-(CH₂)₃CH₂), 37.3 (IMes), 37.0 (Fe-(CH₂)₄CH₂), 34.6, 23.3 (Fe-(CH₂)₅CH₂CH₂), 21.0 (IMes), 14.7 (Fe-(CH₂)₇CH₃). EPR: *g* = [2.122 1.954 1.933] (toluene, 15 K, 9.37 GHz).

(IMes)₃Fe₄S₄(5-Hexenyl) (5): 100 mg of (IMes)₃Fe₄S₄Cl, 0.12 M 5-hexenylmagnesium bromide. The resulting orange-brown solids were washed with pentane (3 x 2 mL). Yield: 53.1 mg (51%). ¹H NMR (400 MHz, C₆D₆, 293 K) δ 256 (s, 2H, Fe-CH₂), 24.5 (s, 2H, Fe-CH₂CH₂), 7.00 (s, 12H, Mes CH), 6.18 (m, 1H, Fe-(CH₂)₄CHCH₂), 6.12 (s, 6H, backbone CH), 4.94 (m, 2H, Fe-

(CH₂)₄CHCH₂), 2.87 (s, 2H, Fe-(CH₂)₃CH₂) 2.32 (s, 18H, Mes *p*-CH₃), 2.05 (s, 36H, Mes *o*-CH₃), 0.54 (s, 2H, Fe-(CH₂)₂CH₂); ¹³C{¹H} NMR (125 MHz, C₆D₆): 147.4 (Fe-(CH₂)₄CHCH₂), 146.0 (IMes), 139.0 (IMes), 133.3 (IMes), 131.2 (IMes), 127.5 (IMes), 115.6 (Fe-(CH₂)₄CHCH₂), 44.5 (Fe-(CH₂)₃CH₂), 37.5 (IMes), 21.3 (IMes). EPR: *g* = [2.121 1.953 1.932] (toluene, 15 K, 9.37 GHz).

(IMes)₃Fe₄S₄(cyclopentylmethyl) (7): 100 mg of (IMes)₃Fe₄S₄Cl, 0.09 M cyclopentylmethylmagnesium bromide. The resulting orange-brown solids were washed with pentane (3 x 2 mL). Yield: 36.8 mg (36%). ¹H NMR (400 MHz, C₆D₆, 293 K) δ 256 (s, 2H, Fe-CH₂), 21.3 (s, 1H, Fe-CH₂CH), 7.01 (s, 12H, Mes CH), 6.15 (s, 6H, backbone CH), 4.27 (s, 2H, cyclopent), 2.85 (s, 2H, cyclopent) 2.33 (s, 18H, Mes *p*-CH₃), 2.06 (s, 36H, Mes *o*-CH₃), 1.84 (s, 2H, cyclopent), -1.63 (s, 2H, cyclopent); ¹³C{¹H} NMR (125 MHz, C₆D₆): δ 145.7 (IMes), 138.6 (IMes), 132.9 (IMes), 130.9 (IMes), 127.8 (IMes), 37.3 (IMes), 34.0 (cyclopent), 21.0 (IMes). EPR: *g* = [2.123 1.954 1.933] (toluene, 15 K, 9.37 GHz).

General method for oxidation of alkylated clusters: The alkylated cluster (1 eq) was mixed with [Cp₂Co][BAr^F₄] (1.2 eq). The solids were suspended in pentane or HMDSO and stirred for 5 min. The solution was filtered to remove cobaltocene. The dark solids were extracted into benzene and filtered through Celite to remove [Cp₂Co][BAr^F₄]. The solvent was removed in vacuo and the residual solids were washed again with pentane. Oxidized clusters, particularly those with β-hydrogens, exhibited some thermal instability and so were freshly generated for each experiment.

[(IMes)₃Fe₄S₄Bn][BAr^F₄] ([2]⁺): The reaction was carried out in pentane. The product was isolated as a red-brown solid. Yield: 28.1 mg (12.7 μmol) on a 27.1 mg (20.0 μmol) scale (64%). ¹H NMR (500 MHz, C₆D₆, 293 K) δ 67.5 (s, 2H, Fe-CH₂), 8.44 (s, 8H, [BAr^F₄]), 7.71 (s, 4H, [BAr^F₄]), 7.17 (s, 2H, benzyl *m*-CH), 6.98 (d, 2H, *J* = 7.6 Hz, benzyl *o*-CH), 6.90 (t, 1H, *J* = 7.6 Hz, benzyl *p*-CH), 6.85 (s, 12H, Mes CH), 5.63 (s, 6H, backbone CH), 2.31 (s, 18H, Mes *p*-CH₃), 1.99 (s, 36H, Mes *o*-CH₃); ¹³C{¹H} NMR (125 MHz, C₆D₆): 162.5 (q, [BAr^F₄]), 140.0 (IMes), 138.8 (IMes), 135.2 ([BAr^F₄]), 134.7 (IMes), 130.0 (IMes), 129.6 (q, [BAr^F₄]), 129.6 (benzyl *m*-CH) 128.2, 127.4 (IMes), 125.4 (benzyl *o*-CH), 125.0 ([BAr^F₄]), 122.1, 121.4 (benzyl *p*-CH), 117.7 ([BAr^F₄]), 23.9 (IMes), 20.5 (IMes). Crystallographic characterization of this complex was obtained by oxidation of (IMes)₃Fe₄S₄Cl with [Cp*₂Fe][OTf] and crystallization by vapor diffusion of pentane into THF at room temperature. [(IMes)₃Fe₄S₄Bn][OTf] can be converted to the [BAr^F₄] salt by addition of NaBAr^F₄ to a THF solution of [(IMes)₃Fe₄S₄Bn][OTf], followed by removal of the solvent in vacuo, extraction into benzene, and filtration through Celite.

[(IMes)₃Fe₄S₄(octyl)][BAr^F₄] ([3]⁺): The reaction was carried out in HMDSO. The product was isolated as a brown solid. Yield: 11.2 mg (5.00 μmol) on a 12.3 mg (9.03 μmol) scale (56%). ¹H NMR (500 MHz, C₆D₆, 293 K) δ 74.7 (s, 2H, Fe-CH₂), 8.45 (s, 8H, [BAr^F₄]), 7.71 (s, 4H, [BAr^F₄]), 6.90 (s, 12H, Mes CH), 5.64 (s, 6H, backbone CH), 2.31 (s, 18H, Mes *p*-CH₃), 2.05 (s, 36H, Mes *o*-CH₃), 1.92 (s, 2H, Fe-(CH₂)₃CH₂), 1.55 (s, 2H, Fe-(CH₂)₂CH₂), 1.46 (m, 6H, Fe-(CH₂)₄CH₂CH₂CH₂), 1.00 (t, 3H, *J* = 6.71 Hz, Fe-(CH₂)₇CH₃), -3.57 (s, 2H, Fe-CH₂CH₂); ¹³C{¹H} NMR (125 MHz, C₆D₆): 162.5 (q, [BAr^F₄]), 140.0 (IMes), 139.0 (IMes), 135.2 ([BAr^F₄]), 134.7 (IMes), 130.0 (IMes), 129.6 (q, [BAr^F₄]), 127.8 (IMes), 125.0 ([BAr^F₄]), 121.6,

117.7 ([BAr^F₄]), 32.2 (octyl), 31.0 (octyl), 28.8 (Fe-(CH₂)₃CH₂), 24.2 (IMes), 23.4 (Fe-(CH₂)₂CH₂), 23.3 (octyl), 20.9 (IMes), 14.4 (Fe-(CH₂)₇CH₃).

[(IMes)₃Fe₄S₄(5-hexenyl)][BAr^F₄] ([5]⁺): The reaction was carried out in HMDSO. The product was isolated as a brown solid. Yield: 20.5 mg (9.27 μmol) on a 21.5 mg (15.9 μmol) scale (59%). ¹H NMR (500 MHz, C₆D₆, 293 K) δ 74.2 (s, 2H, Fe-CH₂), 8.45 (s, 8H, [BAr^F₄]), 7.71 (s, 4H, [BAr^F₄]), 6.89 (s, 12H, Mes CH), 5.95 (m, 1H, Fe-(CH₂)₄CHCH₂), 5.64 (s, 6H, backbone CH), 5.22 (d, 1H, *J* = 17.1 Hz, Fe-(CH₂)₄CHCH₂ trans), 5.14 (d, 1H, *J* = 10 Hz, Fe-(CH₂)₄CHCH₂ cis), 2.60, (q, 2H, *J* = 6 Hz, Fe-(CH₂)₃CH₂), 2.30 (s, 18H, Mes *p*-CH₃), 2.04 (s, 36H, Mes *o*-CH₃), 1.51 (s, 2H, Fe-(CH₂)₂CH₂), -4.00 (s, 2H, Fe-CH₂CH₂). ¹³C{¹H} NMR (125 MHz, C₆D₆): 162.8 (q, [BAr^F₄]), 141.1 (Fe-(CH₂)₄CHCH₂) 140.3 (IMes), 139.3 (IMes), 135.5 ([BAr^F₄]), 135.1 (IMes), 130.3 (IMes), 129.9 (q, [BAr^F₄]), 127.9 (IMes), 125.3 ([BAr^F₄]), 121.9, 118.1 ([BAr^F₄]), 114.5 (Fe-(CH₂)₄CHCH₂), 33.5, (Fe-(CH₂)₃CH₂) 25.0 (Fe-(CH₂)₂CH₂), 24.5 (IMes), 20.9 (IMes).

[(IMes)₃Fe₄S₄(cyclopentymethyl)][BAr^F₄] ([7]⁺): The reaction was carried out in HMDSO. The product was isolated as a brown solid. Yield: 37.4 mg (16.9 μmol) on a 30 mg (22.3 μmol) scale (76%). ¹H NMR (500 MHz, C₆D₆, 293 K) δ 75.0 (s, 2H, Fe-CH₂), 8.40 (s, 8H, [BAr^F₄]), 7.70 (s, 4H, [BAr^F₄]), 6.89 (s, 12H, Mes CH), 5.77 (s, 6H, backbone CH), 2.30 (s, 18H, Mes *p*-CH₃), 2.16 (s, 2H, cyclopent), 2.05 (s, 36H, Mes *o*-CH₃), 1.90 (s, 2H, cyclopent), 1.80 (s, 2H, cyclopent), 1.11 (s, 2H, cyclopent), -3.05 (s, 1H, Fe-CH₂CH); ¹³C NMR (125 MHz, C₆D₆): 163.3 (q, [BAr^F₄]), 140.3 (IMes), 139.3 (IMes), 135.5 ([BAr^F₄]), 135.1 (IMes), 130.4 (IMes),

129.9 (q, [BAr^F₄]), 128.0 (IMes), 125.3 ([BAr^F₄]), 123.0, 118.1 ([BAr^F₄]), 27.6 (cyclopent), 27.4 (cyclopent), 24.5 (IMes), 20.9 (IMes).

General preparation for pyridine-bound clusters: [(IMes)₃Fe₄S₄(Et₂O)][BAr^F₄] was generated in situ by a modification of a previously reported procedure.¹ (IMes)₃Fe₄S₄Cl (100 mg, 0.0769 mmol) was dissolved in benzene (10 mL). A solution of NaBAr^F₄ (68.2 mg, 0.0769 mmol) in Et₂O (2 mL) was added dropwise. The solution was stirred for 5 minutes and then filtered through Celite. The solvent was removed in vacuo to obtain a dark-brown powder. Yield: 117.5 mg (70%). These solids were redissolved in Et₂O and treated with a 1 eq. of a pyridine as a benzene stock solution (0.1 M). Removal of the solvent in vacuo provided the pyridine adducts.

[(IMes)₃Fe₄S₄(DMAP)][BAr^F₄] ([4]⁺): From 20.5 mg (9.31 μmol) of [(IMes)₃Fe₄S₄(Et₂O)][BAr^F₄]. The dark yellow-brown solids were washed with hexanes to remove residual DMAP. Yield: 21 mg (99%). ¹H NMR (500 MHz, C₆D₆/THF (10:1), 293 K) δ 22.8 (s, 2H, DMAP), 14.3 (s, 2H, DMAP), 8.39 (s, 8H, [BAr^F₄]), 7.68 (s, 4H, [BAr^F₄]), 7.27 (s, 6H, DMAP) 6.81 (s, 12H, Mes CH), 6.08 (s, 6H, backbone CH), 2.23 (s, 18H, Mes *p*-CH₃), 2.05 (s, 36H, Mes *o*-CH₃); ¹³C{¹H} NMR (125 MHz, C₆D₆/THF (10:1): 162.8 (q, [BAr^F₄]), 144.8 (IMes), 139.6 (IMes), 135.5 ([BAr^F₄]), 133.5 (IMes), 133.1 (IMes), 131.8 (IMes), 129.9 (q, [BAr^F₄]), 125.3 ([BAr^F₄]), 118.1 ([BAr^F₄]), 36.3 (IMes), 20.9 (IMes). This compound was crystallized as the [OTf] salt. [(IMes)₃Fe₄S₄(THF)][OTf] was formed by addition of an excess of NaOTf to (IMes)₃Fe₄S₄Cl in THF. The solvent was removed in vacuo, the solid was extracted into benzene, the mixture was filtered and the solvent was removed again. The solids were extracted into THF, the solution was filtered, an excess of DMAP was added, and the product was crystallized by vapor diffusion of pentane into the THF solution.

[(IMes)₃Fe₄S₄(pyridine)][BAr^F₄] ([8]⁺): From 27.5 mg (12.5 μmol) of [(IMes)₃Fe₄S₄(Et₂O)][BAr^F₄]. The product was isolated as a dark red-brown solid. Yield: 25.3 mg (92%). ¹H NMR (500 MHz, C₆D₆/THF (10:1), 293 K) δ 18.9 (s, 2H, pyridine), 16.7 (s, 2H, pyridine), 8.41 (s, 8H, [BAr^F₄]), 7.69 (s, 4H, [BAr^F₄]), 6.77 (s, 12H, Mes CH), 6.09 (s, 6H, backbone CH), 2.22 (s, 18H, Mes *p*-CH₃), 2.09 (s, 36H, Mes *o*-CH₃), -0.61 (s, 1H, pyridine); ¹³C{¹H} NMR (125 MHz, C₆D₆/THF (10:1): 162.3 (q, [BAr^F₄]), 144.5 (IMes), 139.4 (IMes), 135.1 ([BAr^F₄]), 134.9 (IMes), 133.2 (IMes), 131.4 (IMes), 129.5 (q, [BAr^F₄]), 125.3 ([BAr^F₄]), 117.7 ([BAr^F₄]), 35.5 (IMes), 20.4 (IMes).

[(IMes)₃Fe₄S₄(4-CF₃-pyridine)][BAr^F₄] ([6]⁺): From 24.3 mg (11.0 μmol) of [(IMes)₃Fe₄S₄(Et₂O)][BAr^F₄]. The product was isolated as a dark green-brown solid. Yield: 24.3 mg (99%). ¹H NMR (500 MHz, C₆D₆/THF (10:1), 293 K) δ 17.2 (s, 2H, pyridine), 16.8 (s, 2H, pyridine), 8.37 (s, 8H, [BAr^F₄]), 7.68 (s, 4H, [BAr^F₄]), 6.76 (s, 12H, Mes CH), 6.11 (s, 6H, backbone CH), 2.21 (s, 18H, Mes *p*-CH₃), 2.15 (s, 36H, Mes *o*-CH₃); ¹³C{¹H} NMR (125 MHz, C₆D₆/THF (10:1): 162.3 (q, [BAr^F₄]), 144.5 (IMes), 139.4 (IMes), 137.1 (IMes) 135.1 ([BAr^F₄]), 133.2 (IMes), 131.3 (IMes), 129.5 (q, [BAr^F₄]), 125.3 ([BAr^F₄]), 117.6 ([BAr^F₄]), 34.7 (IMes), 20.3 (IMes).

B. NMR spectra of compounds

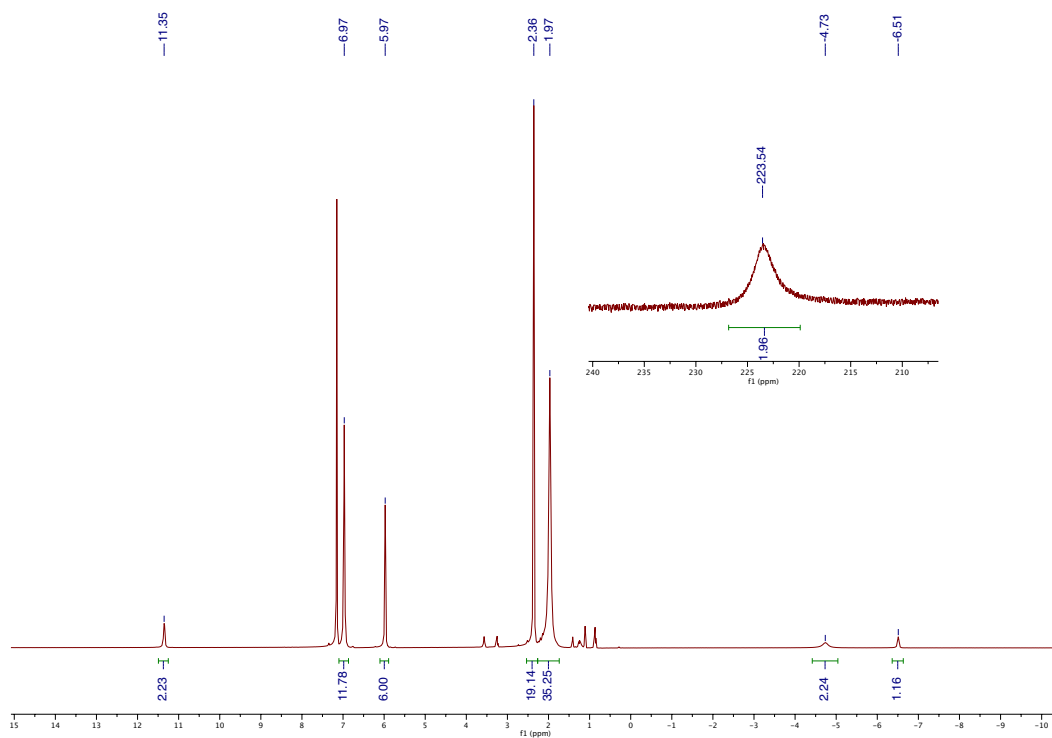


Figure S1: ^1H NMR spectrum of **2** in C_6D_6 at 293 K.

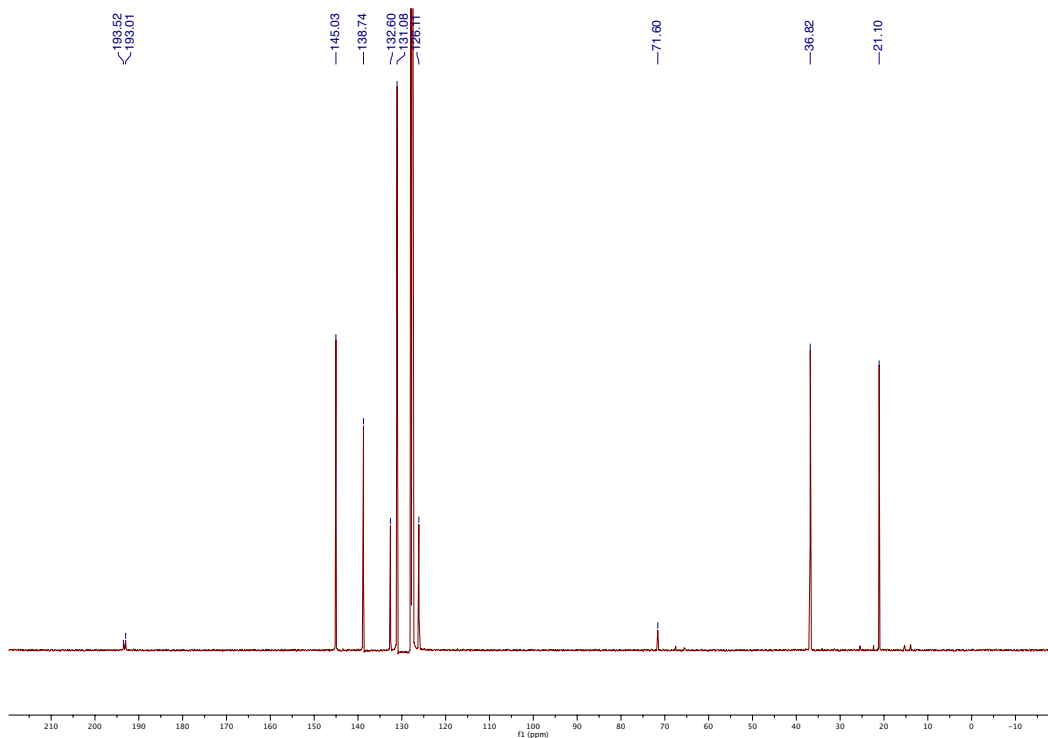


Figure S2: $^{13}\text{C}\{^1\text{H}\}$ NMR spectrum of **2** in C_6D_6 at 293 K.

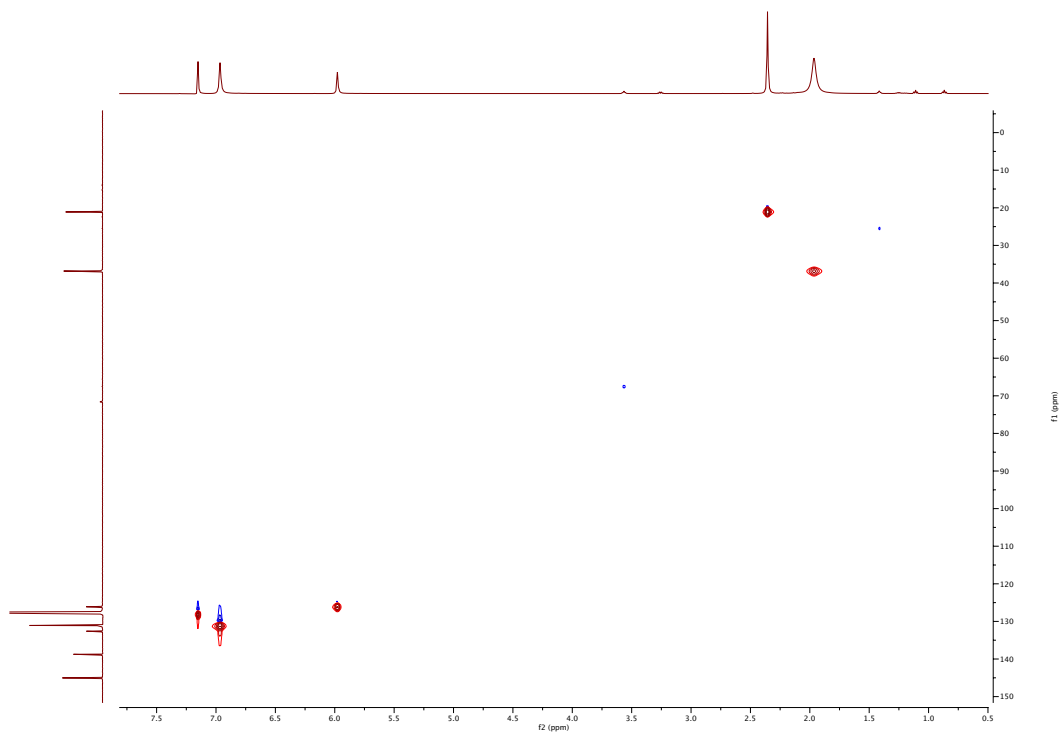


Figure S3: ^1H - ^{13}C multiplicity edited HSQC spectrum of **2** in C_6D_6 at 293 K.

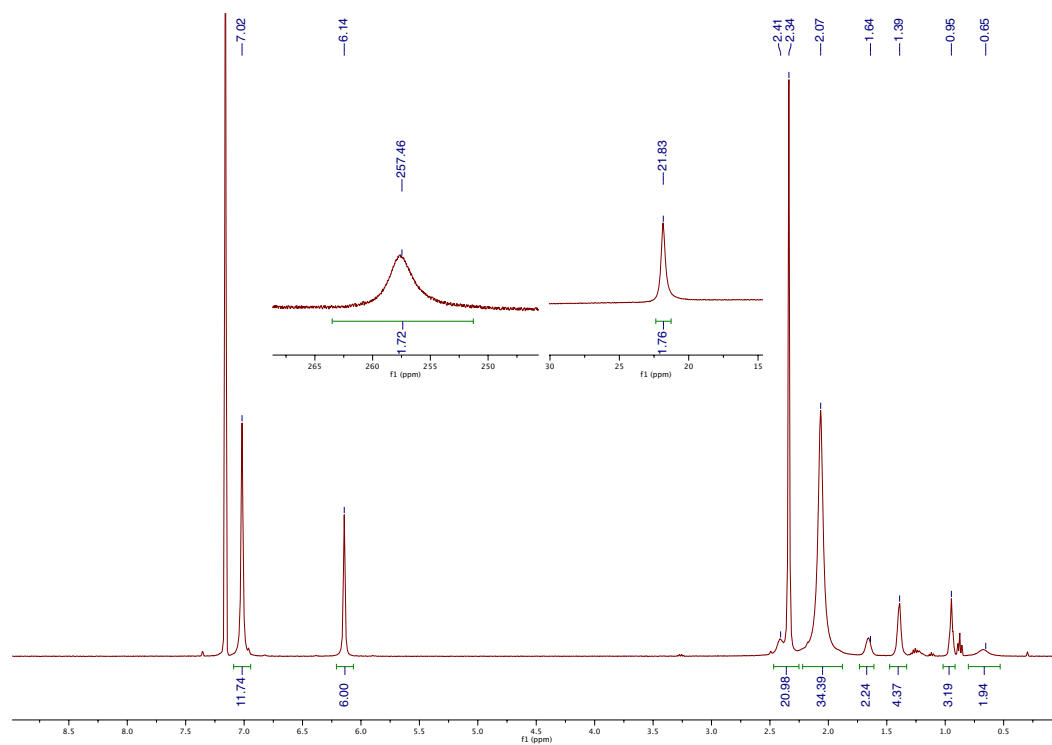


Figure S4: ^1H NMR spectrum of **3** in C_6D_6 at 293 K.

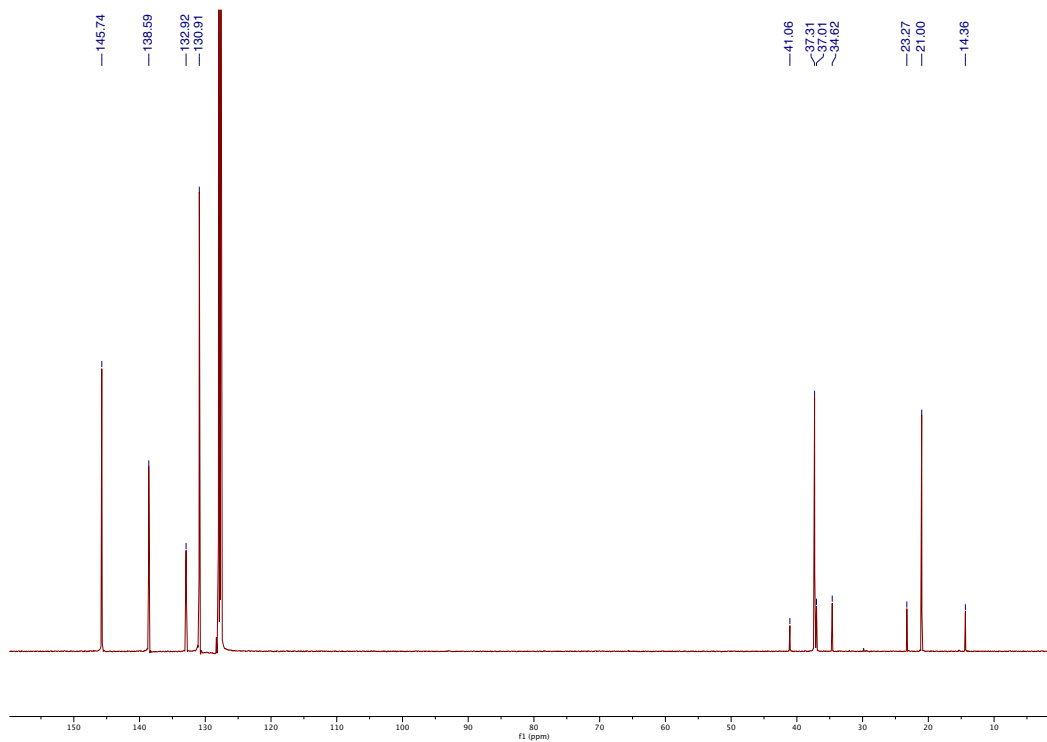


Figure S5: $^{13}\text{C}\{^1\text{H}\}$ NMR spectrum of **3** in C_6D_6 at 293 K.

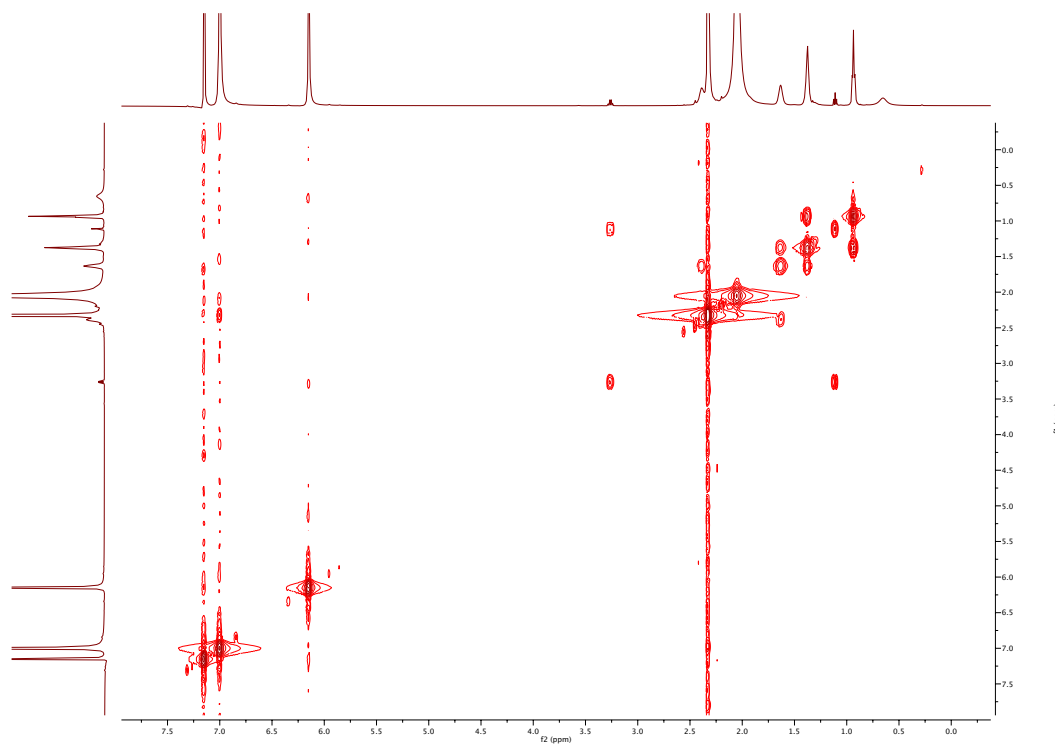


Figure S6: $^1\text{H}\text{-}^1\text{H}$ COSY spectrum of **3** in C_6D_6 at 293 K.

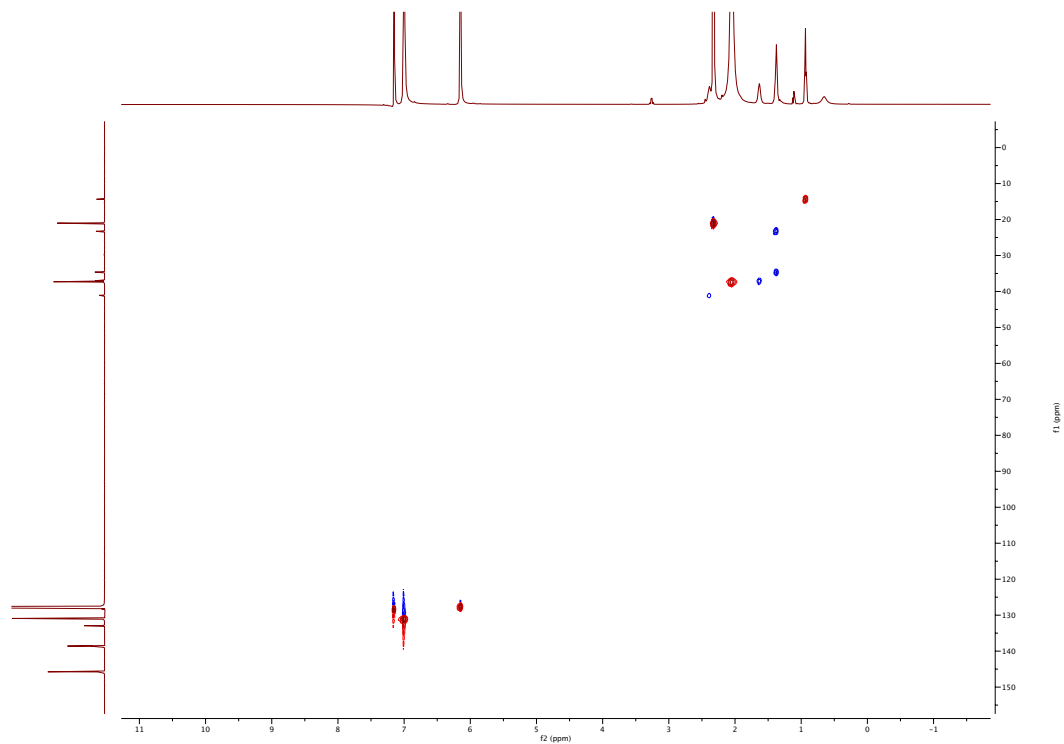


Figure S7: ^1H - ^{13}C multiplicity edited HSQC spectrum of **3** in C_6D_6 at 293 K.

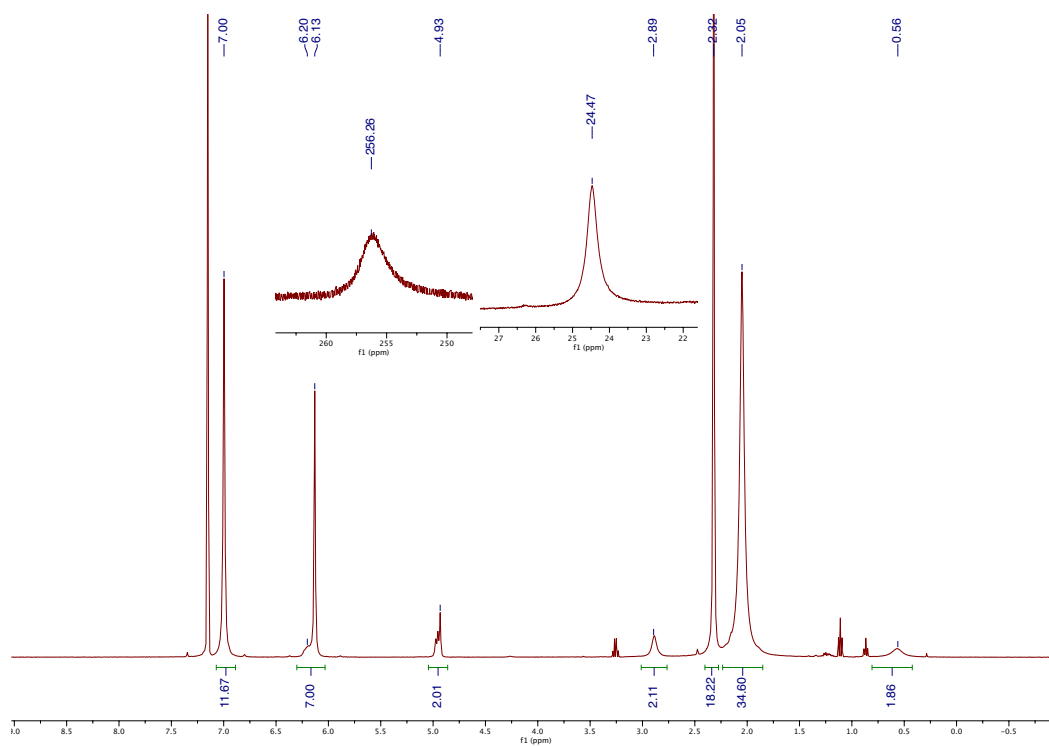


Figure S8: ^1H NMR spectrum of **5** in C_6D_6 at 293 K.

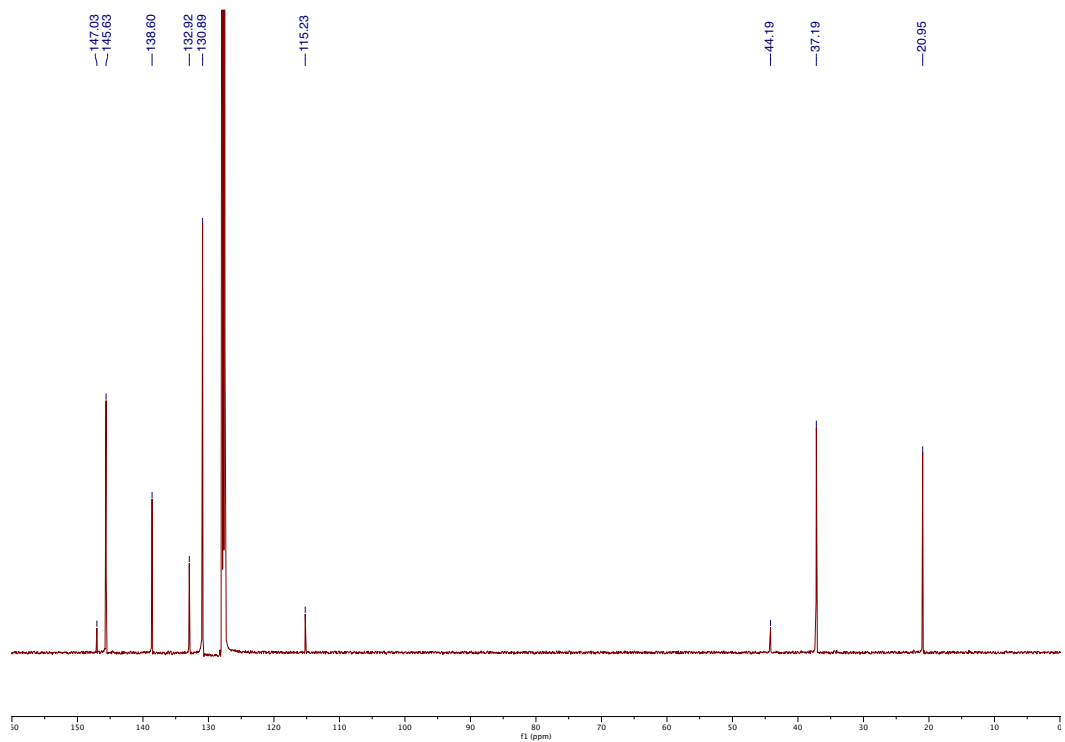


Figure S9: $^{13}\text{C}\{^1\text{H}\}$ NMR spectrum of **5** in C_6D_6 at 293 K.

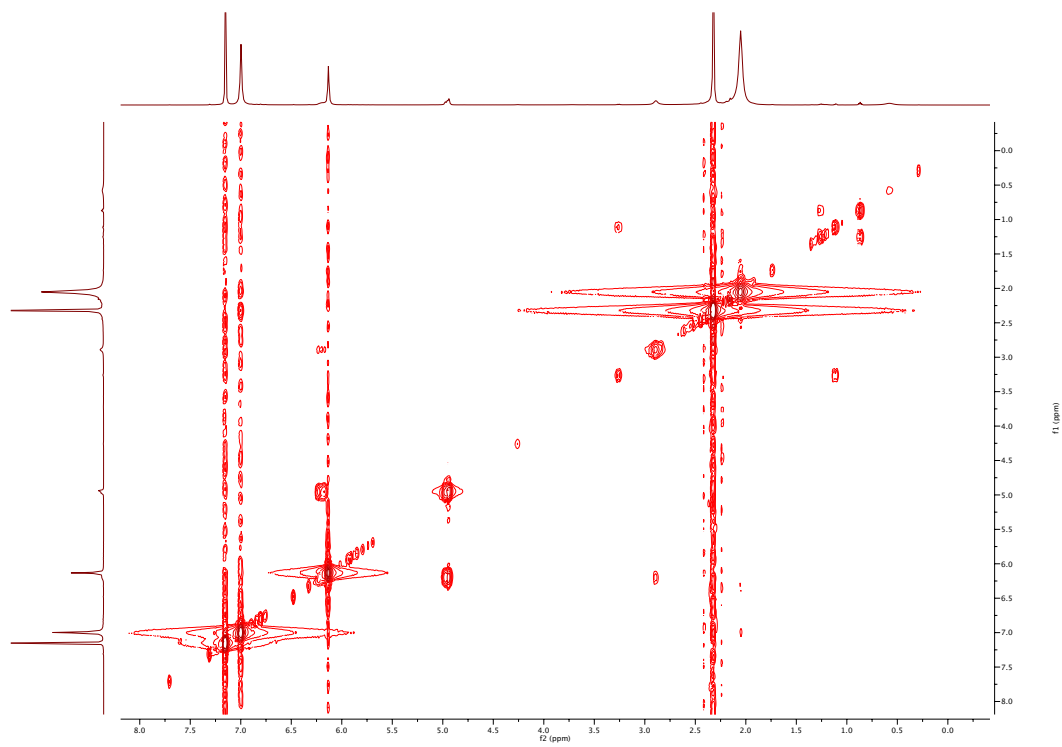


Figure S10: $^1\text{H}\text{-}^1\text{H}$ COSY spectrum of **5** in C_6D_6 at 293 K.

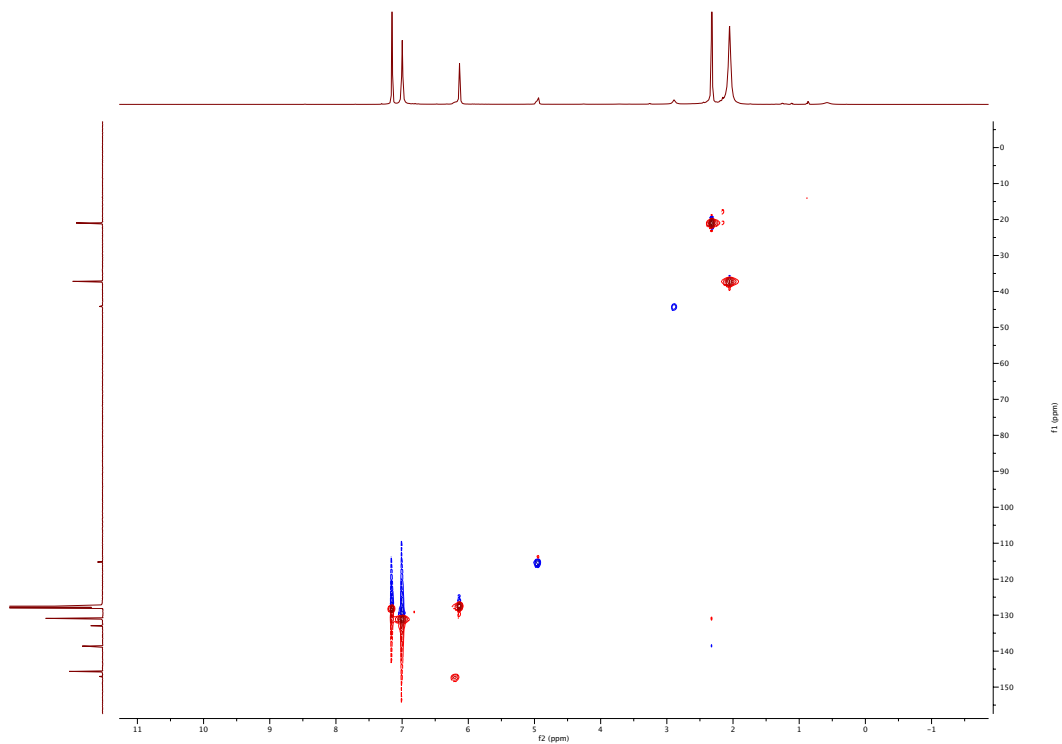


Figure S11: ^1H - ^{13}C multiplicity edited HSQC spectrum of **5** in C_6D_6 at 293 K.

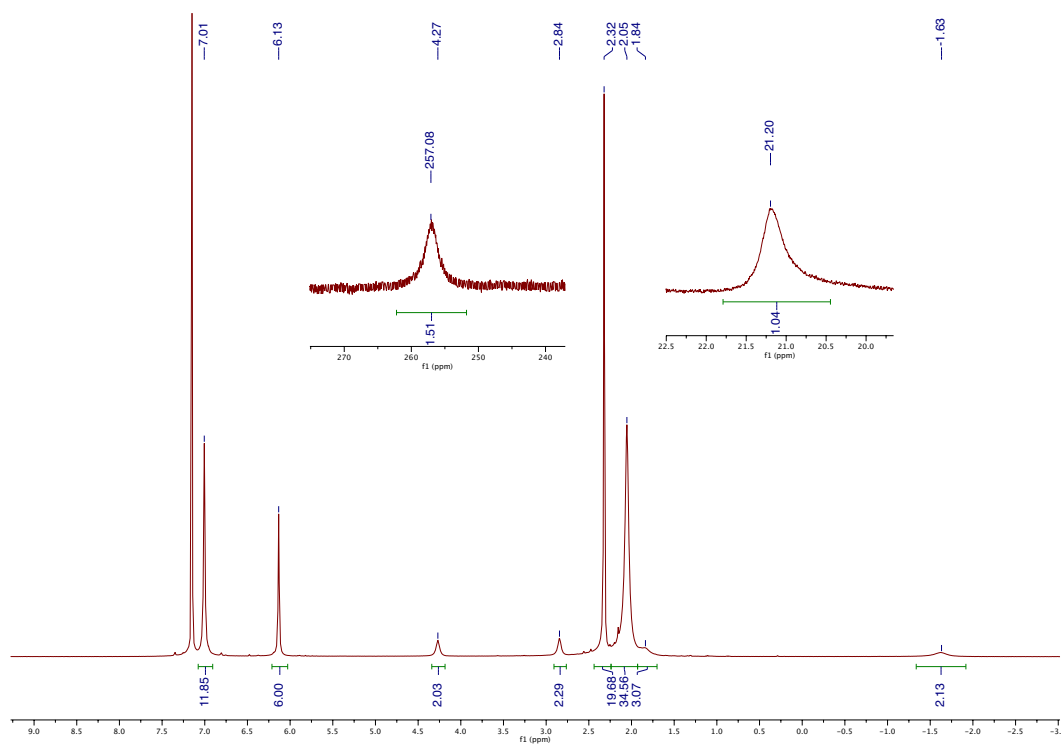


Figure S12: ^1H NMR spectrum of **7** in C_6D_6 at 293 K.

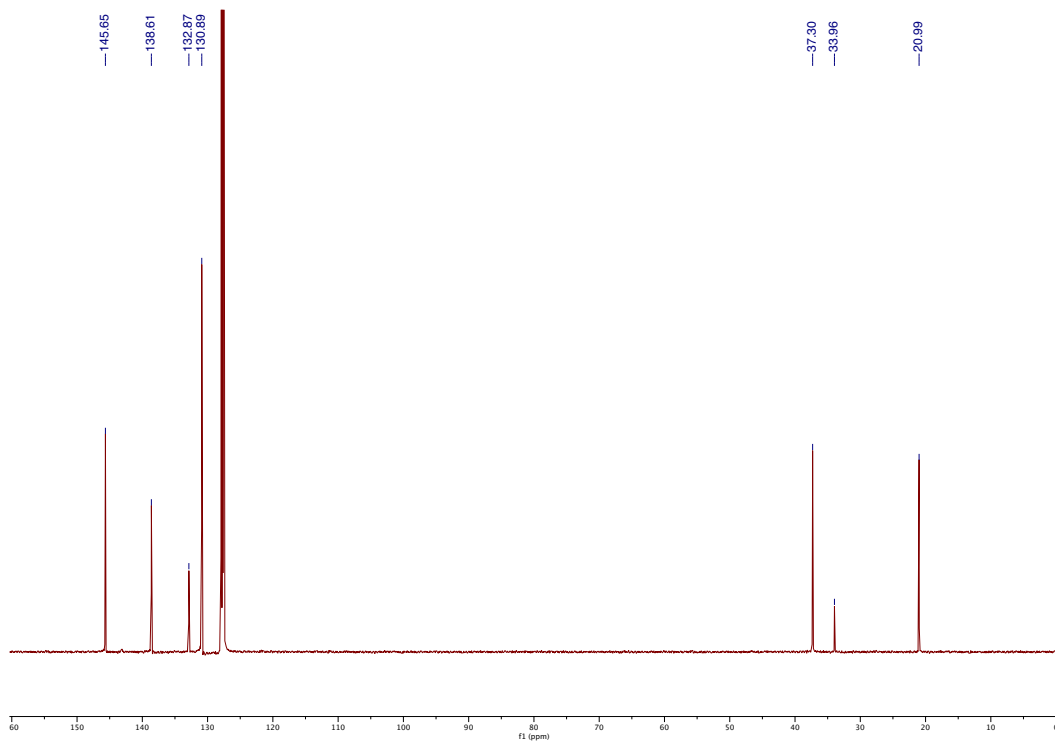


Figure S13: $^{13}\text{C}\{^1\text{H}\}$ NMR spectrum of **7** in C_6D_6 at 293 K.

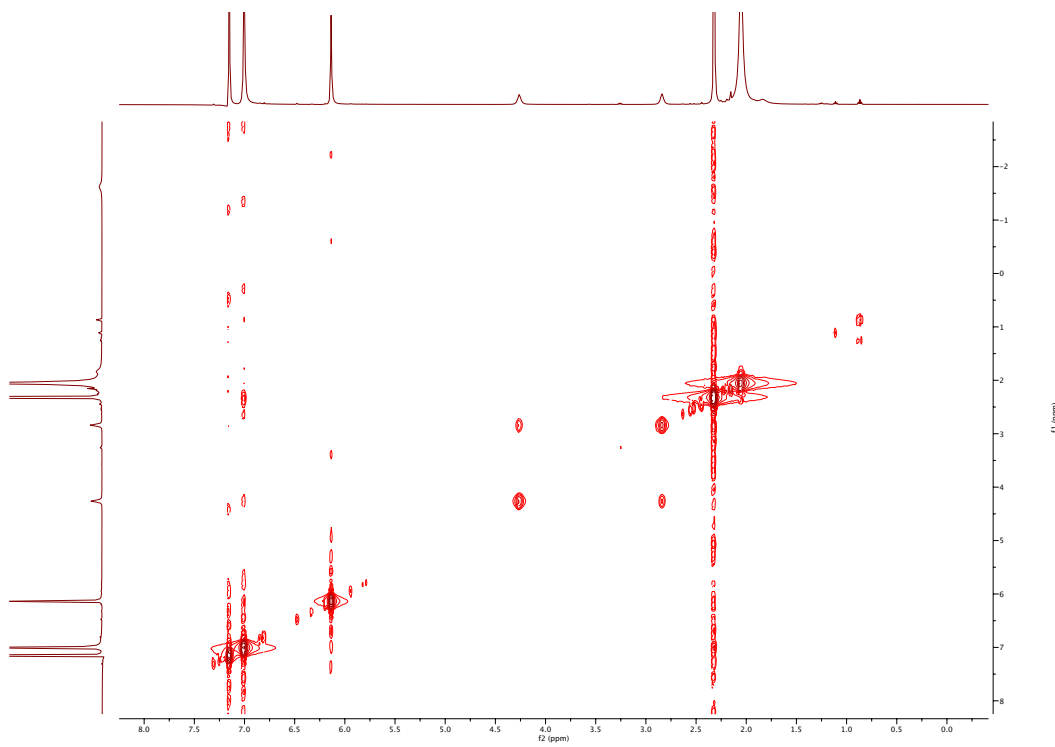


Figure S14: $^1\text{H}\text{-}^1\text{H}$ COSY spectrum of **7** in C_6D_6 at 293 K.

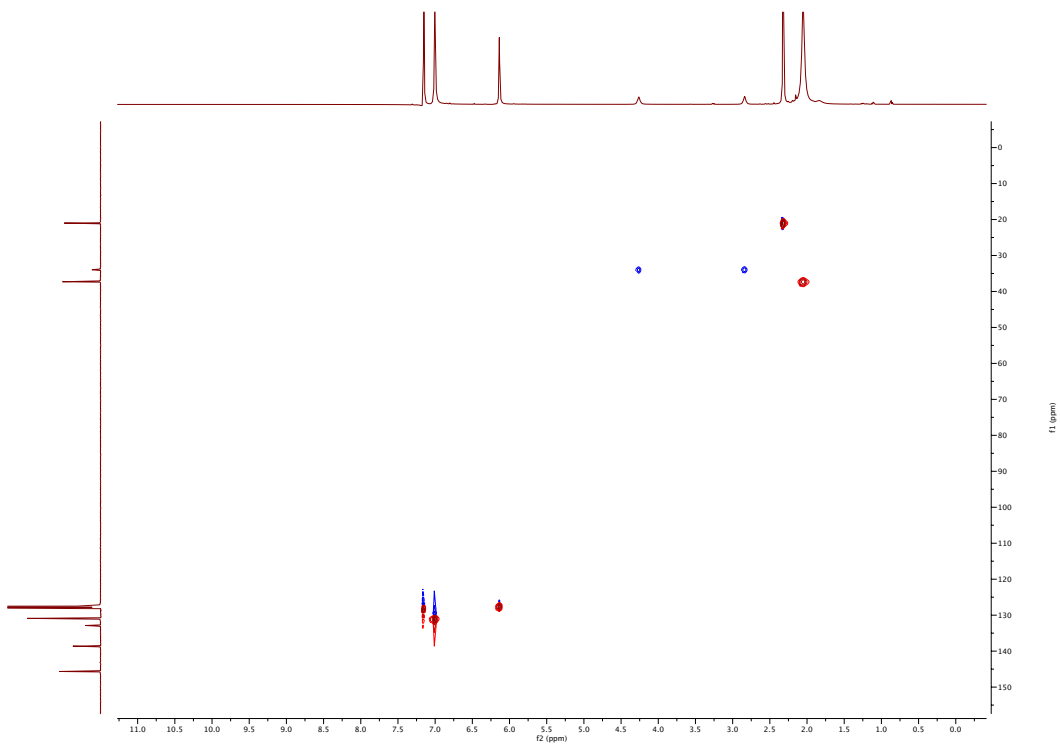


Figure S15: ^1H - ^{13}C multiplicity edited HSQC spectrum of **7** in C_6D_6 at 293 K.

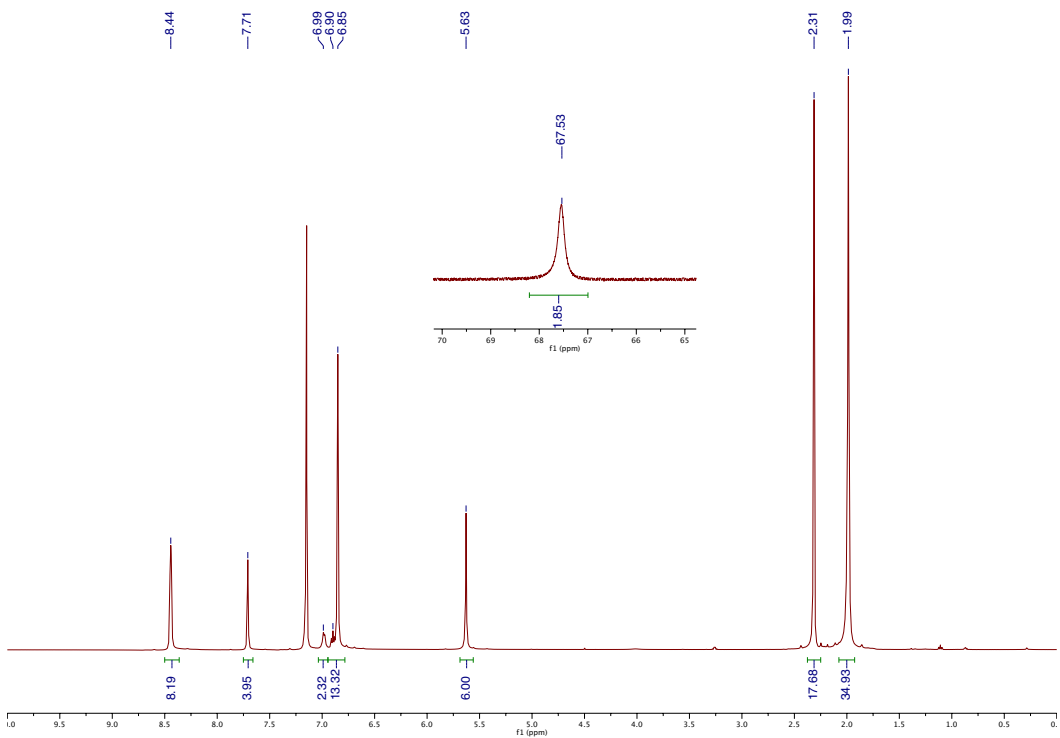


Figure S16: ^1H NMR spectrum of $[\mathbf{2}]^+$ in C_6D_6 at 293 K.

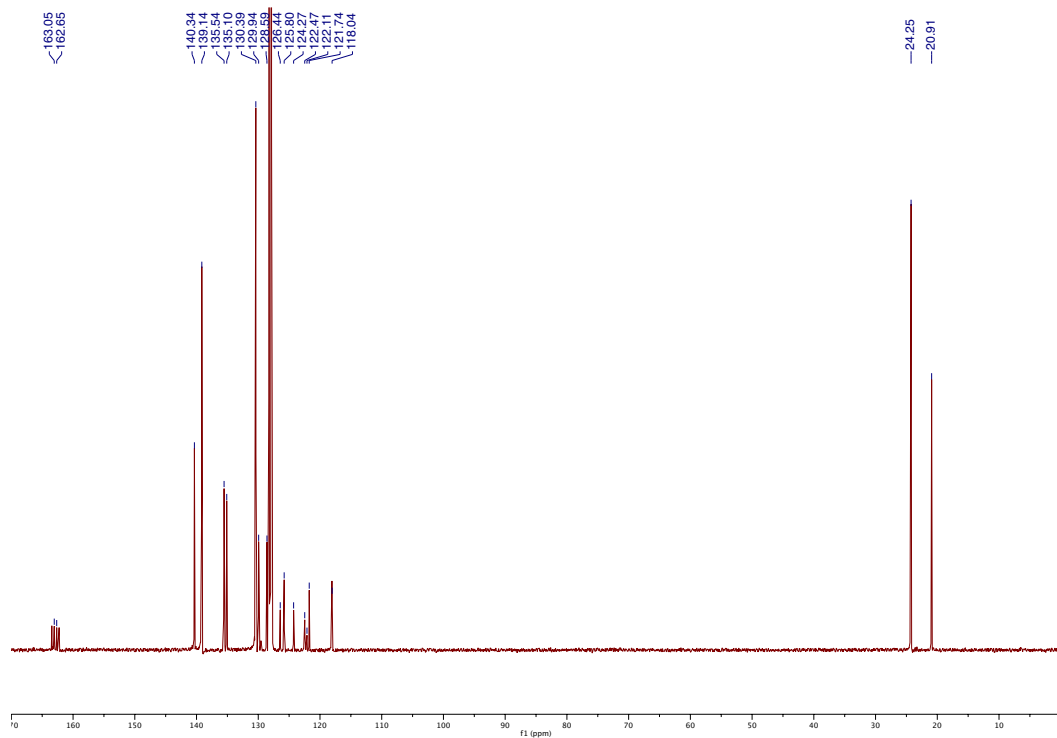


Figure S17: $^{13}\text{C}\{^1\text{H}\}$ NMR spectrum of $[2]^+$ in C_6D_6 at 293 K.

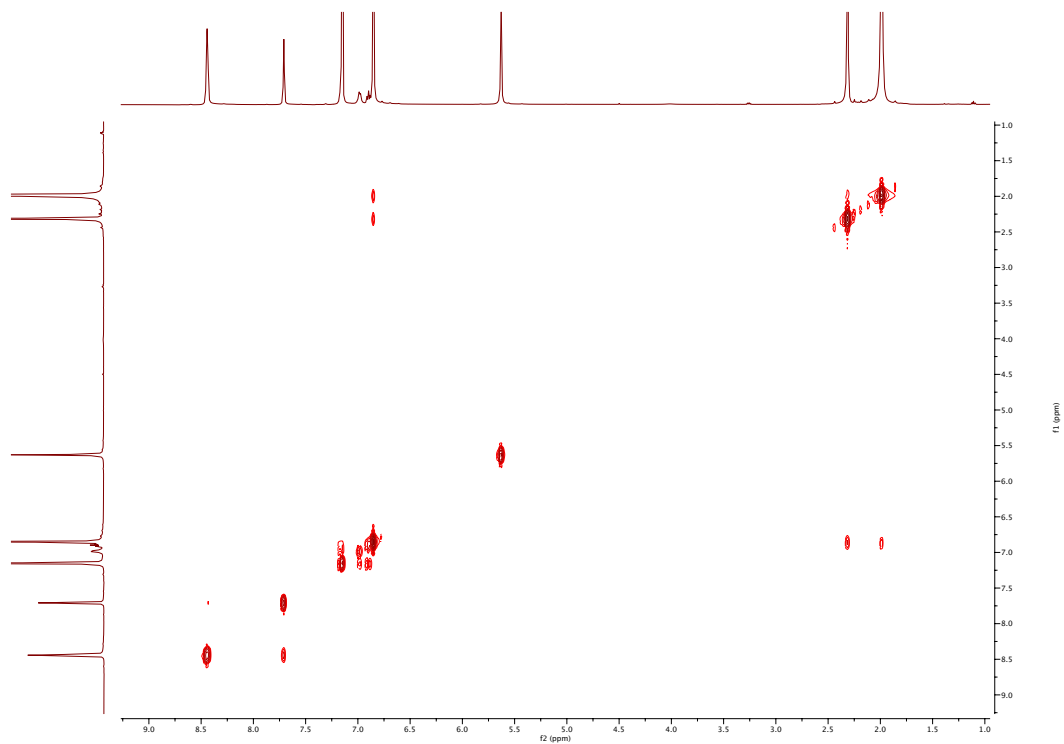


Figure S18: $^1\text{H}\text{-}^1\text{H}$ COSY spectrum of $[2]^+$ in C_6D_6 at 293 K.

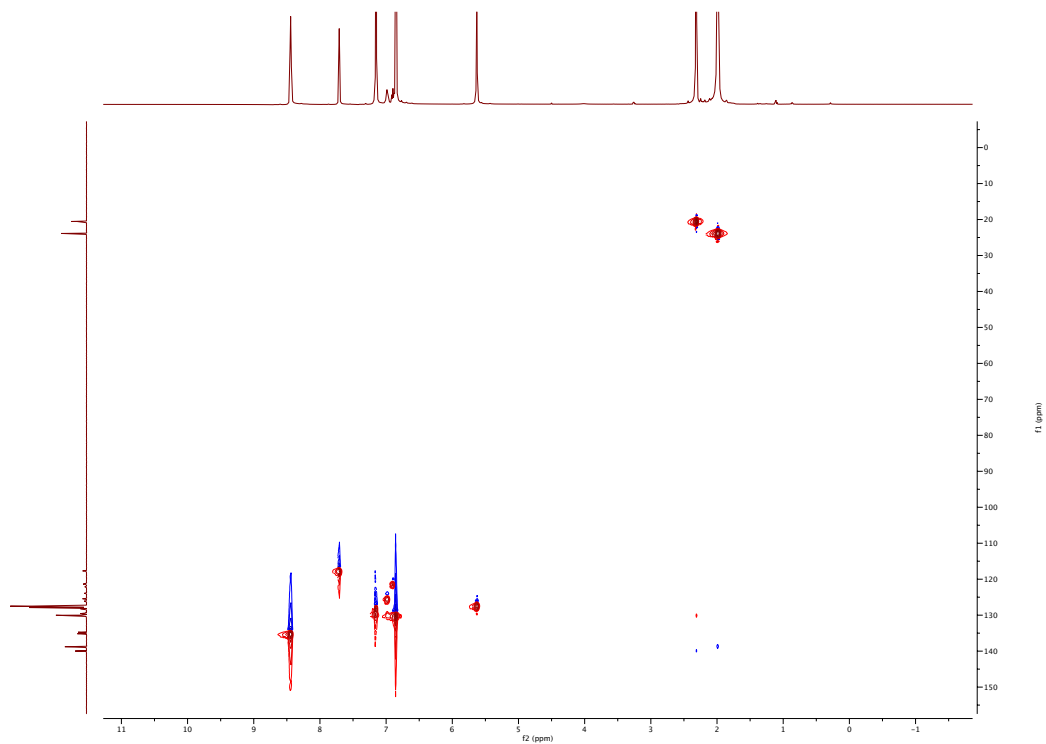


Figure S19: ^1H - ^{13}C multiplicity edited HSQC spectrum of $[\mathbf{2}]^+$ in C_6D_6 at 293 K.

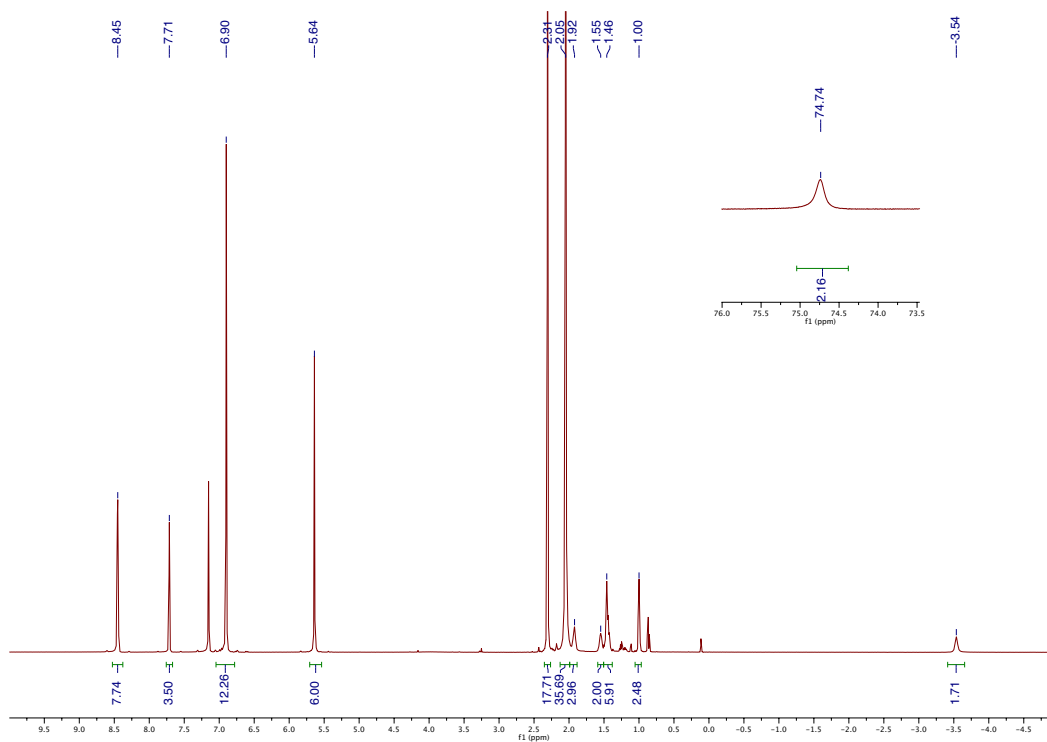


Figure S20: ^1H NMR spectrum of $[\mathbf{3}]^+$ in C_6D_6 at 293 K.

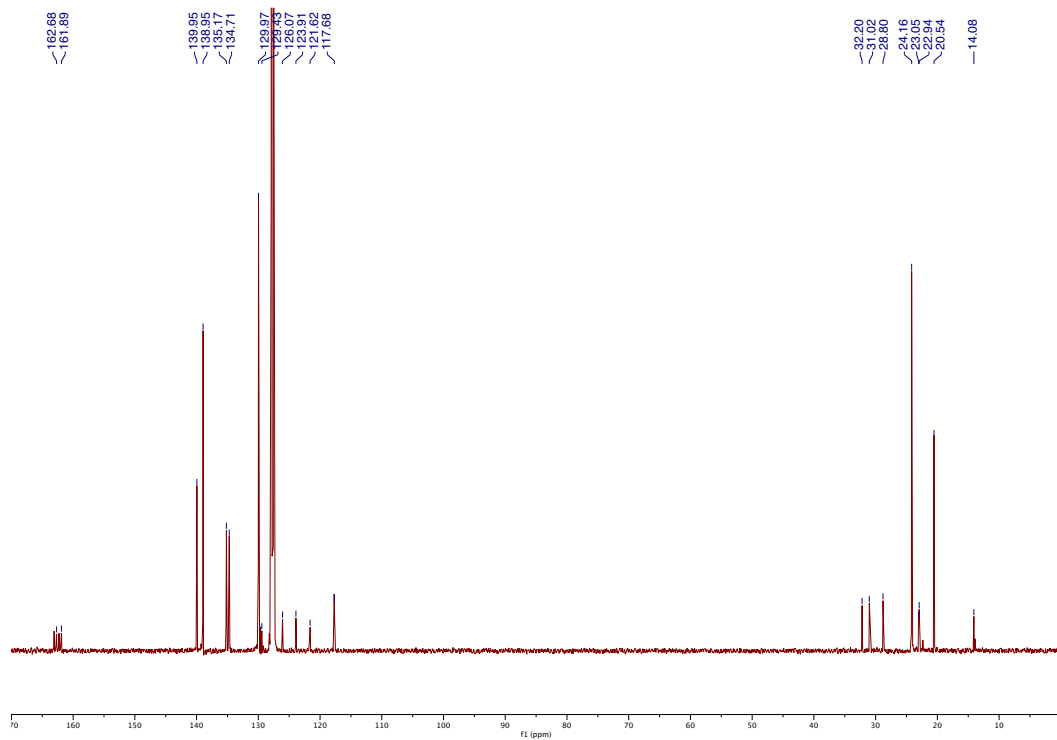


Figure S21: $^{13}\text{C}\{^1\text{H}\}$ NMR spectrum of $[3]^+$ in C_6D_6 at 293 K.

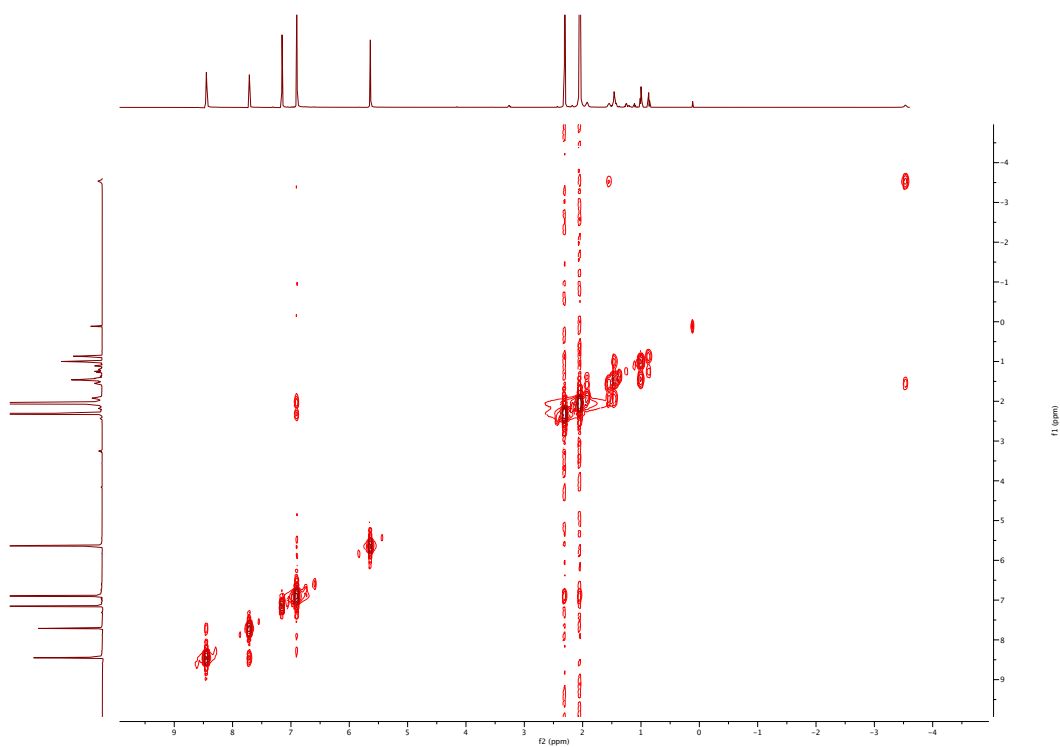


Figure S22: ^1H - ^1H COSY spectrum of $[3]^+$ in C_6D_6 at 293 K.

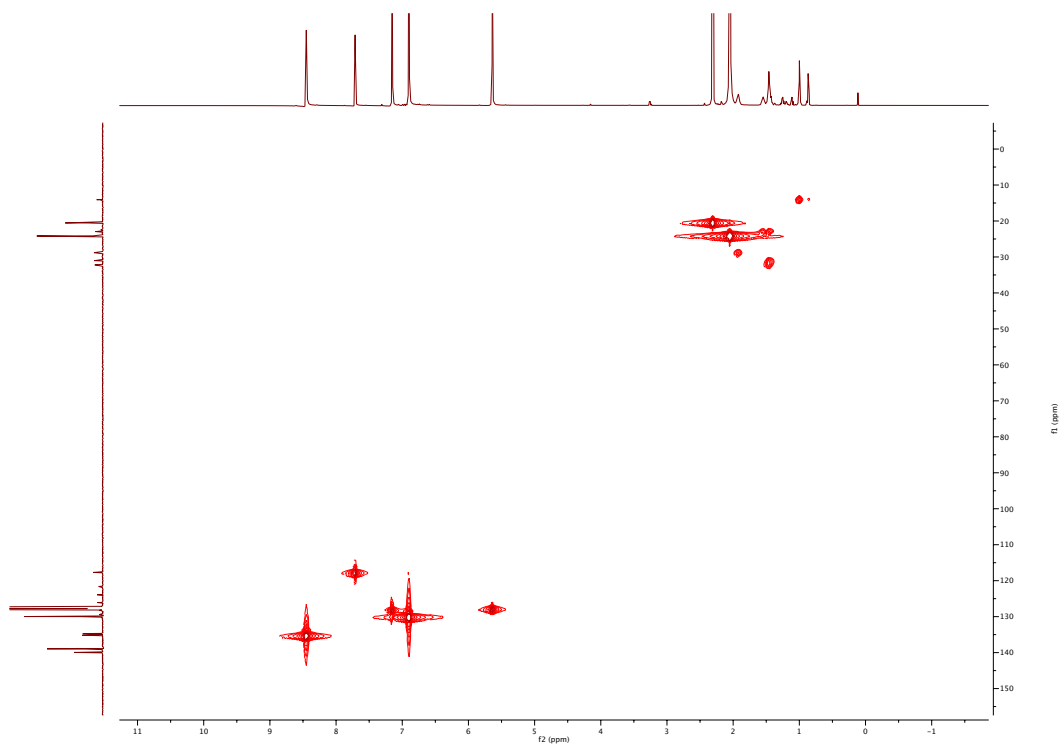


Figure S23: ^1H - ^{13}C HSQC spectrum of $[\mathbf{3}]^+$ in C_6D_6 at 293 K.

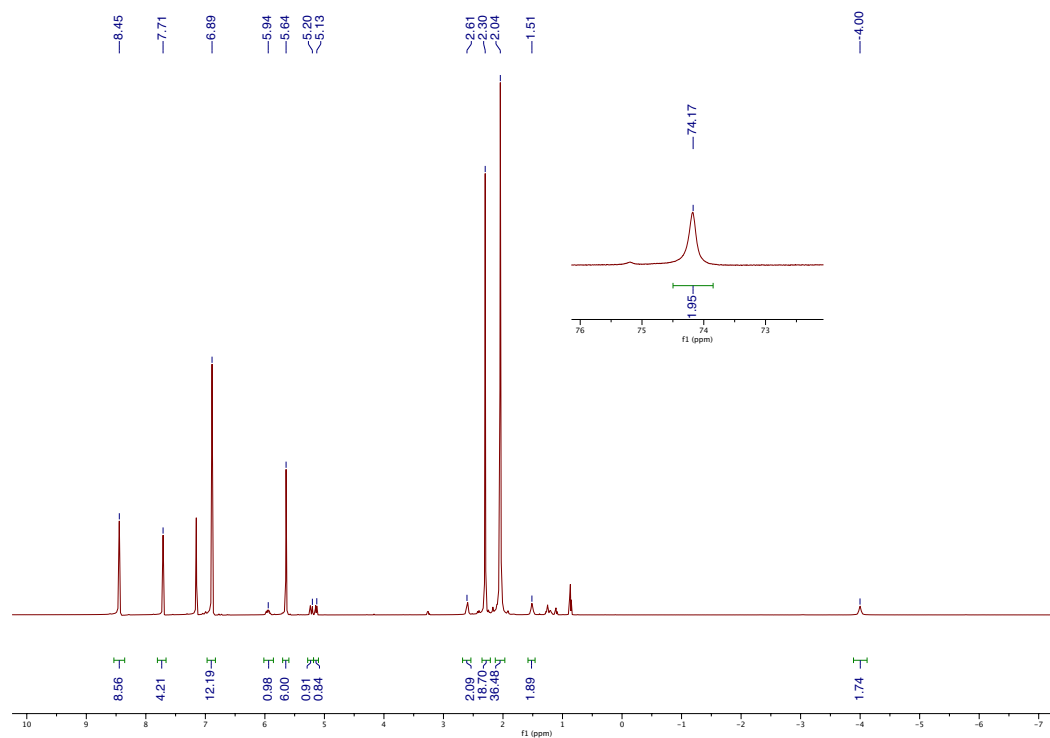


Figure S24: ^1H NMR spectrum of $[\mathbf{5}]^+$ in C_6D_6 at 293 K.

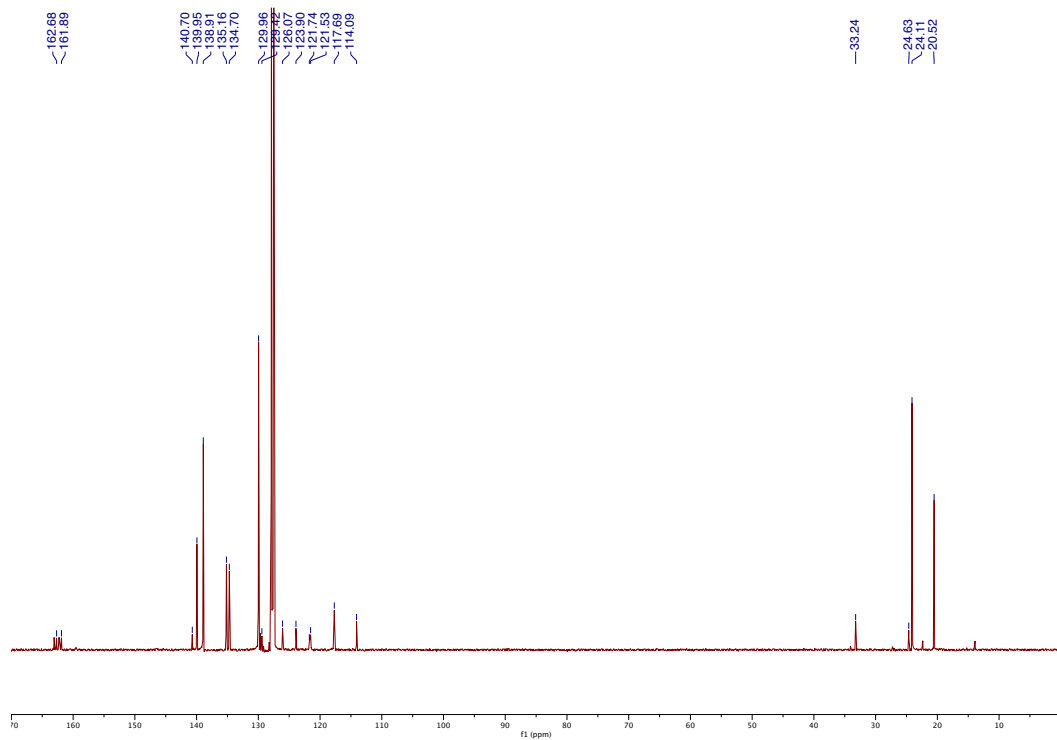


Figure S25: $^{13}\text{C}\{^1\text{H}\}$ NMR spectrum of $[\mathbf{5}]^+$ in C_6D_6 at 293 K.

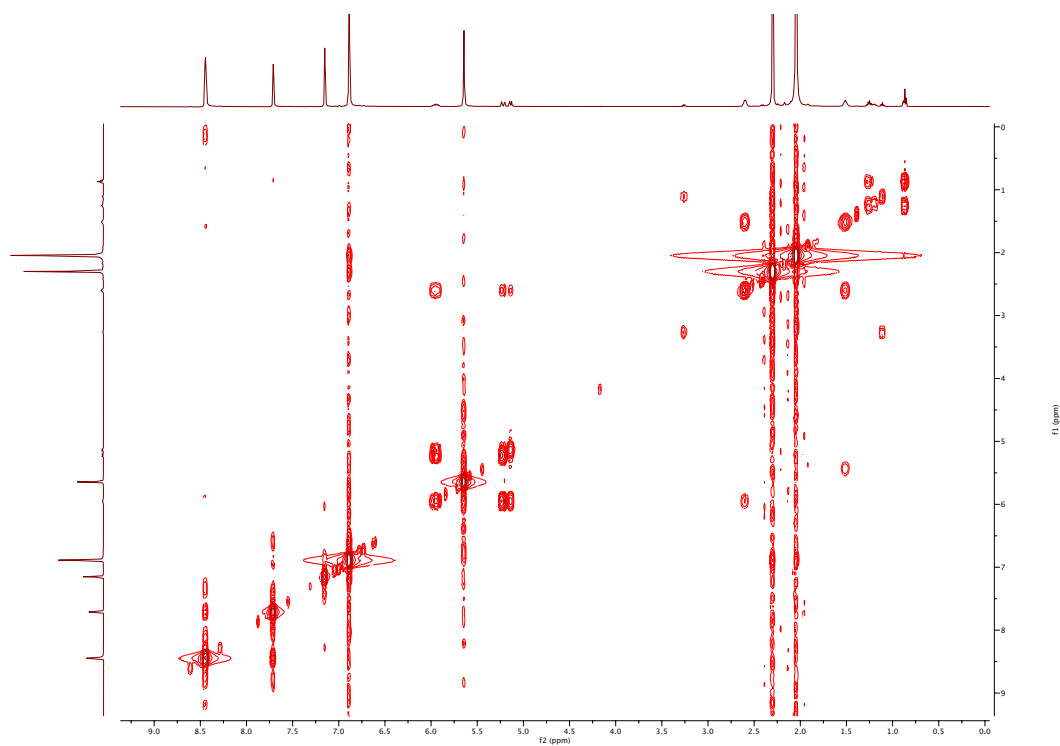


Figure S26: $^1\text{H}\text{-}^1\text{H}$ COSY spectrum of $[\mathbf{5}]^+$ in C_6D_6 at 293 K.

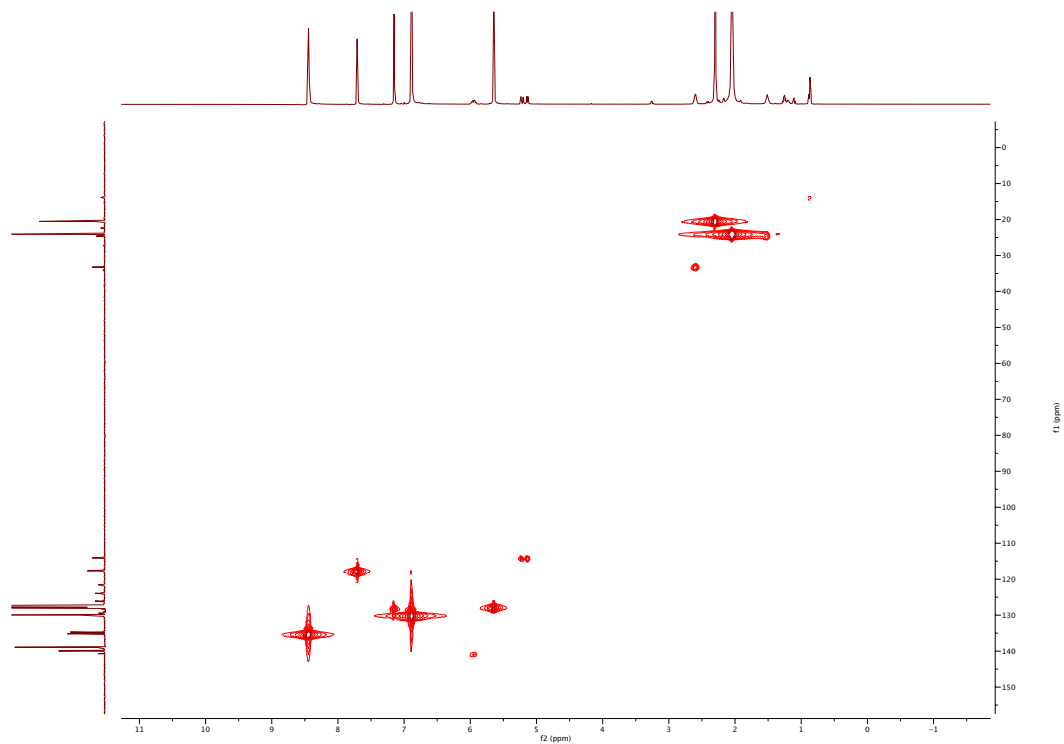


Figure S27: ^1H - ^{13}C HSQC spectrum of $[\mathbf{5}]^+$ in C_6D_6 at 293 K.

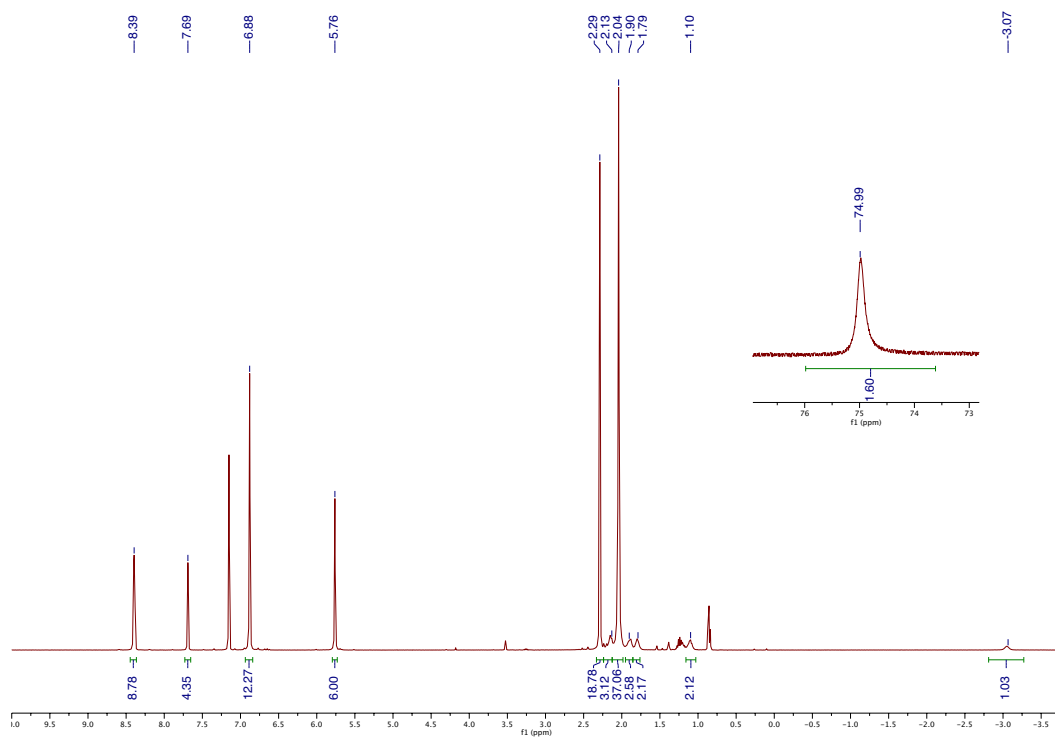


Figure S28: ^1H NMR spectrum of $[\mathbf{7}]^+$ in $\text{C}_6\text{D}_6/\text{d}^8\text{-THF}$ 15:1 at 293 K.

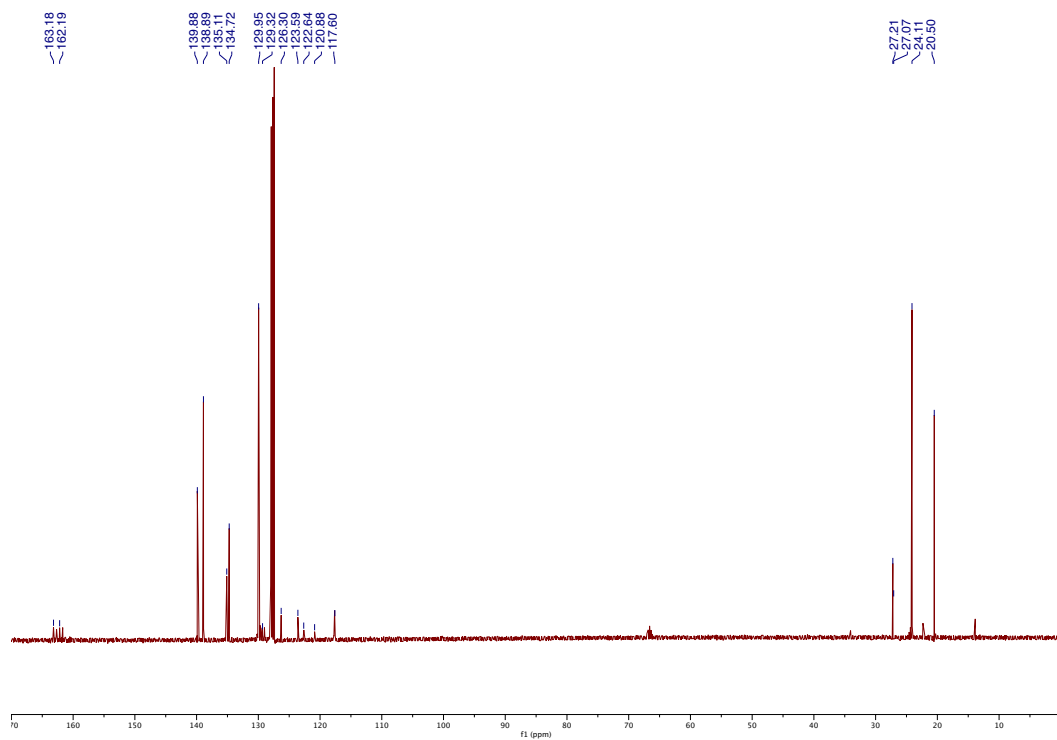


Figure S29: $^{13}\text{C}\{^1\text{H}\}$ NMR spectrum of $[7]^+$ in $\text{C}_6\text{D}_6/\text{d}^8\text{-THF}$ 15:1 at 293 K.

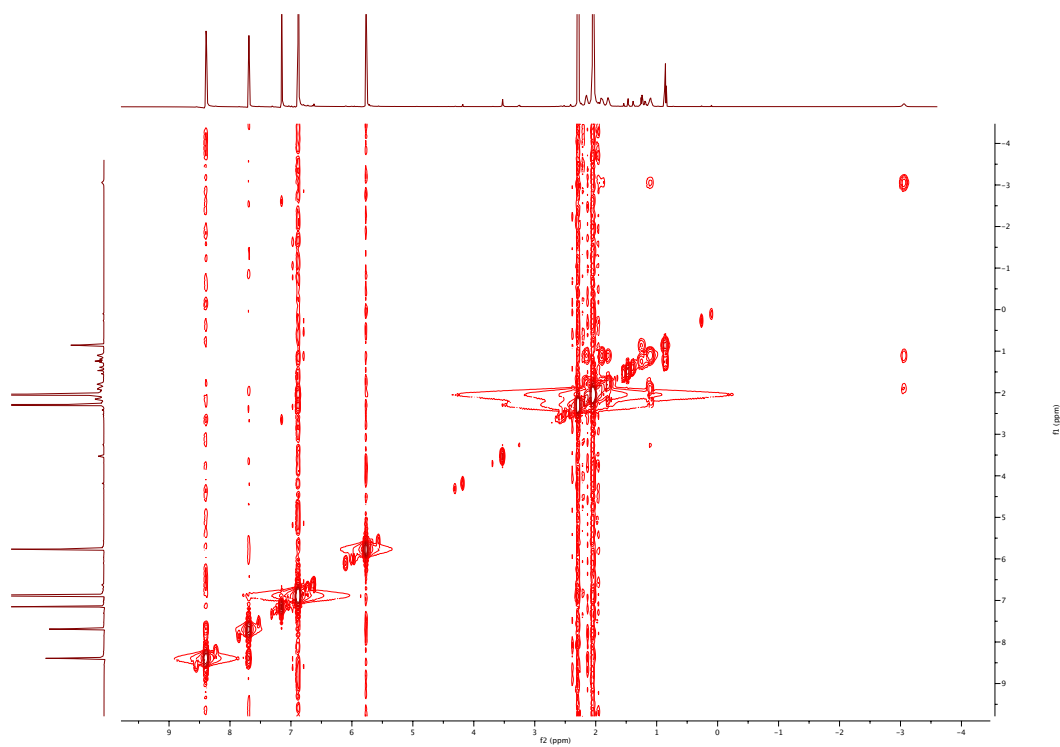


Figure S30: $^1\text{H}\text{-}^1\text{H}$ COSY spectrum of $[7]^+$ in $\text{C}_6\text{D}_6/\text{d}^8\text{-THF}$ 15:1 at 293 K.

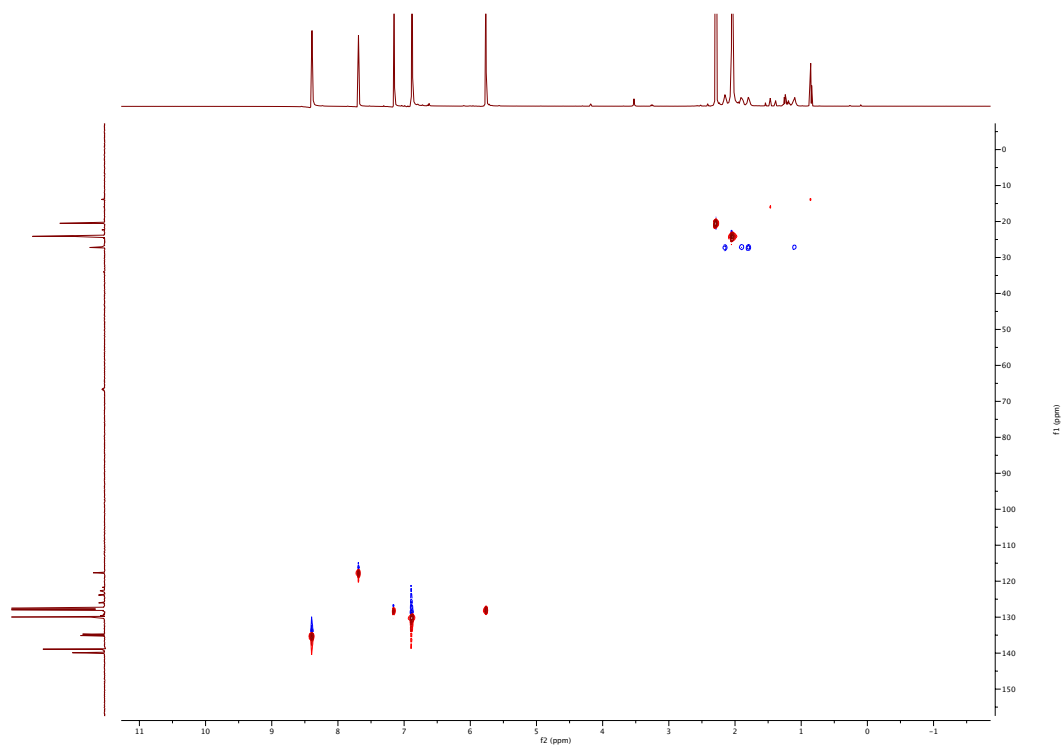


Figure S31: ^1H - ^{13}C multiplicity edited HSQC spectrum of $[\mathbf{7}]^+$ in $\text{C}_6\text{D}_6/\text{d}^8\text{-THF}$ 15:1 at 293 K.

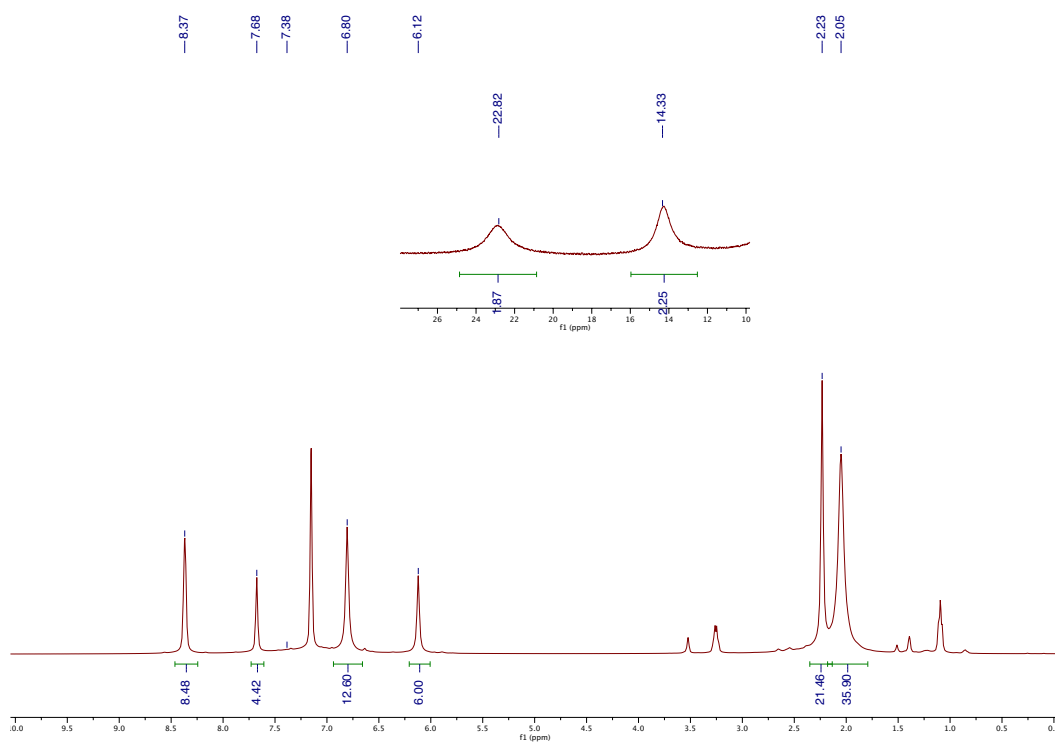


Figure S32: ^1H NMR spectrum of $[\mathbf{4}]^+$ in $\text{C}_6\text{D}_6/\text{d}^8\text{-THF}$ 15:1 at 293 K.

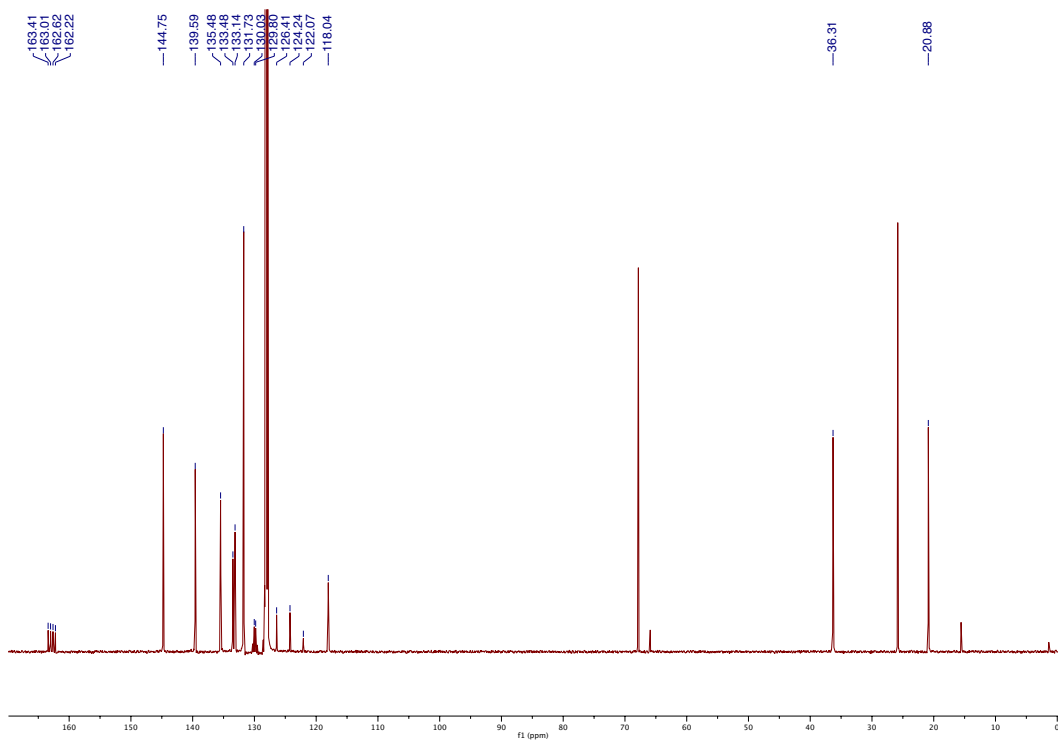


Figure S33: $^{13}\text{C}\{^1\text{H}\}$ NMR spectrum of $[\mathbf{4}]^+$ in $\text{C}_6\text{D}_6/\text{THF}$ 15:1 at 293 K.

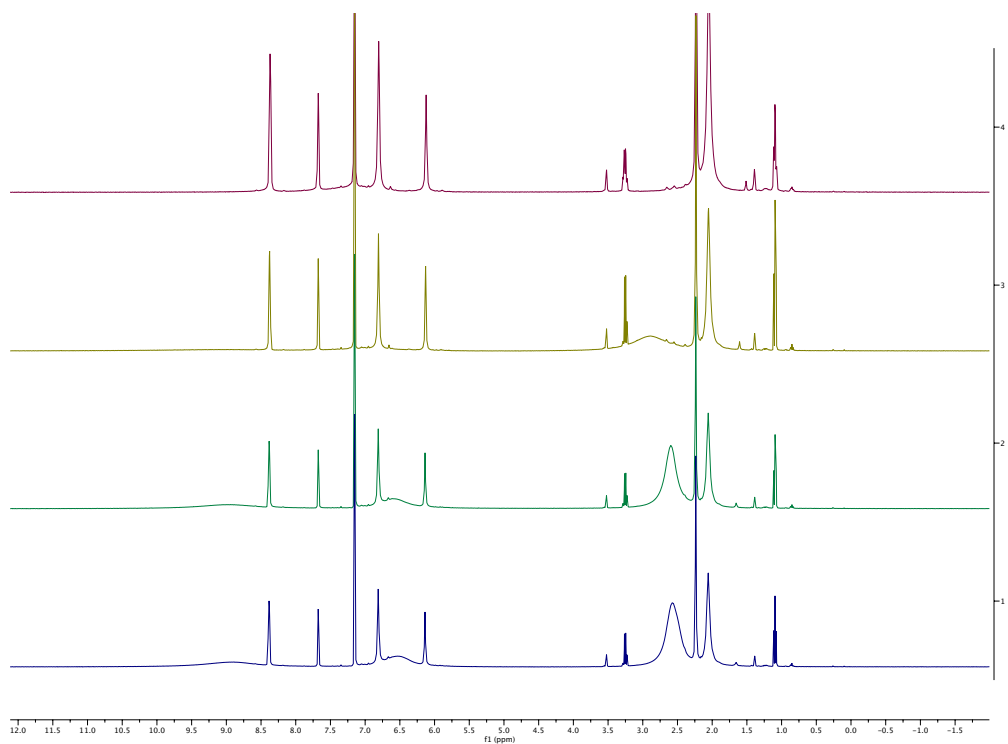


Figure S34: ^1H NMR spectrum of $[\mathbf{4}]^+$ in $\text{C}_6\text{D}_6/\text{d}^8\text{-THF}$ 15:1 at 293 K with 1, 5, 10 and 20 equiv. (top to bottom) of DMAP added.

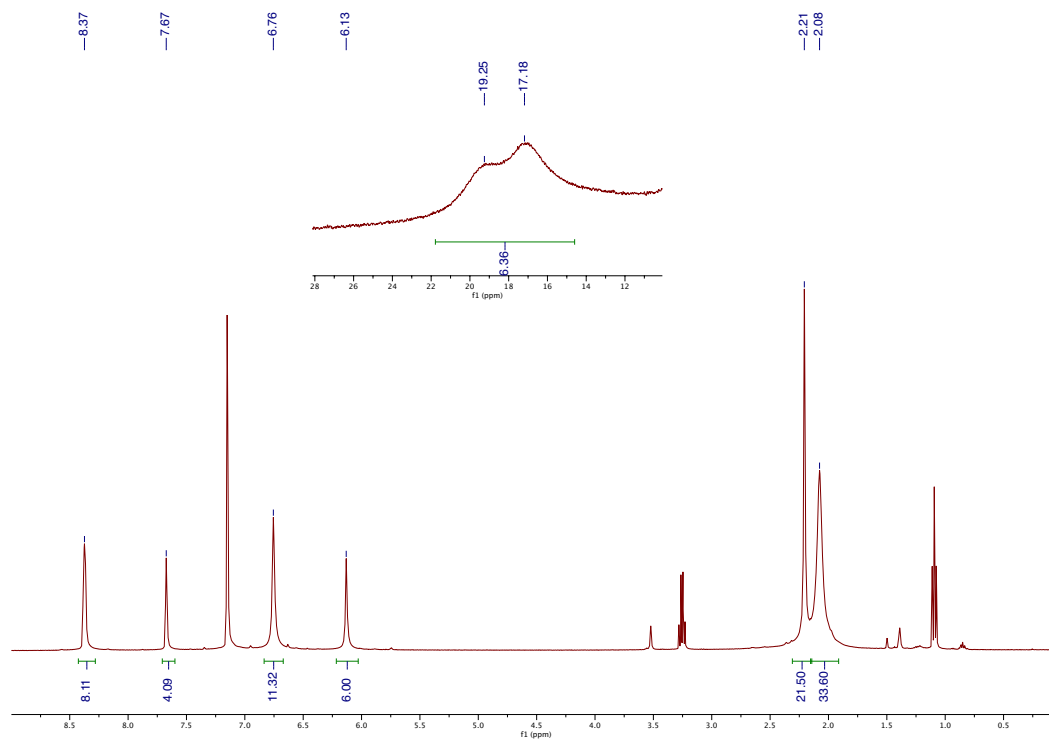


Figure S35: ^1H NMR spectrum of $[\mathbf{8}]^+$ in $\text{C}_6\text{D}_6/\text{d}^8\text{-THF}$ 15:1 at 293 K.

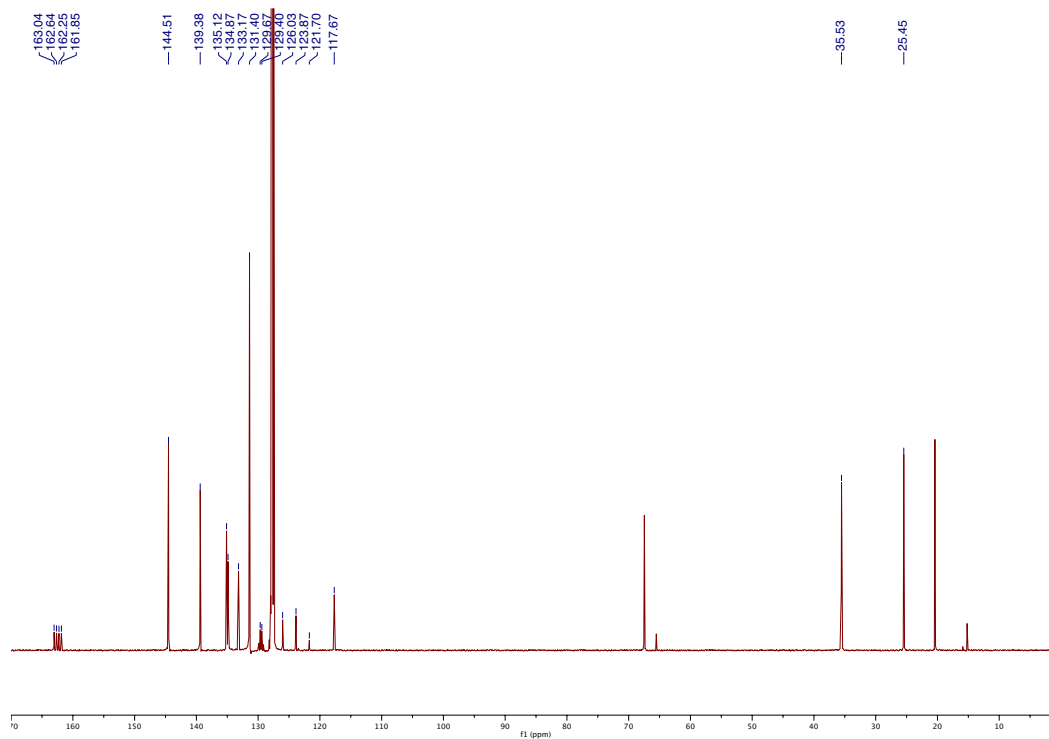


Figure S36: $^{13}\text{C}\{^1\text{H}\}$ NMR spectrum of $[\mathbf{8}]^+$ in $\text{C}_6\text{D}_6/\text{THF}$ 15:1 at 293 K.

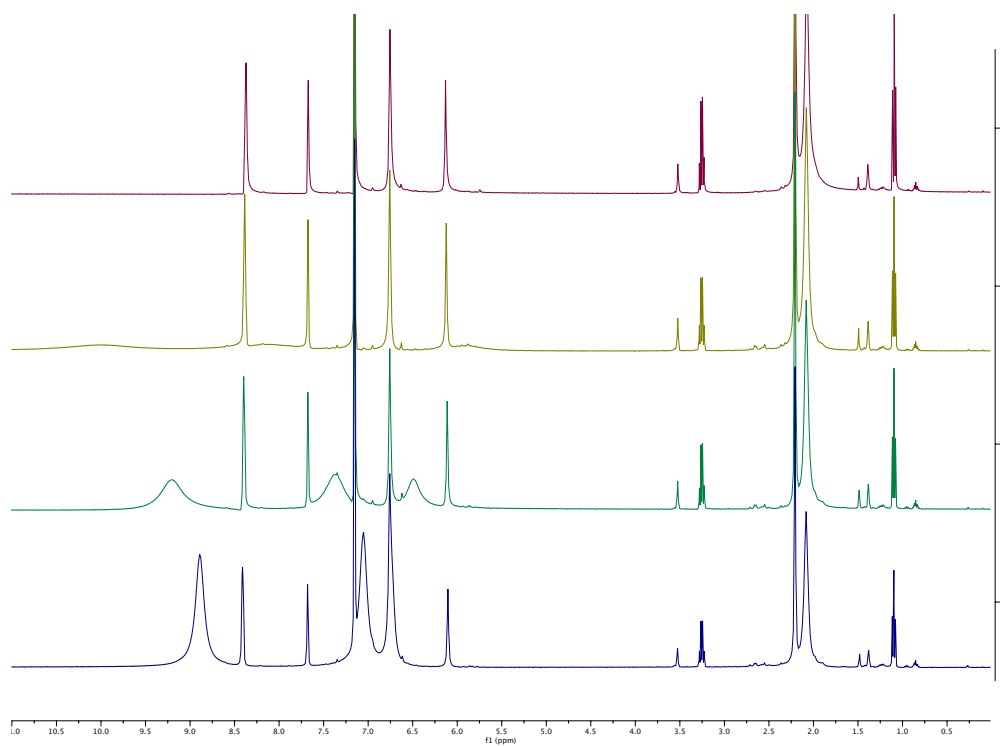


Figure S37: ^1H NMR spectrum of $[\mathbf{8}]^+$ in $\text{C}_6\text{D}_6/\text{d}^8\text{-THF}$ 15:1 at 293 K with 1, 5, 10 and 20 equiv. (top to bottom) of pyridine added.

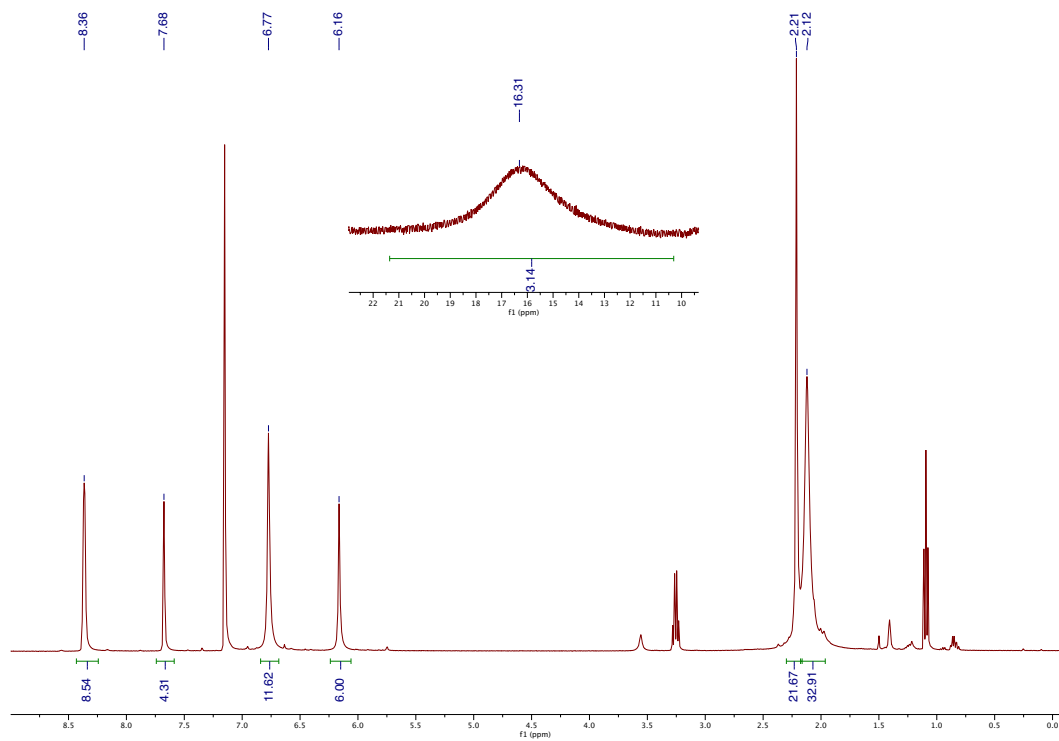


Figure S38: ^1H NMR spectrum of $[\mathbf{6}]^+$ in $\text{C}_6\text{D}_6/\text{d}^8\text{-THF}$ 15:1 at 293 K.

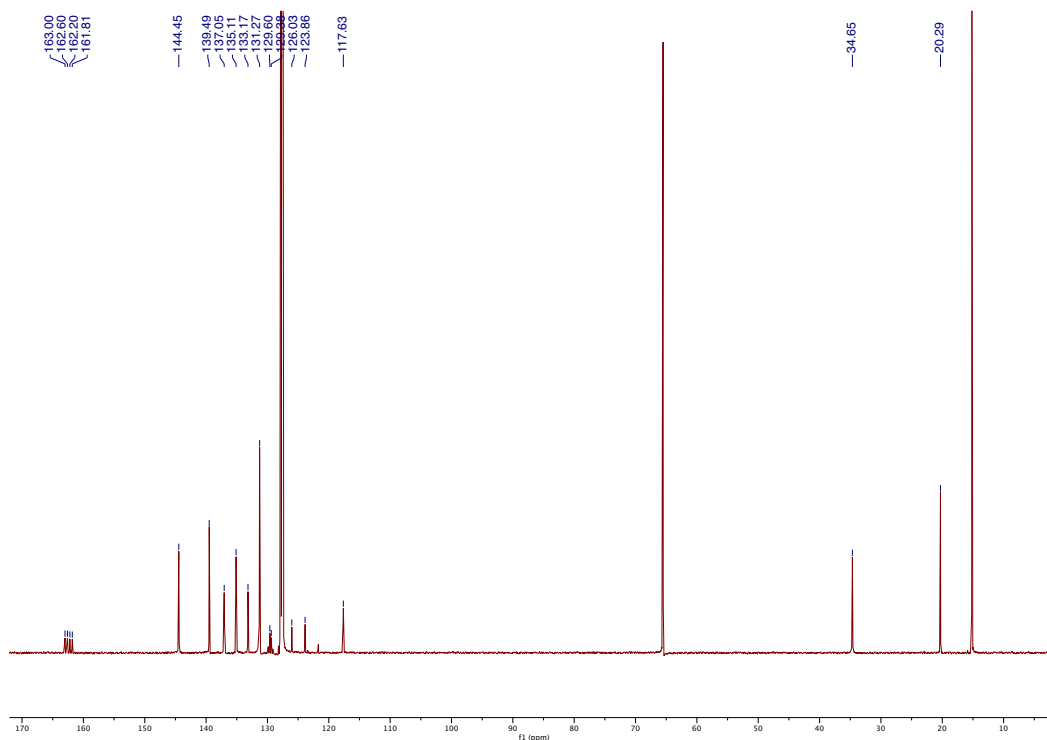


Figure S39: $^{13}\text{C}\{^1\text{H}\}$ NMR spectrum of $[\mathbf{6}]^+$ in $\text{C}_6\text{D}_6/\text{THF}$ 15:1 at 293 K.

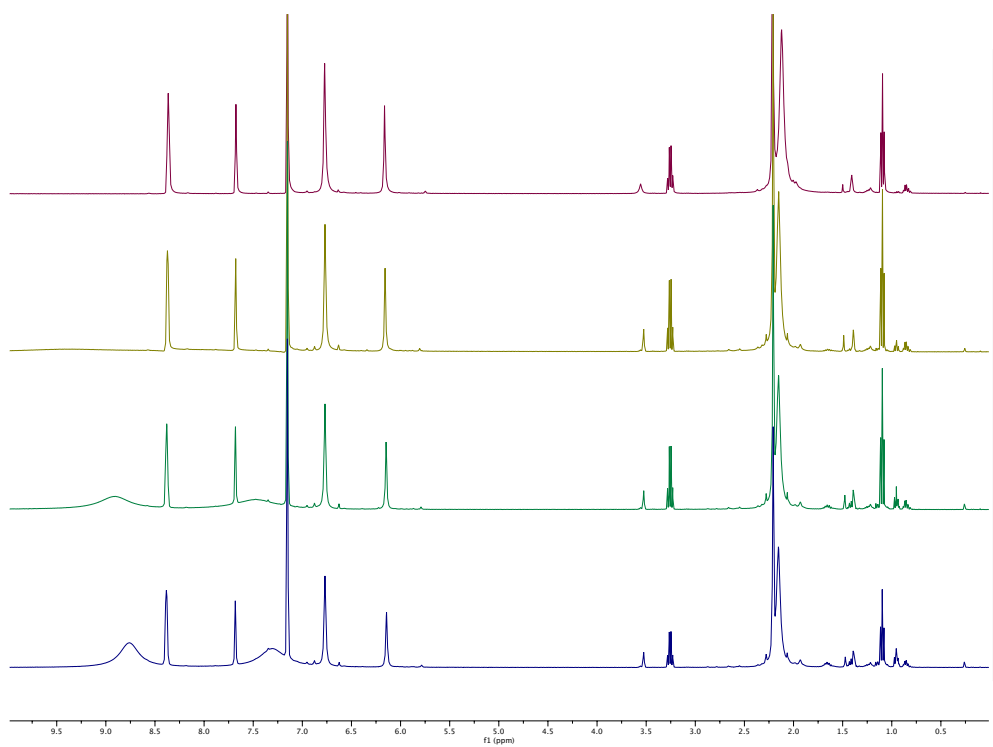


Figure S40: ^1H NMR spectrum of $[\mathbf{6}]^+$ in $\text{C}_6\text{D}_6/\text{d}^8\text{-THF}$ 15:1 at 293 K with 1, 5, 10 and 20 equiv. (top to bottom) of 4- CF_3 -pyridine added.

C. Experimental details and NMR spectra for radical reactions

The products of the reaction between alkylated $[\text{Fe}_4\text{S}_4]^{2+}$ clusters and pyridines were analyzed by ^1H NMR spectroscopy and/or gas chromatography (GC). The GC was calibrated using standards of octane and hexadecane with concentrations between 0.04 and 0.8 mg/mL. An internal standard of HMDSO was added to each trial and a ^1H NMR spectrum was obtained prior to addition of the pyridine to ensure accurate integration of the starting material relative to HMDSO. All NMR spectra were recorded with long delays between scans (30 s) to ensure accurate integrations. Each reaction was performed in triplicate and the reported yields are the average across the three trials. Note that the ^1H NMR features corresponding to the cationic pyridine adducts shift due to fast exchange with excess pyridine (see Fig. S34).

Table S1. Summary of reactions between $[(\text{IMes})_3\text{Fe}_4\text{S}_4\text{R}]^+$ clusters and pyridines in the presence or absence of a radical trap.

R	Base	Trap	R-R (%)	R-H (%)	R-D (%)	R-Sn (%)	Total (%)
Benzyl	DMAP	-	92(3)	4(3)	-	-	96(4)
	DMAP	Bu ₃ SnH	33(3)	34(3)	-	17(3)	84(5)
	DMAP	Bu ₃ SnD	54(3)	7(3)	13(3)	11(3)	85(6)
	CF ₃ py	Bu ₃ SnH	n.d.	55(3)	-	43(3)	98(4)
	quinuclidine	-	90(4)	8(3)	-	-	98(5)
Octyl	DMAP	Bu ₃ SnH	75(8)	n.d.	-	-	75(8)
	DMAP	Bu ₃ SnH	n.d.	56(6)	-	-	56(6)
	CF ₃ py	Bu ₃ SnH	n.d.	52(2)	-	-	52(2)
5-Hexenyl	DMAP	-	99(4) of which 28(2) is uncyclized		-	-	99(4)

1. $[2]^+$ + 20 equiv. DMAP

The reactions were analyzed by ^1H NMR spectroscopy. The amount of bibenzyl was determined using the curve fitting program available in MNova.

2. $[2]^+$ + 20 equiv. DMAP + 20 equiv. Bu_3SnH

The reactions were analyzed by ^1H NMR spectroscopy. The amounts of bibenzyl, toluene, and Bu_3SnBn were determined using the curve fitting program available in MNova.

3. $[2]^+$ + 20 equiv. DMAP + 20 equiv. Bu_3SnD

The reactions were analyzed by ^1H NMR spectroscopy. The amounts of bibenzyl, toluene, d^1 -toluene, and Bu_3SnBn were determined using the curve fitting program available in MNova.

4. $[2]^+$ + 20 equiv. CF_3 -py + 20 equiv. Bu_3SnH

The reactions were analyzed by ^1H NMR spectroscopy. The amounts of toluene and Bu_3SnBn were determined using the curve fitting program available in MNova.

5. $[2]^+$ + 20 equiv. quinuclidine

The reactions were analyzed by ^1H NMR spectroscopy. The reaction mixture was passed through a plug of silica to remove iron-containing species and quinuclidine. The amounts of toluene and bibenzyl were determined using the curve fitting program available in MNova.

6. $[3]^+$ + 20 equiv. DMAP

The reactions were analyzed first by ^1H NMR spectroscopy. The reaction mixture was then passed through a plug of silica to remove iron-containing species and the

silica was washed with benzene to dilute the sample to a total volume of 5 mL.
Product yields were determined by GC.

7. **[3]⁺** + 20 equiv. DMAP + 20 equiv. Bu₃SnH

The reactions were analyzed first by ¹H NMR spectroscopy. The reaction mixture was then passed through a plug of silica to remove iron-containing species and the silica was washed with benzene to dilute the sample to a total volume of 5 mL. Product yields were determined by GC.

8. **[3]⁺** + 20 equiv. CF₃-py + 20 equiv. Bu₃SnH

The reactions were analyzed first by ¹H NMR spectroscopy. The reaction mixture was passed through a plug of silica to remove iron-containing species and the silica was washed with benzene to dilute the sample to a total volume of 5 mL. Product yields were determined by GC.

9. **[5]⁺** + 20 equiv. DMAP

The reactions were analyzed first by ¹H NMR spectroscopy. The reaction mixture was passed through a plug of silica to remove iron-containing species and a second NMR spectrum was obtained.

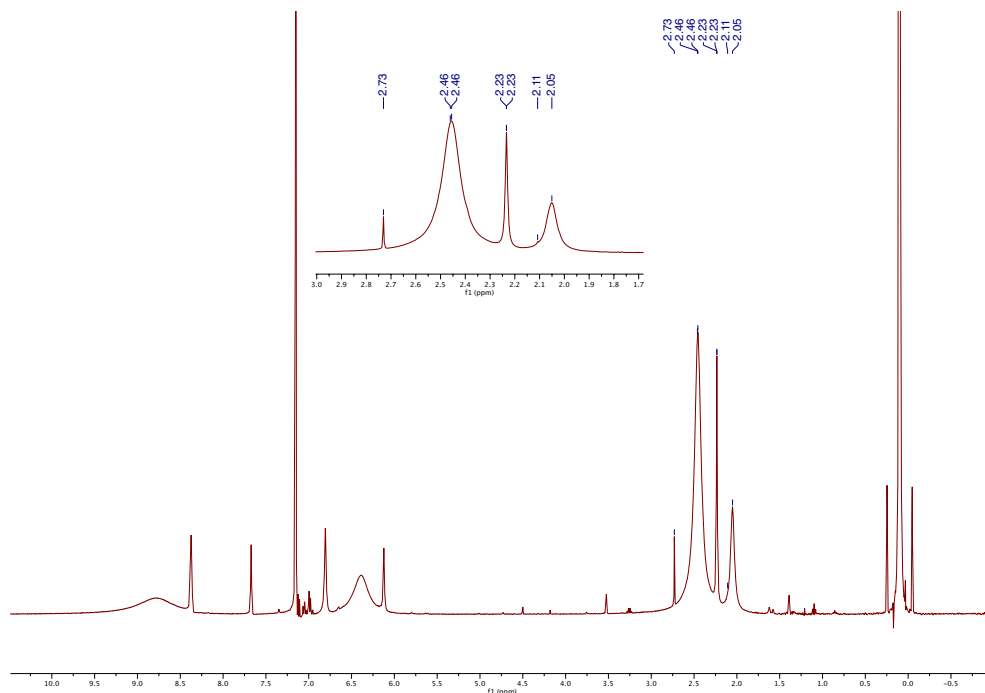


Figure S41: ¹H NMR spectrum of reaction 1: addition of DMAP to **[2]**⁺. Inset shows toluene (2.11 ppm) and bibenzyl (2.73 ppm).

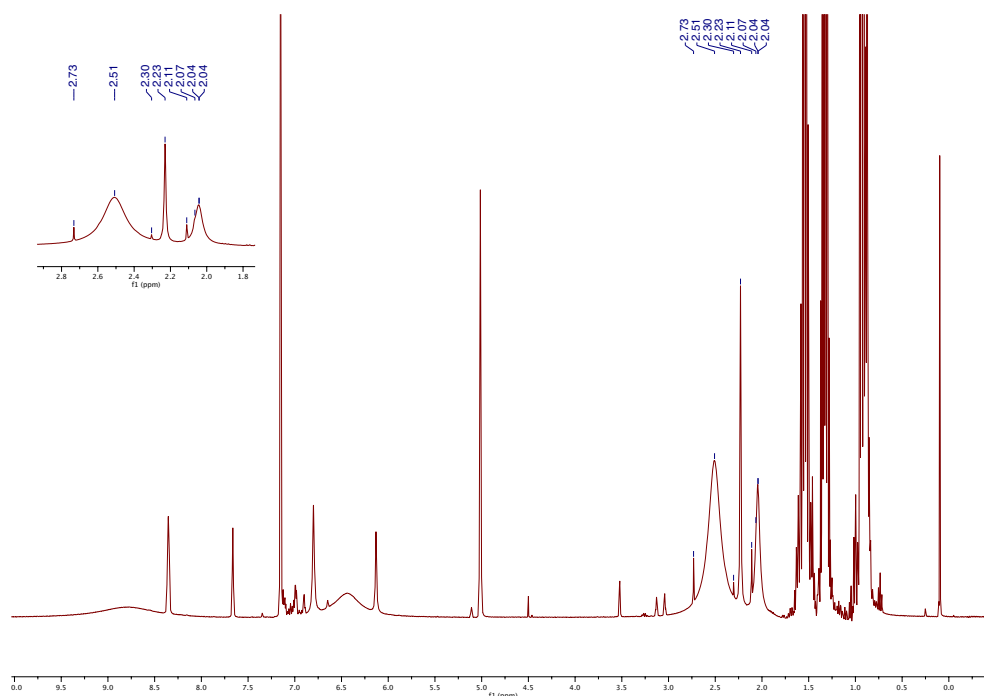


Figure S42: ¹H NMR spectrum of reaction 2: addition of DMAP to **[2]**⁺ in the presence of Bu₃SnH. Inset shows toluene (2.11 ppm), Bu₃SnBn (2.30 ppm) and bibenzyl (2.74 ppm).

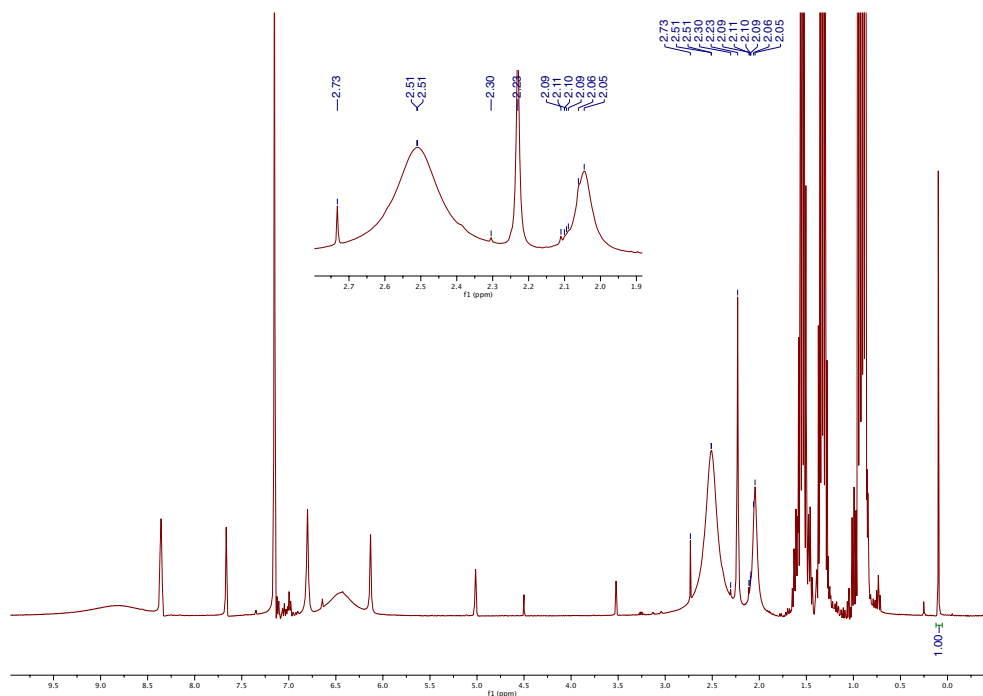


Figure S43: ^1H NMR spectrum of reaction 3: addition of DMAP to $[2]^+$ in the presence of Bu_3SnD . Inset shows toluene (2.11 ppm), d^1 -toluene (2.09 ppm) Bu_3SnBn (2.30 ppm) and bibenzyl (2.74 ppm).

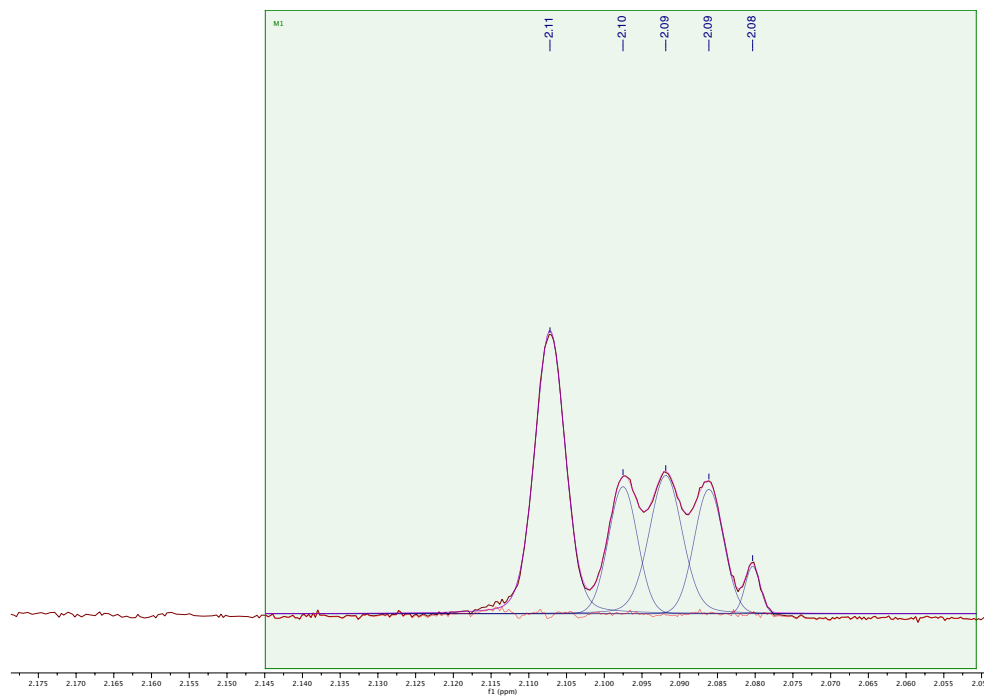


Figure S44: ^1H NMR spectrum of reaction 3 after vacuum transfer of the volatile material. Toluene (2.11 ppm) and d^1 -toluene (1:1:1 triplet, 2.09 ppm) are visible. The peak at 2.08 ppm is a ^{13}C satellite peak from residual DMAP.

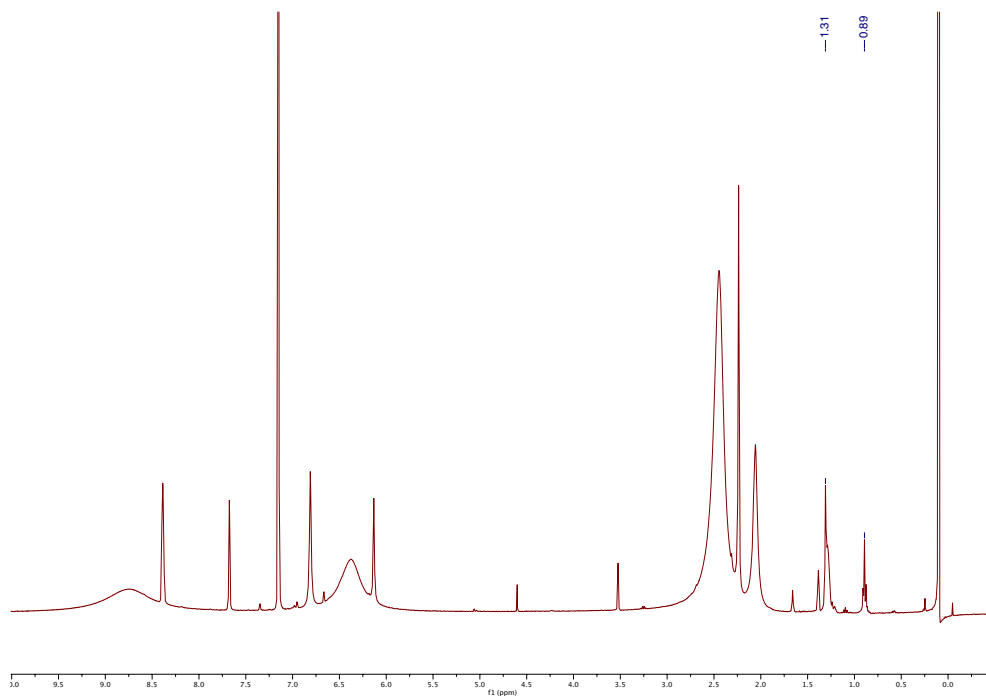


Figure S47: ¹H NMR spectrum of reaction 6: addition of DMAP to **[3]**⁺. Hexadecane appears as overlapping peaks at 0.89 and 1.31 ppm.

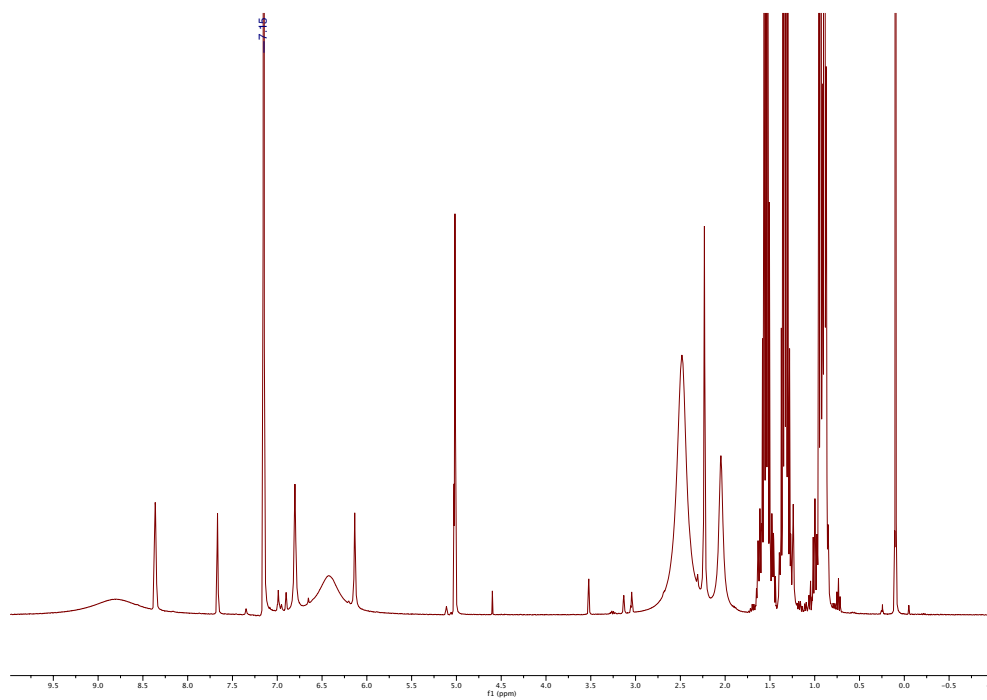


Figure S48: ¹H NMR spectrum of reaction 7: addition of DMAP to **[3]**⁺ in the presence of Bu₃SnH. Hexadecane and octane are obscured by excess Bu₃SnH.

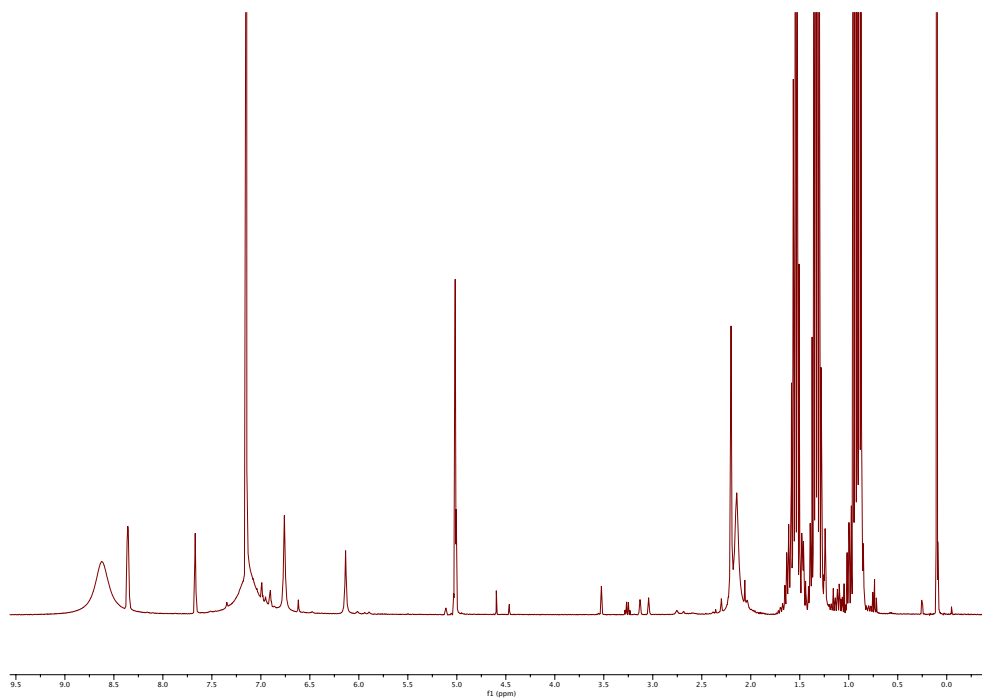


Figure S49: ¹H NMR spectrum of reaction 8: addition of 4-CF₃-py to [3]⁺ in the presence of Bu₃SnH. Hexadecane and octane are obscured by excess Bu₃SnH.

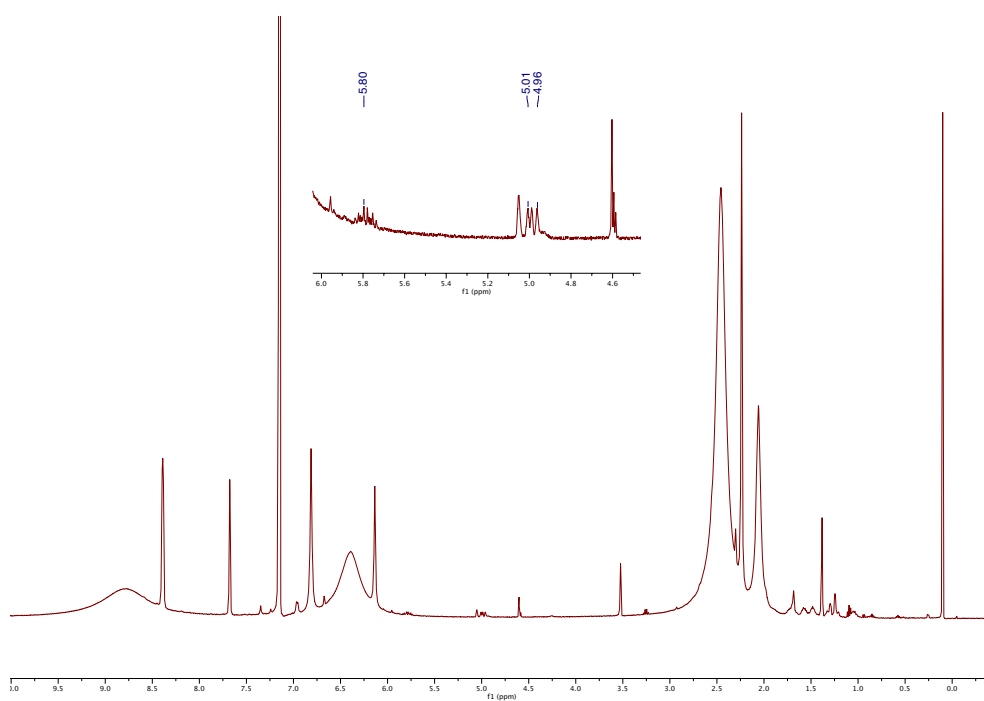


Figure S50: ¹H NMR spectrum of reaction 9: addition of DMAP to [5]⁺. Inset shows the alkene resonances.

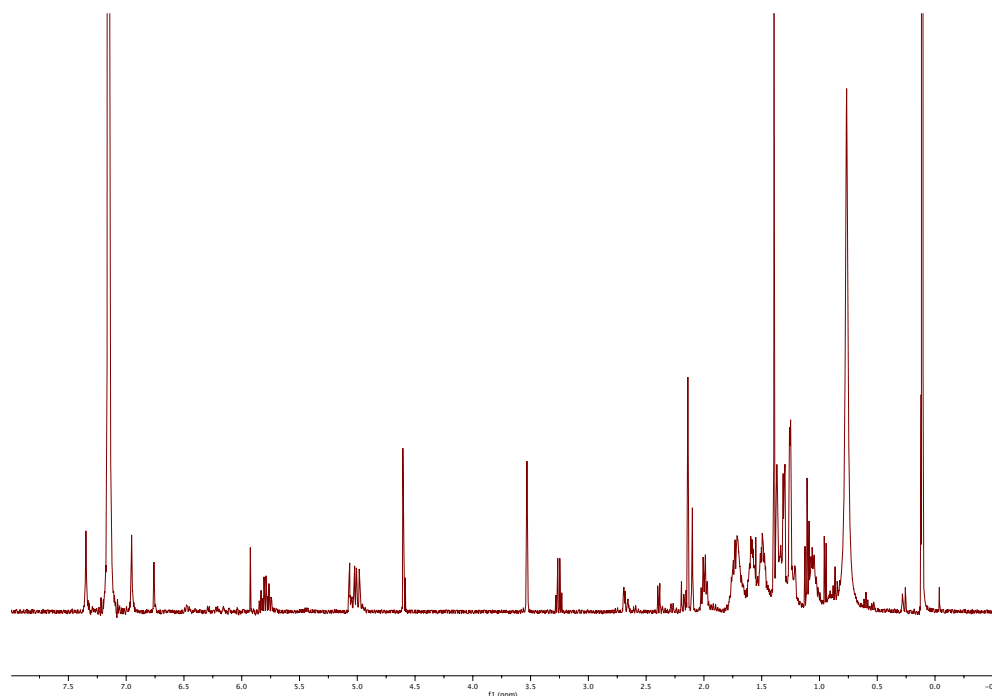


Figure S51: ^1H NMR spectrum of reaction 9 after running the reaction mixture through a plug of silica. Integration of the alkene resonances at 5.8 and 5.0 ppm relative to the alkyl region (1.9 through 0.9 ppm) and the internal standard gave the percentage of alkyl groups that still contained alkene resonances.

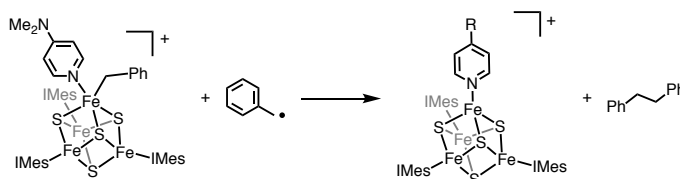
D. Discussion of the mechanism of the radical release reaction

The radicals generated by Fe–C bond homolysis from the pyridine-bound intermediate discussed in the main text (Scheme 2) can undergo subsequent reactions to generate C–C coupled organic fragments by several conceivable mechanisms:

A) Reaction with the starting material, $[2]^+$



B) Reaction with the 5-coordinate intermediate



C) Free-radical coupling with a second free alkyl radical



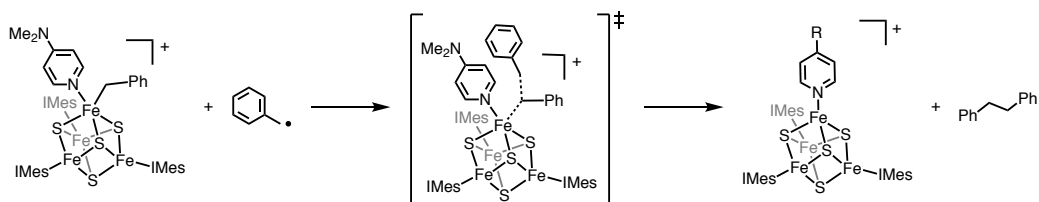
Reaction C is unlikely because free radicals are reactive and are expected to be present at a very low concentration, disfavoring direct second-order coupling. Additionally, only hexadecane was formed in the reaction of $[3]^+$ with DMAP; if reaction C was occurring we would expect to observe octane and octene (resulting from H-atom abstraction from one octyl radical by another) in addition to hexadecane.⁷ Based on these observations, reaction C can be ruled out.

Between reactions A and B, we consider reaction A unlikely because it would entail generating a three-coordinate apical Fe site. For these reasons, reaction B most likely accounts for the formation of coupled organic products. Moreover, reaction B, but not A, is consistent with the following observations:

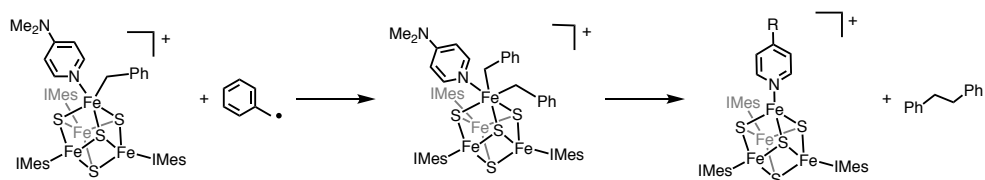
- The reaction of $[2]^+$ with DMAP occurs more cleanly for more donating pyridines. This is because there is a higher concentration of the 5-coordinate intermediate present when the pyridine is a stronger ligand, resulting in faster C–C coupling.
- With more donating pyridines (DMAP), C–C coupling occurs at a competitive rate to Sn–H abstraction. With a weakly donating pyridine ($\text{CF}_3\text{-py}$), Sn–H abstraction completely outcompetes C–C coupling. This is consistent with having a lower concentration of the 5-coordinate intermediate present with less donating pyridines, leading to slower C–C coupling. The rate of Sn–H activation is independent of the pyridine used.

For mechanism B, C–C coupling could occur by either an $\text{S}_{\text{H}}2$ mechanism or by oxidative addition and reductive elimination (see below). Experimentally differentiating between these possibilities is challenging.

1) $\text{S}_{\text{H}}2$ mechanism (concomitant Fe–C bond cleavage and C–C bond formation)



2) Oxidative addition/reductive elimination



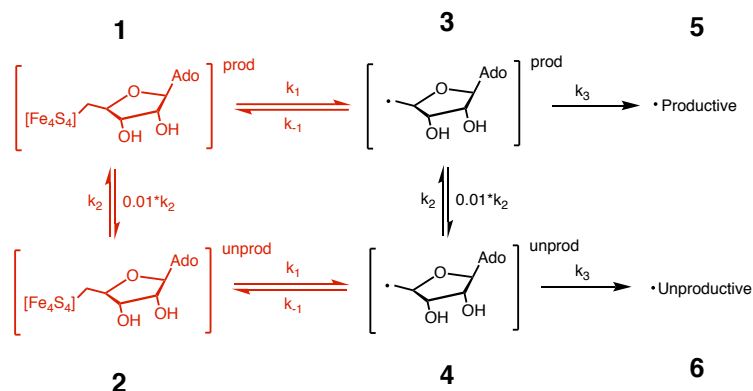
Finally, we note that additional, radical-derived products are observed in reactions involving Bu_3SnH . These include the expected H-atom abstraction product(s), and, in the case of $[\mathbf{2}]^+$, Bu_3SnBn , which may form by:

- i) Reaction of $\text{Bu}_3\text{Sn}\cdot$ or Bu_6Sn_2 with benzyl radicals
- ii) Reaction of $\text{Bu}_3\text{Sn}\cdot$ or Bu_6Sn_2 with $[\mathbf{2}]^+$ or the 5-coordinate intermediate

Reaction ii seems more likely than reaction i since benzyl radicals, $\text{Bu}_3\text{Sn}\cdot$, and Bu_6Sn_2 are all present at small concentrations in this reaction. However, further differentiation of these mechanisms is beyond the scope of this discussion.

E. Kinetic simulations

To simulate the reaction outcomes for our model system, we used MATLAB to symbolically solve the system of differential equations that describes the kinetic model in the presence and the absence of the organometallic intermediate.



In the presence of the organometallic intermediate:

$$\frac{d[1]}{dt} = -k_1[1] + k_{-1}[3] - 0.01 \cdot k_2[1] + k_2[2]$$

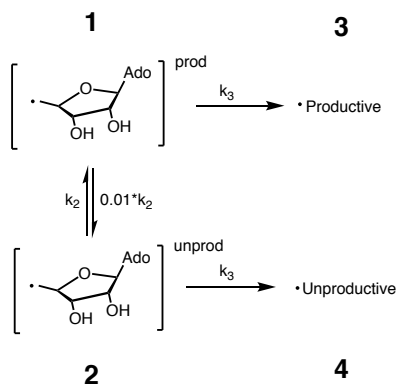
$$\frac{d[2]}{dt} = -k_1[2] + k_{-1}[4] + 0.01 \cdot k_2[1] - k_2[2]$$

$$\frac{d[3]}{dt} = k_1[1] - k_{-1}[3] - 0.01 \cdot k_2[3] + k_2[4] - k_3[3]$$

$$\frac{d[4]}{dt} = k_1[2] - k_{-1}[4] + 0.01 \cdot k_2[3] + k_2[4] - k_3[4]$$

$$\frac{d[5]}{dt} = k_3[3]$$

$$\frac{d[6]}{dt} = k_3[4]$$



$$\frac{d[1]}{dt} = -0.01 * k_2[1] + k_2[2] - k_3[1]$$

$$\frac{d[2]}{dt} = 0.01 * k_2[1] - k_2[2] - k_3[2]$$

$$\frac{d[3]}{dt} = k_3[1]$$

$$\frac{d[4]}{dt} = k_3[2]$$

Carrying out these simulations requires assumptions for the rate constants k_1 , k_{-1} , k_2 , k_{-2} , and k_3 .

The initial choices for rate constants are outlined below:

k_{-1} : The reactions of open-shell metal fragments with organic radicals have been widely studied,^{8,9} and the rate constant for recombination of the metal center with the organic radical consistently approaches the diffusion limit (10^{10} s^{-1}). This allows us to estimate that reformation of the Fe–C bond (k_{-1}) occurs at least as fast as the diffusion limit. As such, we set k_{-1} to 10^{11} s^{-1} ; the absolute rate constant is unimportant in our simulations so long as this process is the fastest in the system.

k_1 : The percentage of the 5'-dAdo• that is masked as an Fe–C bond is dictated by the equilibrium constant between Fe-bound and “free” 5'-dAdo•, which is equivalent to the bond dissociation free energy (BDFE) for the Fe–C bond. Estimating the BDFE from the half-life of the organometallic intermediate in pyruvate-formate lyase activating enzyme ($\sim 10^0 \text{ min}$ at 170 K)¹⁰ conflates the barrier to Fe–C homolysis and the barrier for X–H activation. Nevertheless, with the assumption that Fe–C bond homolysis is rate limiting (i.e., that the X–H activation barrier does not contribute to the observed half-life) and that the barrier for recombination is small, we approximate the BDFE as $\sim 11 \text{ kcal/mol}$ using the Eyring equation and $t_{1/2} = \ln(2)/k$ for a first-order reaction. A bond strength of $\sim 11 \text{ kcal/mol}$ corresponds to a difference in forward and reverse rate constants on the order of 10^8 , and we can therefore approximate $k_1 = 10^3 \text{ s}^{-1}$.

k₃: For the reasons outlined above, it is difficult to estimate the barrier for X–H activation from the available data. Consistent with the assumption that Fe–C bond homolysis is rate-limiting, we set the rate of H-atom abstraction ($k_3 = 10^5 \text{ s}^{-1}$) such that X–H activation is faster than Fe–C bond homolysis ($k_1 = 10^3 \text{ s}^{-1}$). We use the same rate of X–H activation in the “productive” and “unproductive” states; any difference in these rates will quantitatively change the selectivity of the reaction but not affect the qualitative conclusions of these simulations.

k₂ and k₋₂: The dynamical processes that affect the selectivity in radical SAM enzymes could occur on a wide range of time scales, from 10^0 to 10^{15} s^{-1} .^{11,12} It is difficult to determine *a priori* which processes are important for X–H abstraction selectivity and therefore which time scales to consider. As such, we varied the rates of state interconversion in our simulations, initially with $k_2 = 10^2 \text{ s}^{-1}$ and $k_{-2} = 1 \text{ s}^{-1}$ (both being slower than X–H activation and Fe–C bond homolysis). In all simulations, we set $k_{-2} = 0.01 \cdot k_2$ such that the “productive” state is thermodynamically favored by $\sim 2 \text{ kcal/mol}$ and we allowed the system to convert between productive and unproductive states with either the organometallic species or the 5'-dAdo• present.

In addition to the figures discussed in the text, contour plots can be generated that explore the interdependence of the rate constants, in particular how the rates of state interconversion and X–H activation simultaneously contribute to product selectivity.

We began with Fe–C homolysis rates as defined above ($k_1 = 10^3 \text{ s}^{-1}$ and $k_{-1} = 10^{11} \text{ s}^{-1}$). Each trace (Fig. S51) is drawn as a 50/50 selectivity contour with the region above and to the left of the trace corresponding to the region of selectivity for the productive reaction and the region below and to the right of the trace corresponding to the region of selectivity for the unproductive reaction. The black line shows the selectivity in the absence of the organometallic intermediate.

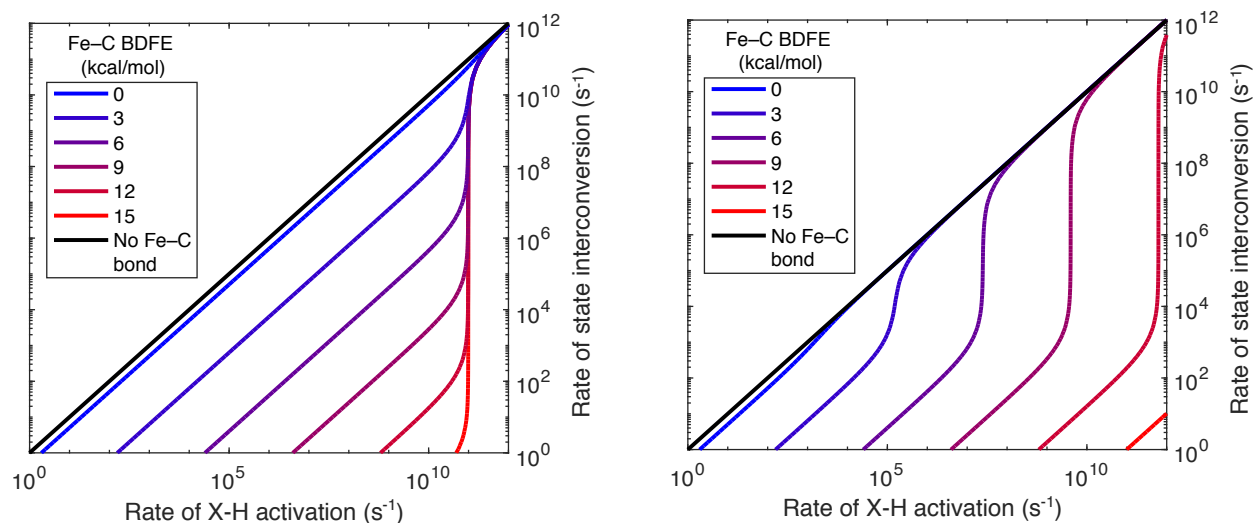


Figure S52: Contour plots for the kinetic model showing the interdependence of the modelled rate constants. On the left k_1 was varied ($k_{-1} = 10^{11} \text{ s}^{-1}$) and on the right k_{-1} was varied ($k_1 = 10^3 \text{ s}^{-1}$) to give the desired bond strength. Contours were drawn at 50% selectivity. The black lines show the 50% selectivity level in the absence of the organometallic species.

The region between each trace and the black line is the range of kinetic parameters for which the presence of the organometallic intermediate is expected to increase selectivity.

From these plots we can see that a stronger Fe–C bond leads to a larger range of kinetic parameters for which high selectivity can be achieved. In Figure S51 (left), the selectivity contours in the presence of the organometallic intermediate depart from the black line at the point where the Fe–C bond reformation is faster than X–H activation. This emphasizes that the low barrier to Fe–C bond reformation following homolysis is critical for allowing the organometallic intermediate to function as a protective mechanism during catalysis.

Matlab script for solving the system of differential equations and plotting figures 4E,4F and S51

1. Solve differential eq, with organometallic intermediate

```
clear

GC=1.987e-3; %gas constant

%Defining system of equations and solving it symbolically
syms a(t) b(t) c(t) d(t) e(t) f(t) m n o k p
cond=[a(0)==0,b(0)==0,c(0)==0,d(0)==1,e(0)==0,f(0)==0];
eqns= [diff(a,t)== -(m*a - k*c) - (p*n*a - n*b),...
       diff(b,t)== -(m*b - k*d) + (p*n*a - n*b),...
       diff(c,t)== (m*a - k*c) - o*c - (p*n*c - n*d),...
       diff(d,t)== (m*b - k*d) - o*d + (p*n*c - n*d),...
       diff(e,t)== o*c,...
       diff(f,t)== o*d];
sol=dsolve(eqns,cond);
% saves functions so they can be called later
a=matlabFunction(sol.a);
b=matlabFunction(sol.b);
c=matlabFunction(sol.c);
d=matlabFunction(sol.d);
e=matlabFunction(sol.e);
f=matlabFunction(sol.f);

% a is organometallic in productive state
% b is organometallic in unproductive state
% c is 5'-dAdo in productive state
% d is 5'-dAdo in unproductive state
% e is productive product
% f is unproductive product

% m is homolysis rate (k1)
% n is unproductive to productive conversion rate (k2)
% o is abstraction rate (k3)
% k is Fe-C bond formation rate (k-1)
% p is productive to unproductive conversion rate divided by k2 (k-2/k2)
```

2. Plot 1D traces for varying the interconversion rate (4E)

```
%sets figure up
FigHandle = figure;
set(FigHandle,'Position',[1000, 1000, 240, 200]);
box on

%sets range and points for x-values
range=30;
increment=0.1;
offset=-10;
loopsize=range/increment;
points=zeros(loopsize,5);

%loops over different values of Fe-C bond strength
for r=0:4:12
    BDFE=r; %each value of Fe-C BDFE
```

```

s=r/4+1; %indexing values
BDFEf(s,1)=BDFE; %saving BDFEs

Keq=exp(-BDFE/(GC*298)); %converting from BDFE to equilibrium
    constant (k1/k-1=keq)

k=1*10.^11; %value for k-1
m=k*Keq; %getting homolysis rate from equilibrium constant (keq*k-
    1=k1)
mx(s,1)=m; %saving values of homolysis rate

o=1*10^5; %value for k3
p=0.01; % energy difference between productive and unproductive
    state
t=1e100000000; %evaluates solution at steady state

%evaluates equation for each value of interconversion rate
for i=1:loopsize
    j=(i*increment)+offset; %generates values for state
        interconversion rate
    n=1*10^j; %varying the rate of state interconversion
    points(i,1)=n; %saving rates of interconversion
    subrad=e(k,m,n,o,p,t); %solving diff eq for each set of
        parameters, for productive product
    v=s+1; %creating an index for each point
    points(i,v)=subrad*100; %converting to percent and saving
end

semilogx(points(:,1),points(:,v),'-',
    'MarkerSize',0.25,'linewidth',0.5,'color',[r+2]/15 0 0);
hold on
end

%sets plot parameters
axis([10^-10 10^15 0 100]);
h=gca;
h.FontSize=6;
xlabel('rate of state interconversion (s-1)')
ylabel('Percentage productive radical')

```

3. Plot 1D traces for varying the abstraction rate (4F)

```

%sets figure up
FigHandle = figure;
set(FigHandle,'Position', [1000, 1000, 240,200]);
box on

%sets range and points for x-values
range=30;
increment=0.1;
offset=-10;
loopsize=range/increment;
points=zeros(loopsize,2);

%loops over different values of Fe-C bond strength

```

```

for r=0:4:12
    BDFE=r; %each value of Fe-C BDFE
    s=r/4+1; %indexing to save values
    BDFEf(s,1)=BDFE; %saving BDFEs

    Keq=exp(-BDFE/(GC*298)); %converting back from BDFE to equilibrium
        constant (k1/k-1=keq)

    k=1*10.^11; %value for k-1
    m=k*Keq; %getting homolysis rate from equilibrium constant
        (keq*k-1=k1)
    mx(s,1)=m; %saving values of homolysis rate

    n=1*10^2; %setting rate of state interconversion
    p=0.01; % energy difference between productive and unproductive
        state
    t=1e100000000; %timeline for simulation

    %evaluates equation for each value of interconversion rate
    for i=1:loopsize %indexing
        j=(i*increment)+offset; %generates values for C-H activation
            rate
        o=1*10^j; %varying rate of C-H activation
        points(i,1)=o; %saving values for rate of C-H activation
        subrad=e(k,m,n,o,p,t); %solving diff eq for each set of
            parameters, for productive product
        v=s+1; %creating an index for each point
        points(i,v)=subrad*100; %converting to percent and saving
    end
    semilogx(points(:,1),points(:,v),'-',
        'MarkerSize',0.25,'linewidth',0.5,'color',[(r+2)/15 0 0]);
    hold on
end

%plot parameters
box on
h=gca;
h.FontSize=6;
axis([10^-10 10^15 0 100]);
xlabel('rate of C-H activation (s-1)')
ylabel('Percentage productive radical')

```

4. Plot first contour plot (S51 left)

```

%sets figure parameters
FigHandle = figure;
set(FigHandle,'Position', [1000, 1000, 360, 300]);
box off

%Sets range of parameters to look over
for r=0:3:15
    % generating values for parameters
    r=15-r;
    s=(r/3)+1;
    v=0:0.1:12;

```

```

%Generates a matrix of points with spacing and range defined by v
[X,Y]=meshgrid(v);

%stores BDFE and converts to Keq
BDFE=r;
BDFEf(s,1)=BDFE;
Keq=exp(-BDFE/(GC*298));

%model parameters, generates m from Keq
k=1*10.^11;
m=k*Keq;
n=1*10.^Y;
o=1*10.^X;
t=1e100000;
p=0.01;

%evaluates differential equation
subrad=e(k,m,n,o,p,t);
hold on
%plots only the 50% selectivity contour
contour(o,n,subrad,[0.5 0.5], 'color',[r/15 0 1-
r/15], 'linewidth',1.5);
end

%defines plot parameters
ax=gca;
set(ax, 'xscale', 'log', 'yscale', 'log', 'YAxisLocation', 'right');
box on
ax.FontSize=12;

%plots the line corresponding to no organometallic intermediate
nofecx=0:0.1:13;
nofecx=1.*10.^nofecx;
nofecy=nofecx;
axis([10^0 10^12 10^0 10^12]);
plot(nofecx,nofecy, 'color',[0 0 0], 'linewidth',1.5);

xlabel('Rate of X-H activation (s-1)')
ylabel('Rate of state interconversion (s-1)')
legend('0', '3', '6', '9', '12', '15', 'No Fe-C
bond', 'location', 'northwest');

```

5. Plot second contour plot (S51 right)

```

FigHandle = figure;
set(FigHandle, 'Position', [1000, 1000, 360, 300]);
box off

%Sets range of parameters to look over
for r=0:3:15

% generating values for parameters
s=r/3+1;
v=0:0.1:12;

```

```

%Generates a matrix of points with spacing and range defined by v
[X,Y]=meshgrid(v);

%stores BDFE and converts to Keq
BDFE=r;
BDFEr(s,1)=BDFE;
Keq=exp(-BDFE/(GC*298));

%model parameters, generates k from Keq
m=1*10.^3;
k=m/Keq;
kr(s,1)=k;
n=1*10.^Y;
o=1*10.^X;
t=1e1000;
p=0.01;

%evaluates differential equation
subrad=e(k,m,n,o,p,t);
hold on

%plots only the 50% selectivity contour
contour(o,n,subrad,[0.5,0.5], 'color',[r/15 0 1-
r/15], 'linewidth',1.5);
end

%plots the line corresponding to no organometallic intermediate
nofecx=0:0.1:12;
nofecx=1.*10.^nofecx;
nofecy=nofecx;
plot(nofecx,nofecy, 'color',[0 0 0], 'linewidth',1.5);

%defines plot parameters
box on
axis([10^0 10^12 10^0 10^12]);
h=gca;
h.FontSize=12;
set(h, 'xscale', 'log', 'yscale', 'log', 'YAxisLocation', 'right');
xlabel('Rate of X-H activation (s-1)')
ylabel('Rate of state interconversion (s-1)')
legend('0', '3', '6', '9', '12', '15', 'No Fe-C
bond', 'location', 'northwest');

```

6. Solve differential eq, without organometallic intermediate

```

clear

%Defining system of equations and solving it symbolically
syms c(t) d(t) e(t) f(t) n o p
cond=[c(0)==0,d(0)==1,e(0)==0,f(0)==0];
eqns= [diff(c,t)== - o*c - (p*n*c -n*d),...
diff(d,t)== - o*d + (p*n*c - n*d),...
diff(e,t)== o*c,...
diff(f,t)== o*d];
% saves functions so they can be called later
sol=dsolve(eqns,cond);
c=matlabFunction(sol.c);

```

```

d=matlabFunction(sol.d);
e=matlabFunction(sol.e);
f=matlabFunction(sol.f);

% c is 5'-dado in productive state
% d is 5'-dado in unproductive state
% e is productive product
% f is unproductive product

% n is unproductive to productive conversion rate (k2)
% o is abstraction rate (k3)
% p is productive to unproductive conversion rate divided by k2
(k-2/k2)

```

7. Plot 1D traces for varying the interconversion rate

```

%sets range and points for x-values
range=20;
increment=0.1;
offset=-9;
loopsize=range/increment;
points=zeros(loopsize,3);

%evaluates equation for each value of interconversion rate
for i=1:loopsize
    j=(i*increment)+offset; %index values of n

    n=1*10^j; %varying the rate of state interconversion
    o=1*10^5; %set the abstraction rate
    p=0.01; %energy difference between productive and unproductive state
    points(i,1)=n; %saves the values of n

    t=1e1000; %evaluates solution at steady state

    subrad=e(n,o,p,t);%solves for productive product
    points(i,2)=subrad*100; %saves percent productive radical
end

semilogx(points(:,1),points(:,2),'-','color','black','linewidth',0.5);
%plots on same plot as other script
axis([10^-10 10^15 0 100])
hold on

```

8. Plot 1D traces for varying the X-H abstraction rate

```

%sets range and points for x-values
range=20;
increment=0.1;
offset=-9;
loopsize=range/increment;
points=zeros(loopsize,3);

%evaluates equation for each value of abstraction rate
for i=1:loopsize %index
    j=(i*increment)+offset; %indexes values for o

```

```
n=1*10^2; %sets state interconversion rate
o=1*10^j; %varies abstraction rate
points(i,1)=o; %saves values of abstraction rate

t=1e1000; %evaluates solution at steady state

subrad=e(n,o,t); %evaluates diff eq for each value
points(i,2)=subrad*100; %saves percent productive radical
end
semilogx(points(:,1),points(:,2),'-', 'color', 'black', 'linewidth', 0.5);
    %plots on same plot as other script
axis([10^-10 10^15 0 100])
hold on
```

F. EPR Spectra

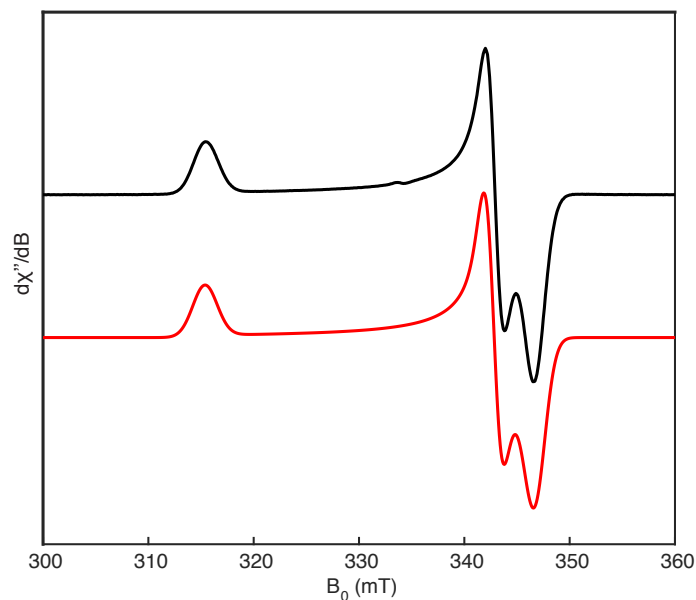


Figure S53: X-Band CW EPR spectrum of **2** (1 mM) in toluene at 15 K (black) and simulation (red). Microwave power: 16 μ W, microwave frequency: 9.370 GHz. Simulation parameters: $g = [2.123 \ 1.953 \ 1.931]$, g -strain = $[0.017 \ 0.008 \ 0.012]$.

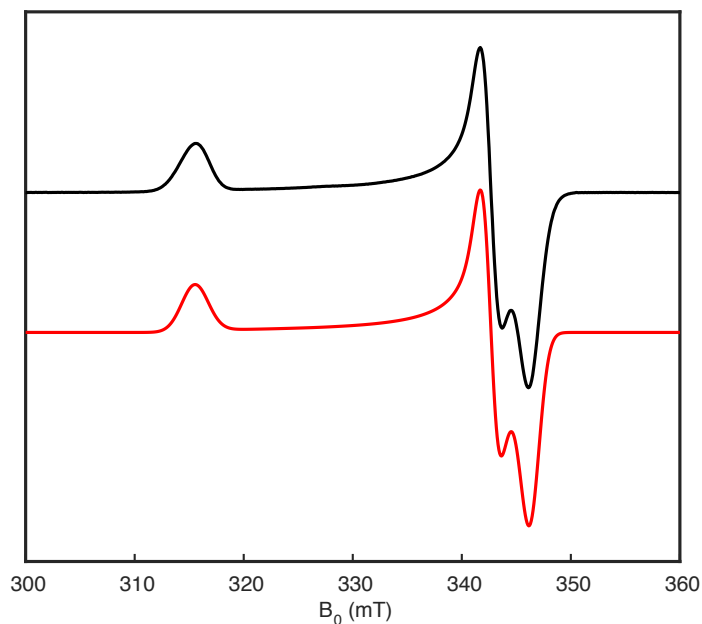


Figure S54: X-Band CW EPR spectrum of **3** (1 mM) in toluene at 15 K (black) and simulation (red). Microwave power: 16 μ W, microwave frequency: 9.370 GHz. Simulation parameters: $g = [2.122 \ 1.954 \ 1.934]$, g -strain = $[0.018 \ 0.008 \ 0.010]$.

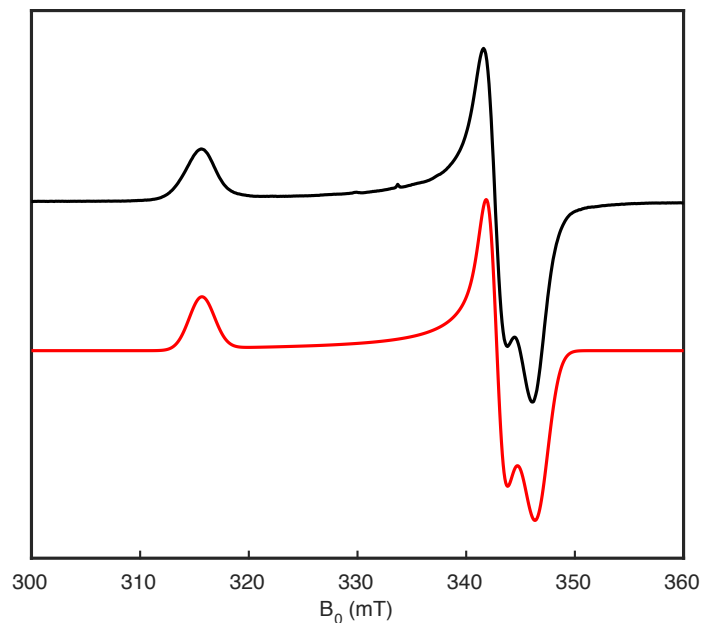


Figure S55: X-Band CW EPR spectrum of **5** (1 mM) in toluene at 15 K (black) and simulation (red). Microwave power: 16 μ W, microwave frequency: 9.369 GHz. Simulation parameters: $g = [2.121 \ 1.953 \ 1.932]$, $g\text{-strain} = [0.017 \ 0.008 \ 0.013]$.

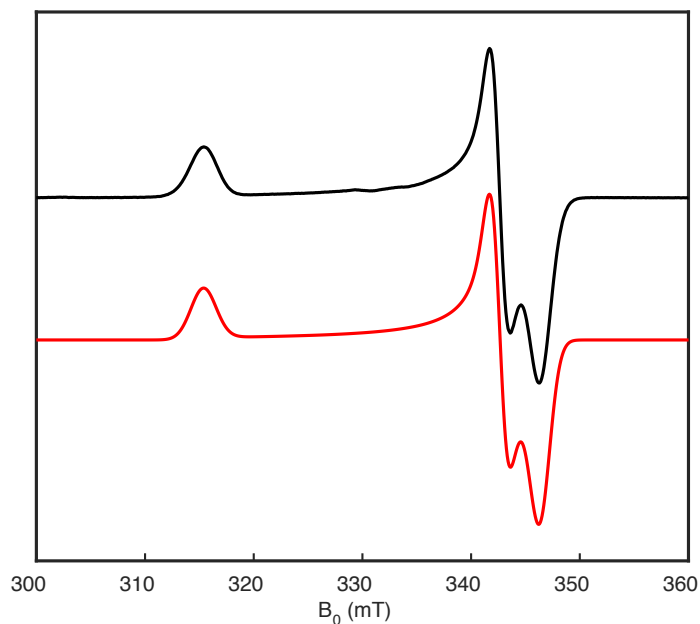


Figure S56: X-Band CW EPR spectrum of **7** (1 mM) in toluene at 15 K (black) and simulation (red). Microwave power: 16 μ W, microwave frequency: 9.371 GHz. Simulation parameters: $g = [2.123 \ 1.954 \ 1.933]$, $g\text{-strain} = [0.017 \ 0.008 \ 0.011]$.

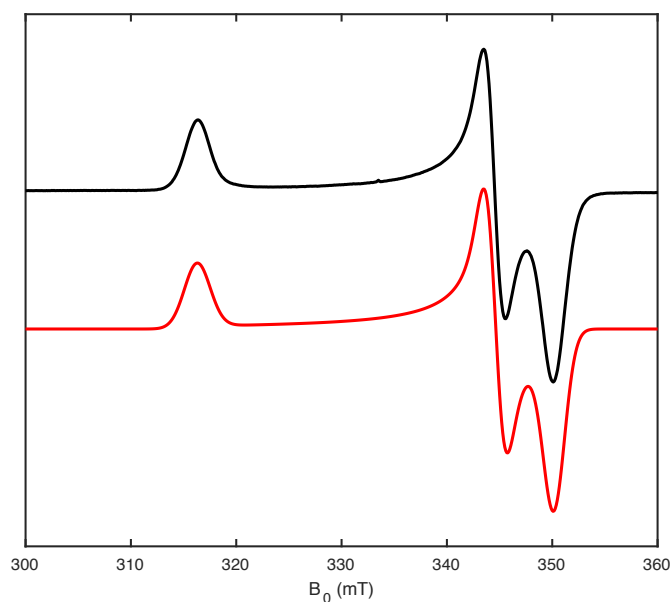


Figure S57: X-Band CW EPR spectrum of **[4]⁺** (1 mM) in 10:1 toluene:THF at 15 K (black) and simulation (red). Microwave power: 63 μ W, microwave frequency: 9.369 GHz. Simulation parameters: $g = [2.117 \ 1.943 \ 1.912]$, $g\text{-strain} = [0.018 \ 0.010 \ 0.012]$.

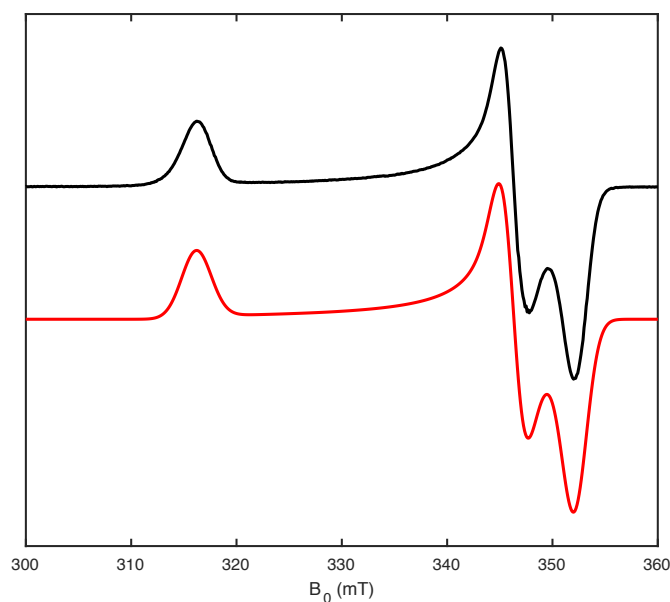


Figure S58: X-Band CW EPR spectrum of **[6]⁺** (1 mM) in 10:1 toluene:THF at 15 K (black) and simulation (red). Microwave power: 16 μ W, microwave frequency: 9.368 GHz. Simulation parameters: $g = [2.117 \ 1.933 \ 1.901]$, $g\text{-strain} = [0.021 \ 0.013 \ 0.014]$.

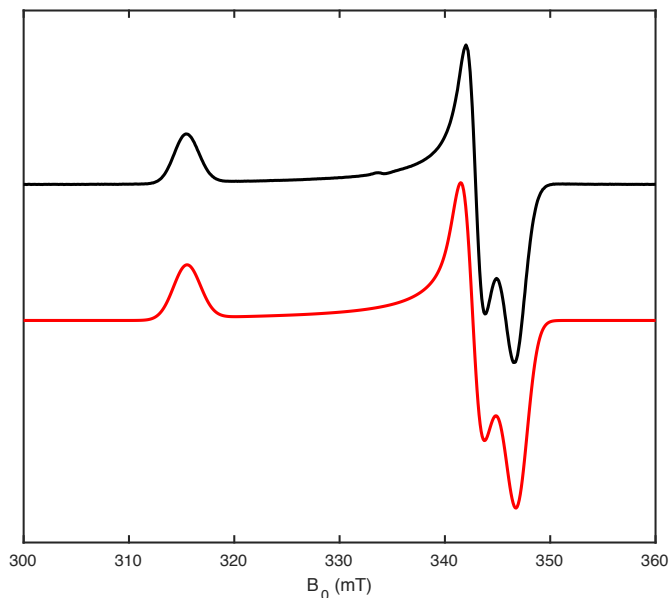


Figure S59: X-Band CW EPR spectrum of **[8]⁺** (1 mM) in 10:1 toluene:THF at 15 K (black) and simulation (red). Microwave power: 16 μ W, microwave frequency: 9.370 GHz. Simulation parameters: $g = [2.122 \ 1.954 \ 1.930]$, $g\text{-strain} = [0.019 \ 0.01 \ 0.012]$.

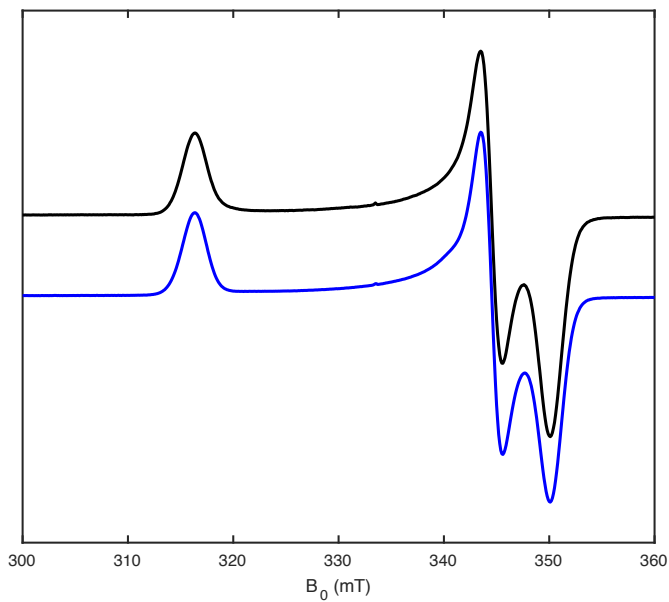


Figure S60: Overlaid X-Band CW EPR spectrum of **[4]⁺** (1 mM) (black) and the product of the reaction between **[2]⁺** and DMAP (blue) in 10:1 toluene:THF at 15 K (black). Microwave power: 16 μ W, microwave frequency: 9.369 GHz.

G. IR Spectra

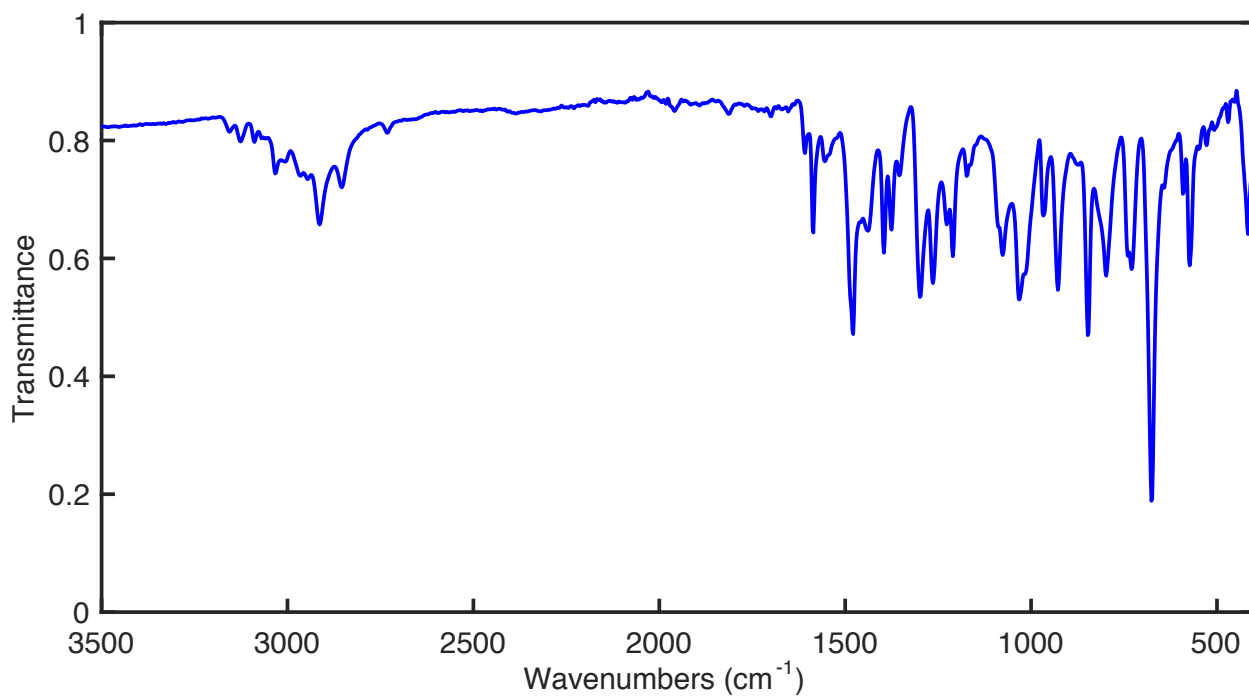


Figure S61: IR spectrum of **2**.

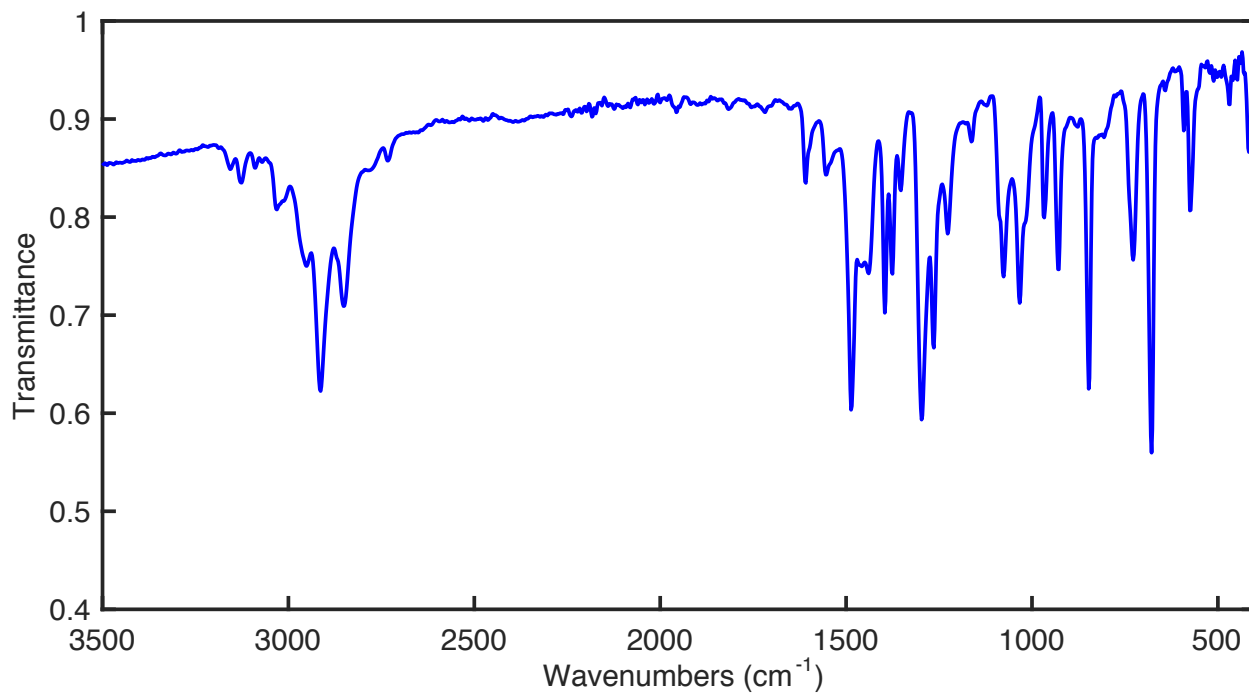


Figure S62: IR spectrum of **3**.

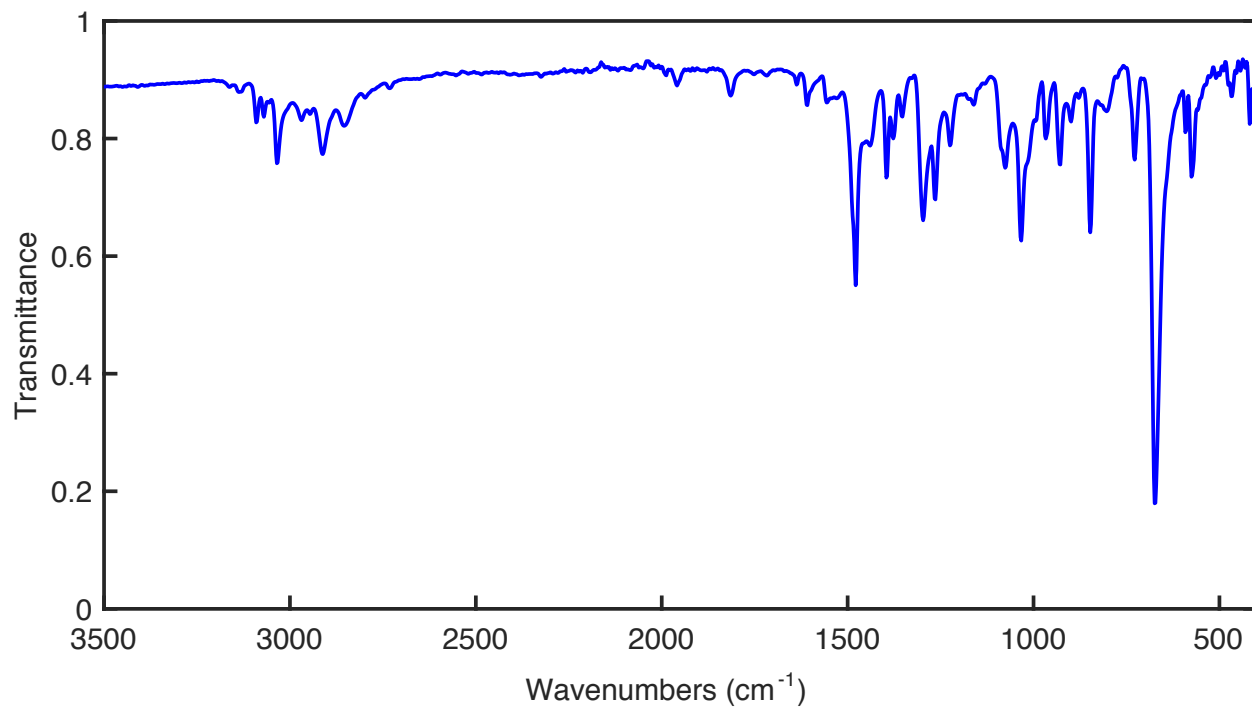


Figure S63: IR spectrum of **5**.

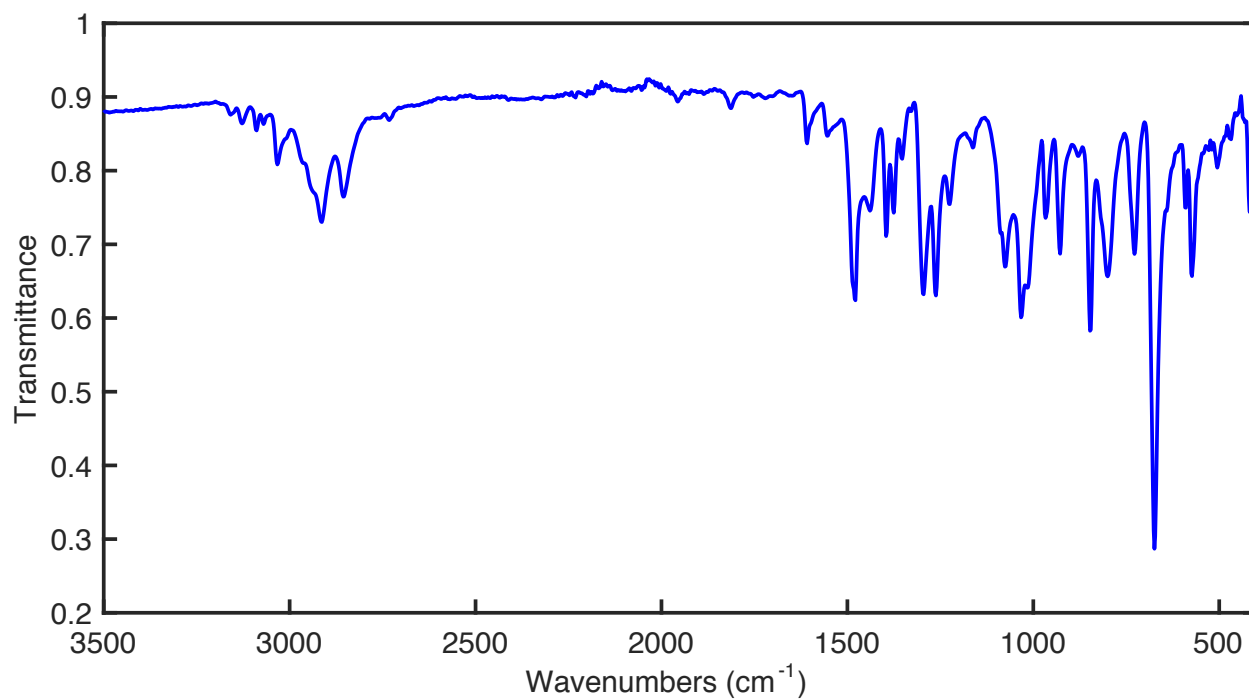


Figure S64: IR spectrum of **6**.

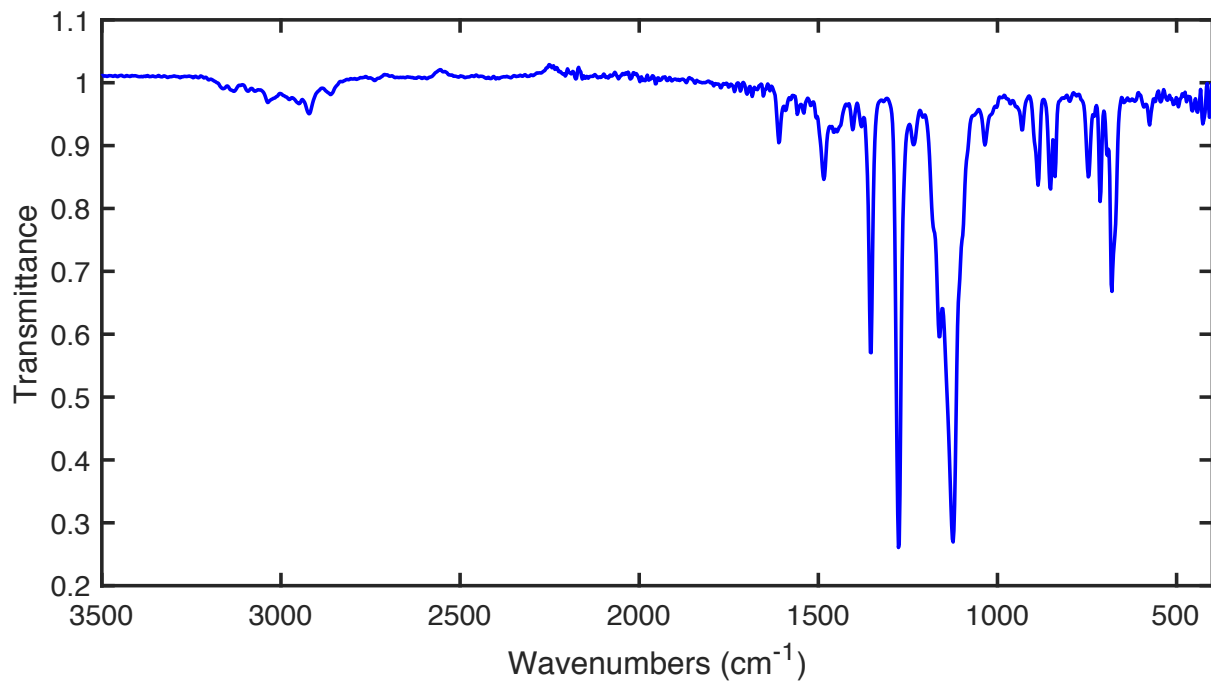


Figure S65: IR spectrum of [2]⁺.

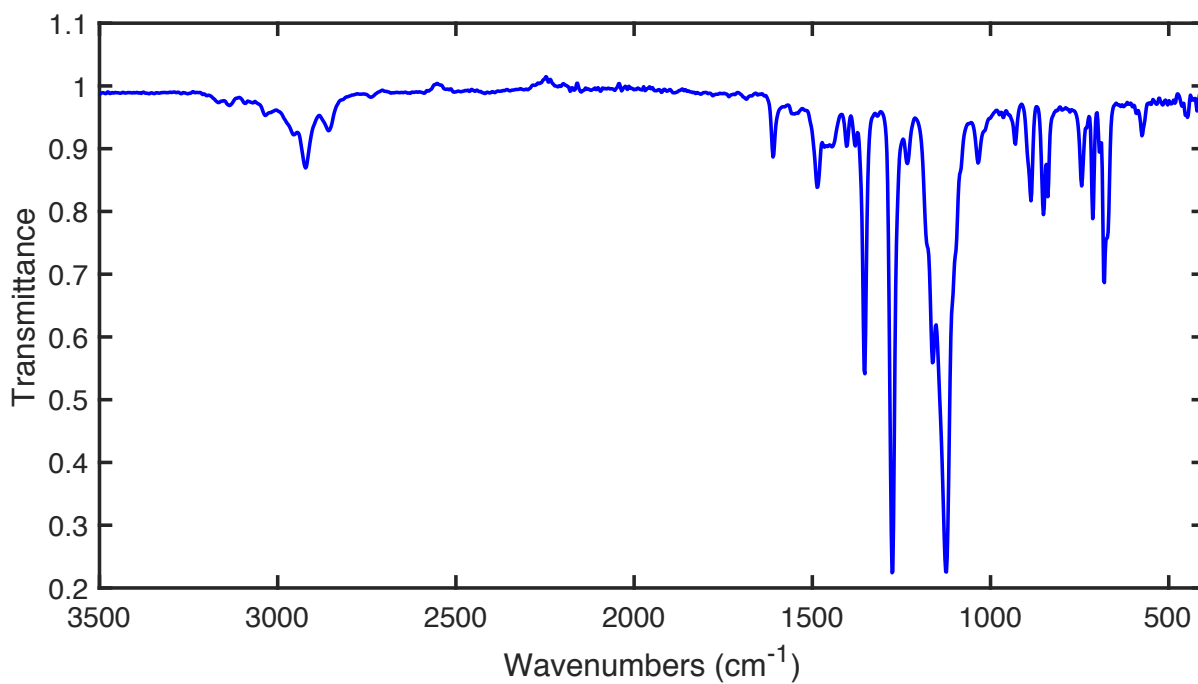


Figure S66: IR spectrum of [3]⁺.

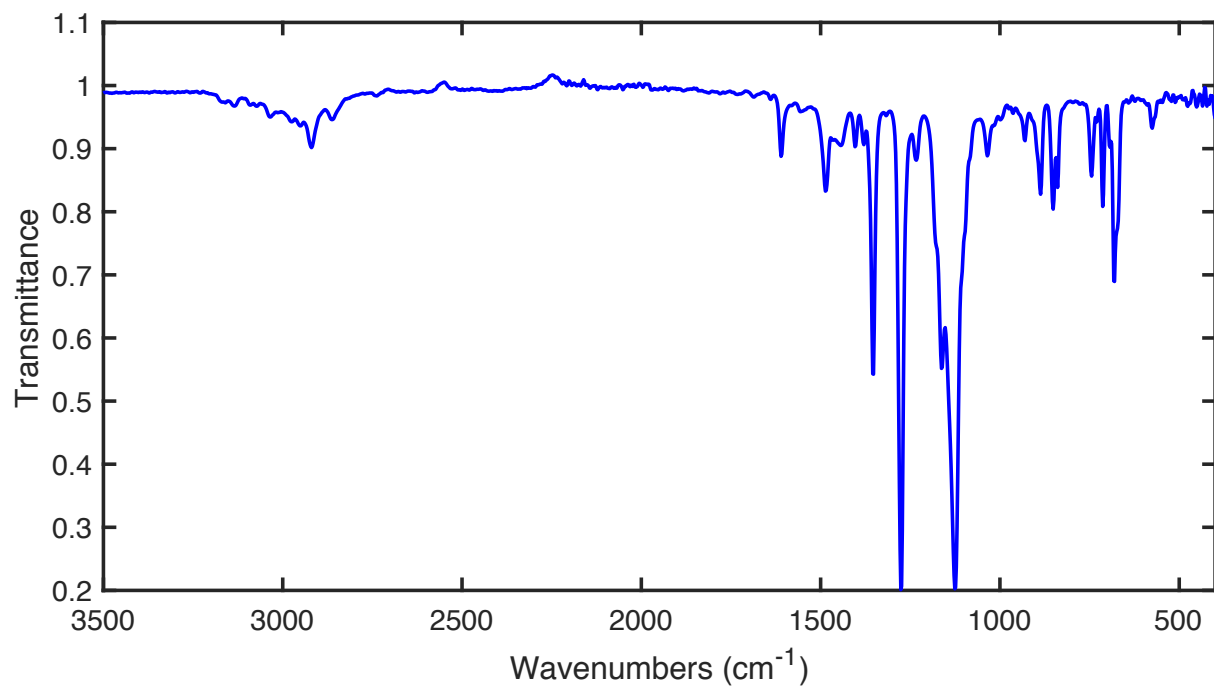


Figure S67: IR spectrum of [5]⁺.

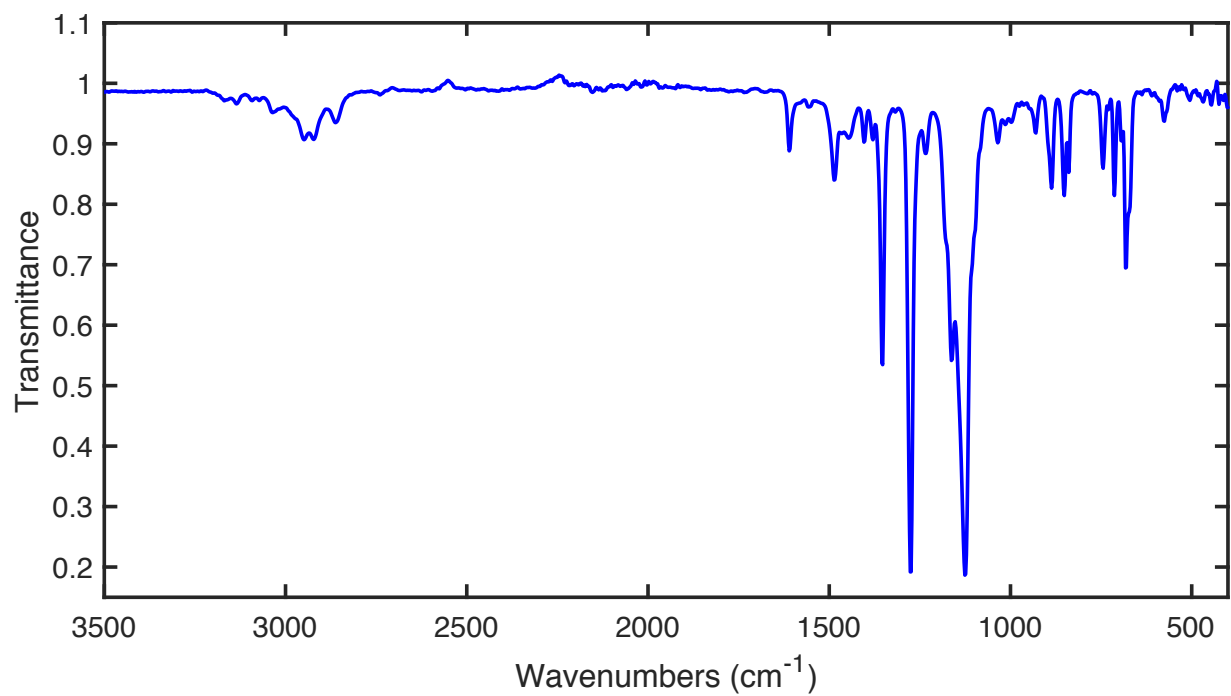


Figure S68: IR spectrum of [7]⁺.

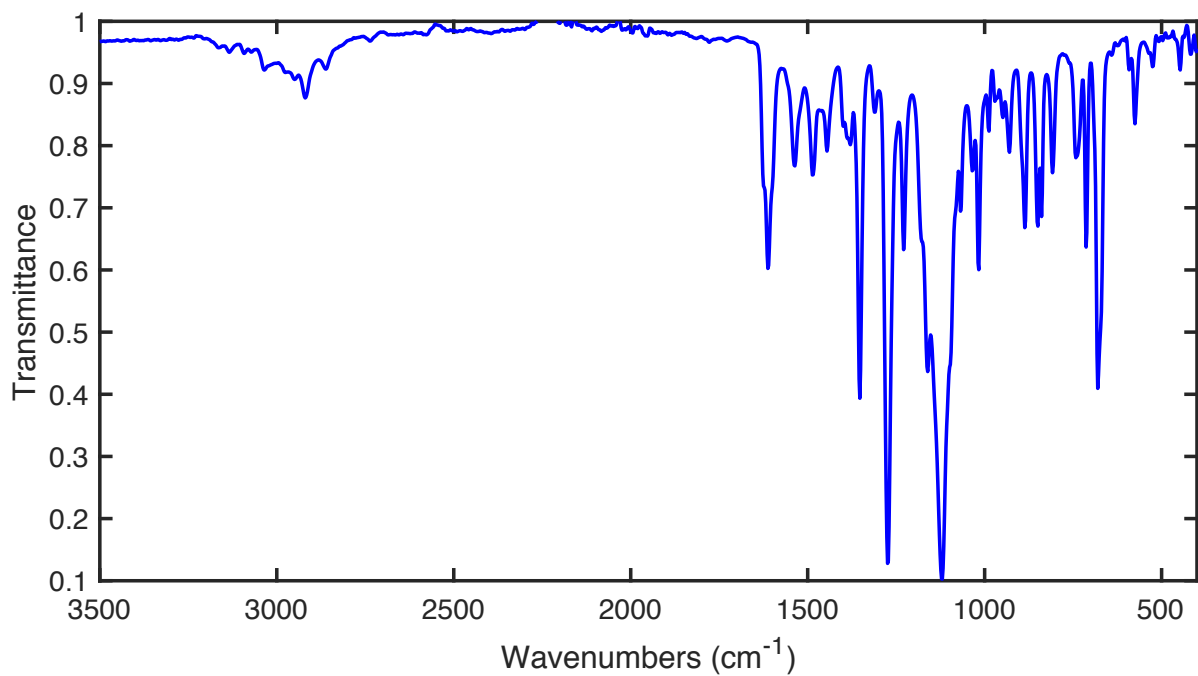


Figure S69: IR spectrum of [4]⁺.

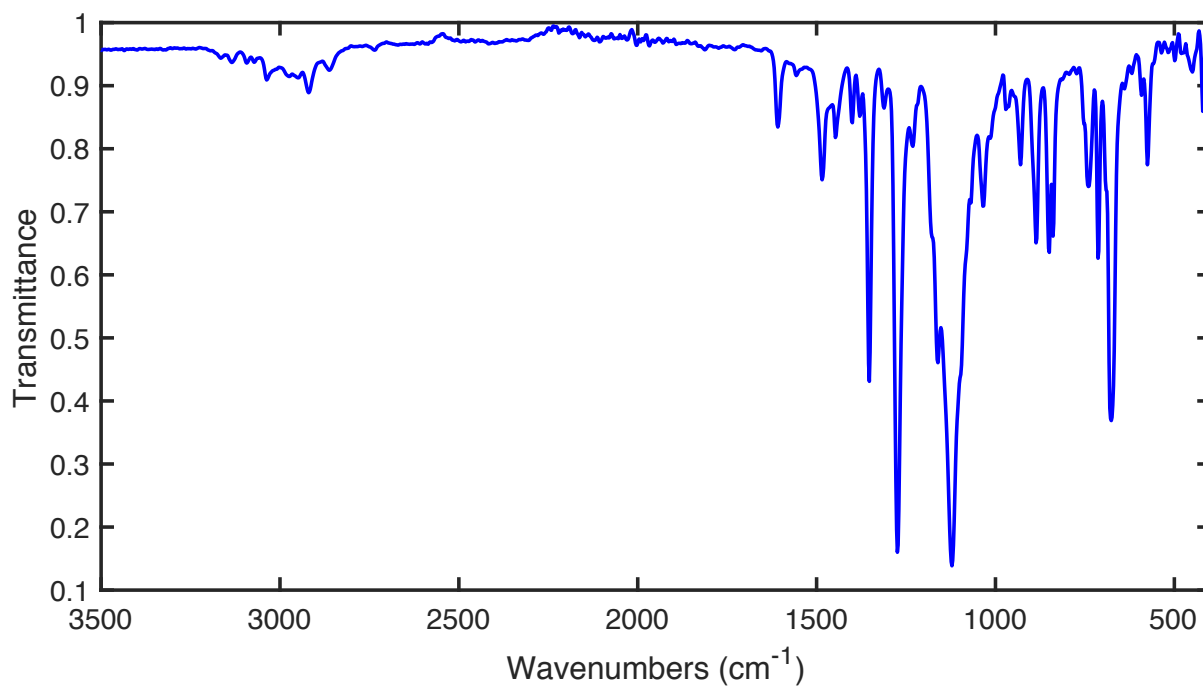


Figure S70: IR spectrum of [8]⁺.

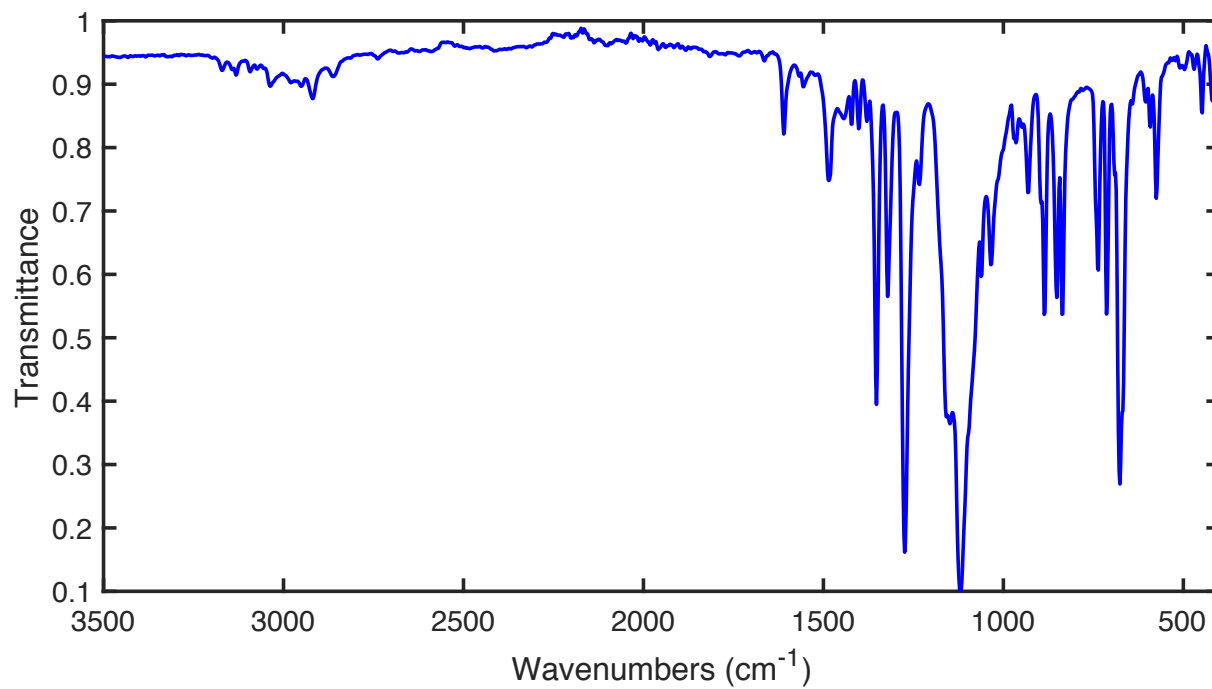


Figure S71: IR spectrum of $[6]^+$.

H. UV-Vis spectra

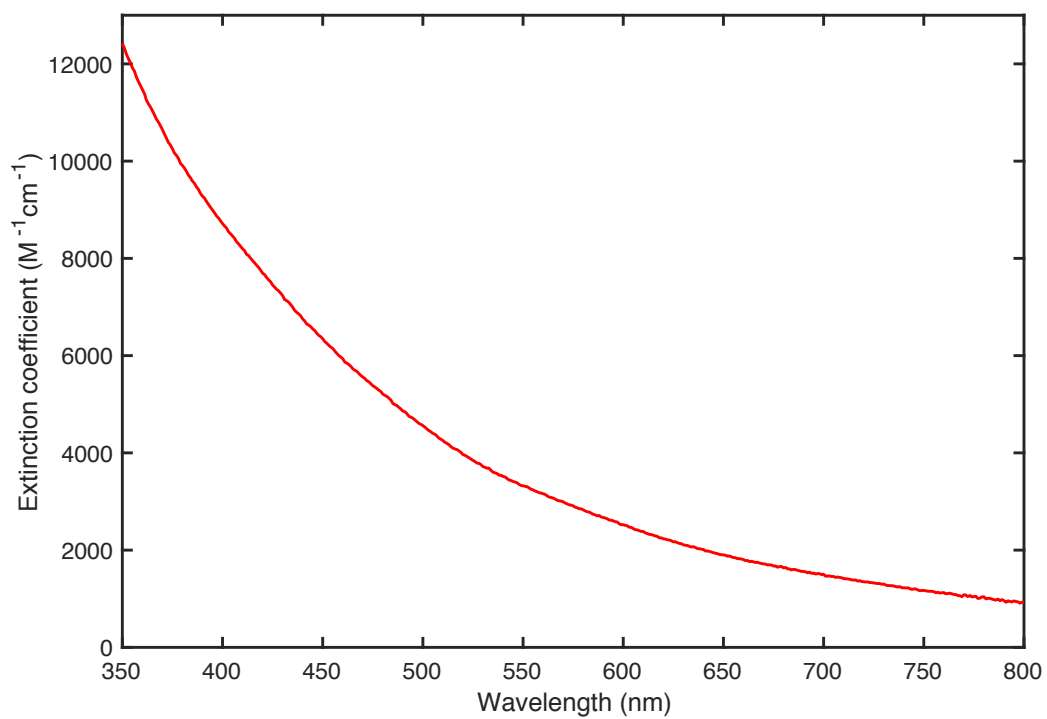


Figure S72: UV-Vis spectrum of **2** in THF.

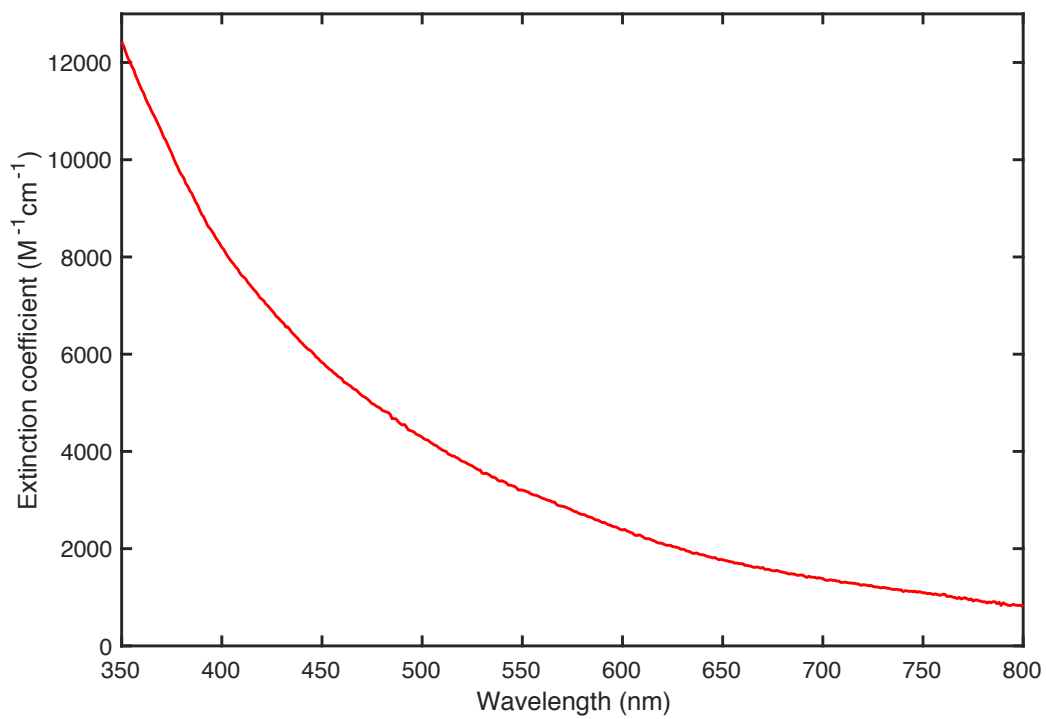


Figure S73: UV-Vis spectrum of **3** in THF.

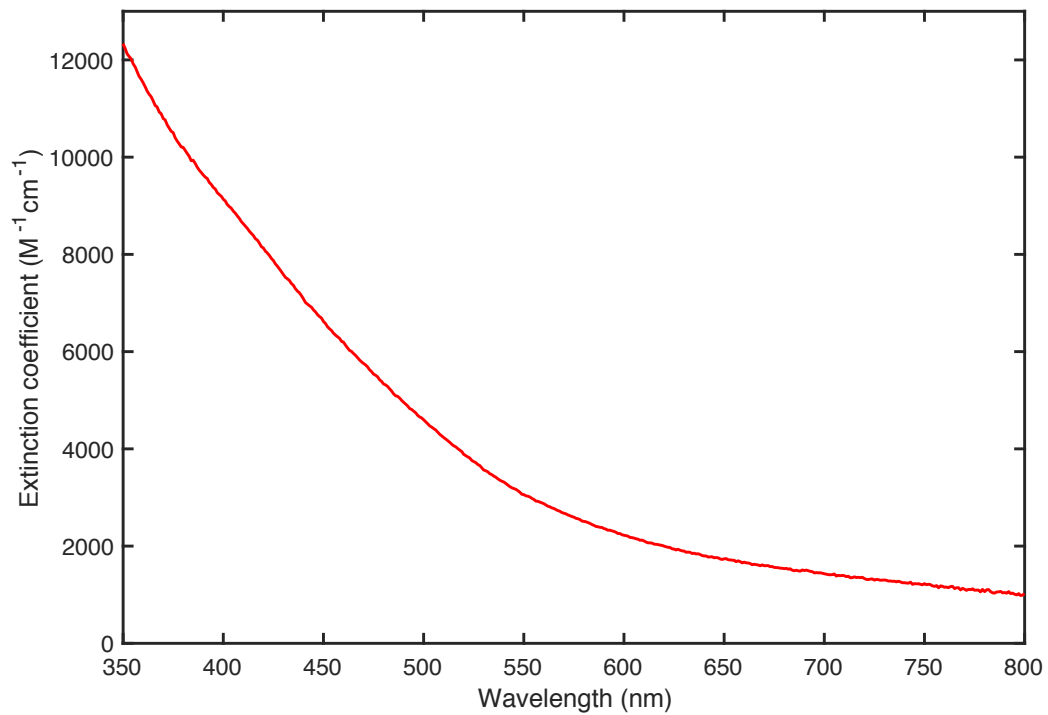


Figure S74: UV-Vis spectrum of **5** in THF.

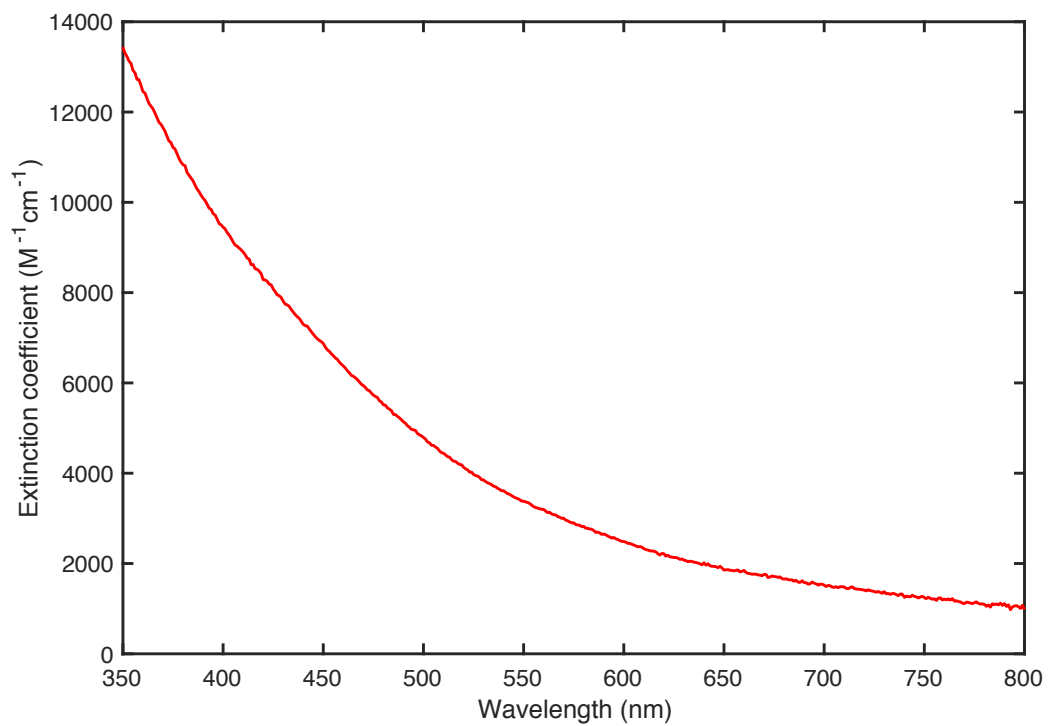


Figure S75: UV-Vis spectrum of **7** in THF.

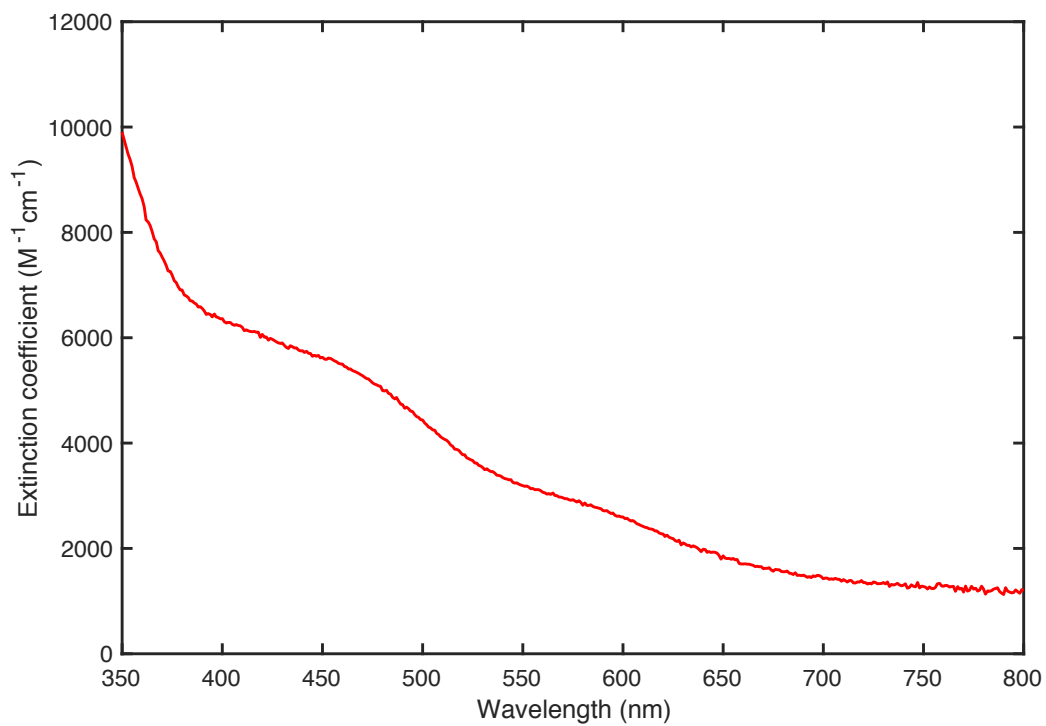


Figure S76: UV-Vis spectrum of [2]⁺ in toluene.

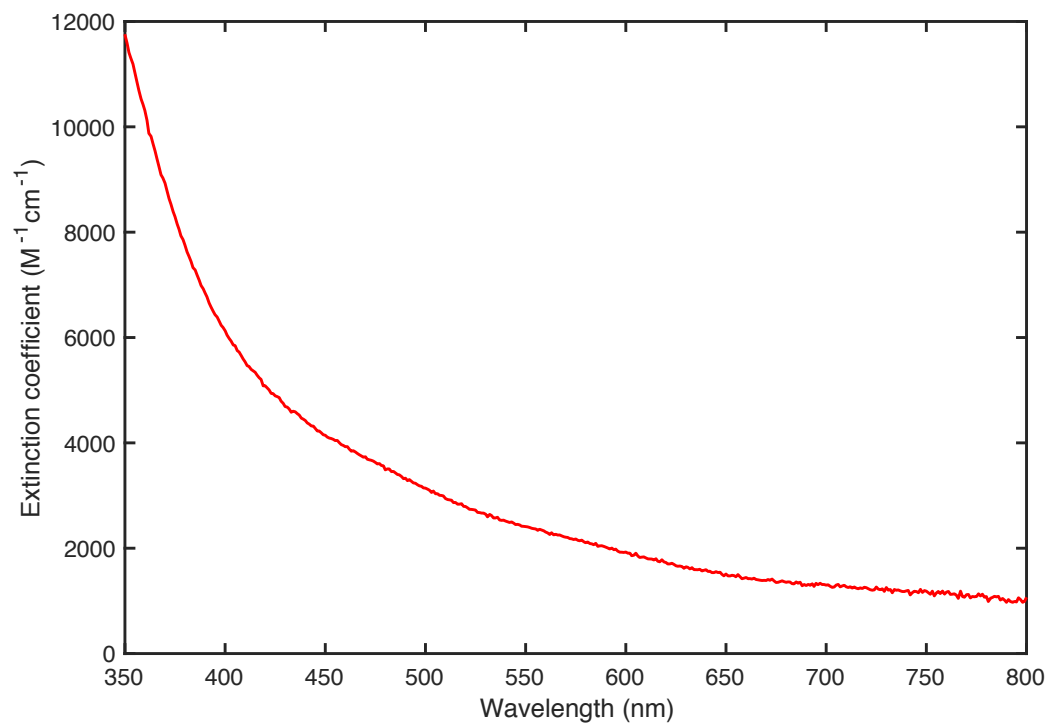


Figure S77: UV-Vis spectrum of [3]⁺ in toluene.

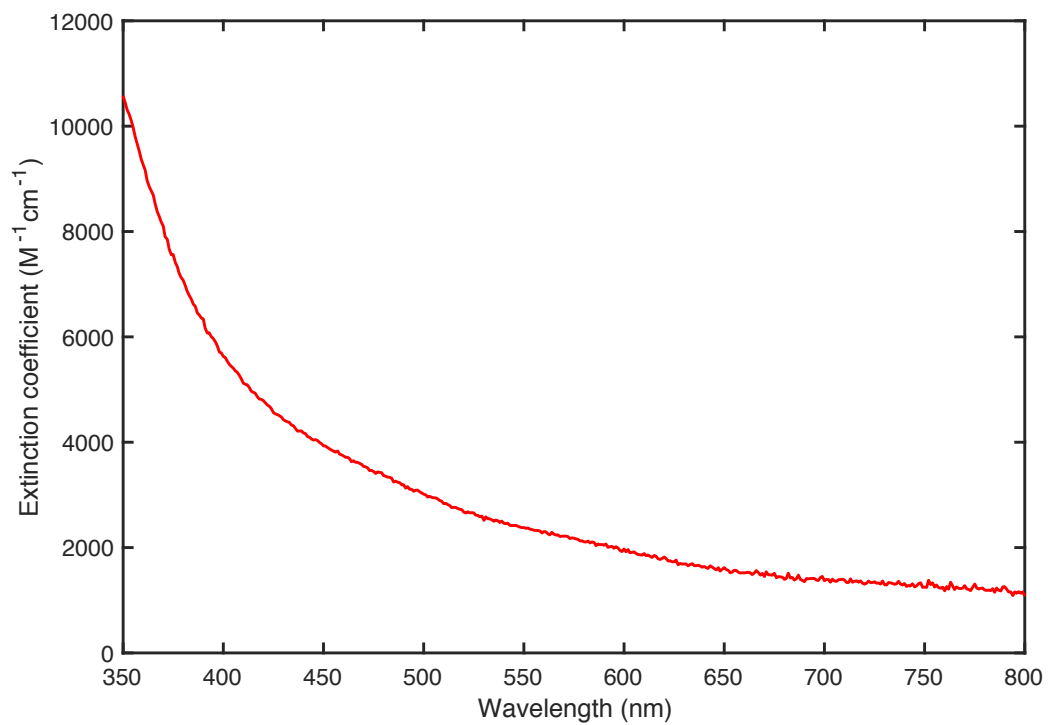


Figure S78: UV-Vis spectrum of [5]⁺ in toluene.

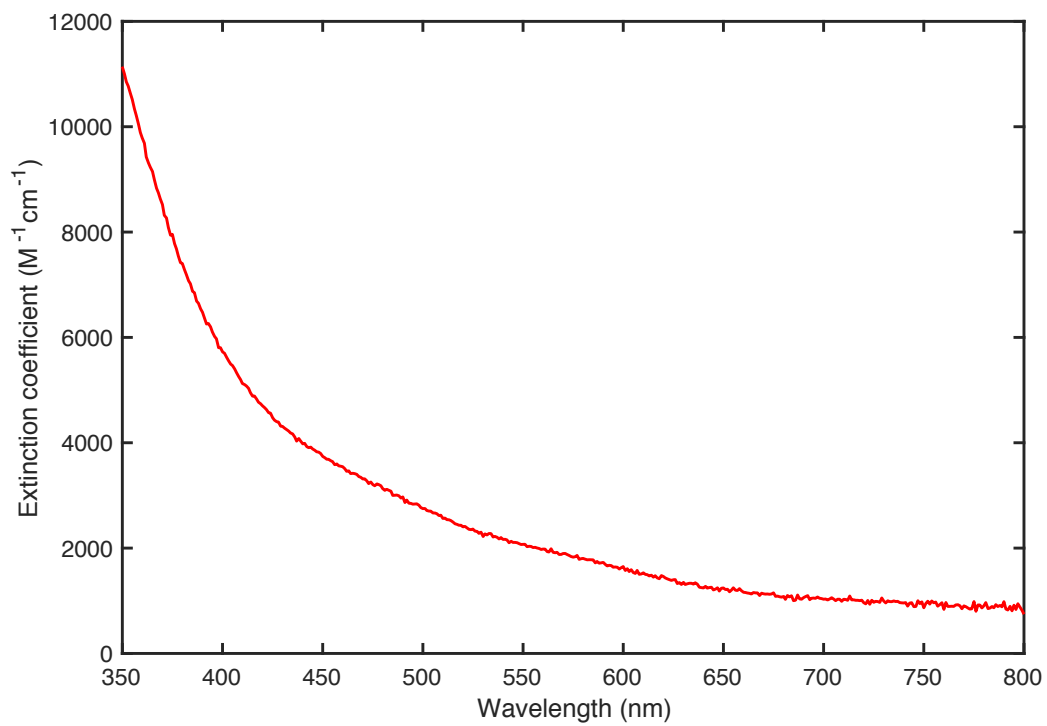


Figure S79: UV-Vis spectrum of [7]⁺ in toluene.

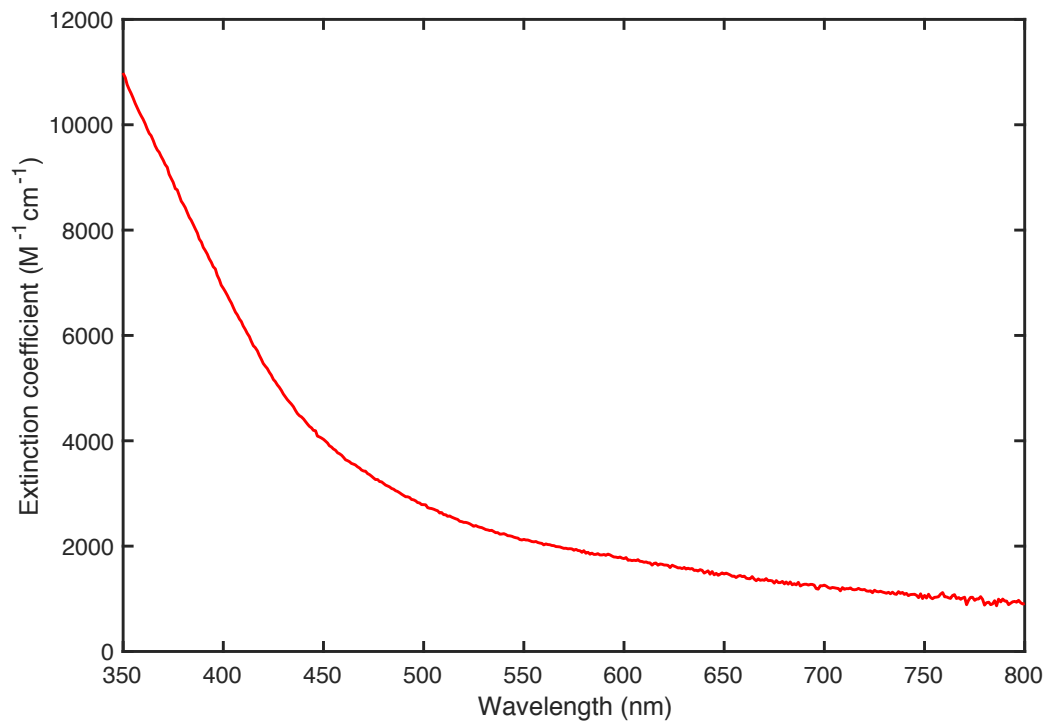


Figure S80: UV-Vis spectrum of [4]⁺ in toluene.

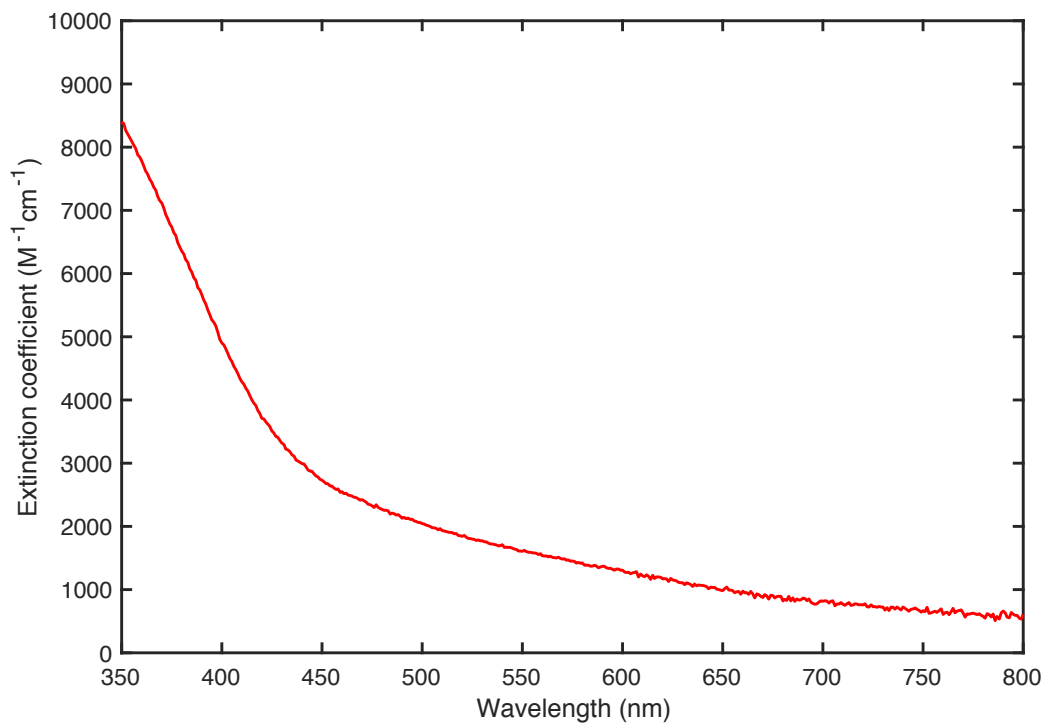


Figure S81: UV-Vis spectrum of [8]⁺ in toluene.

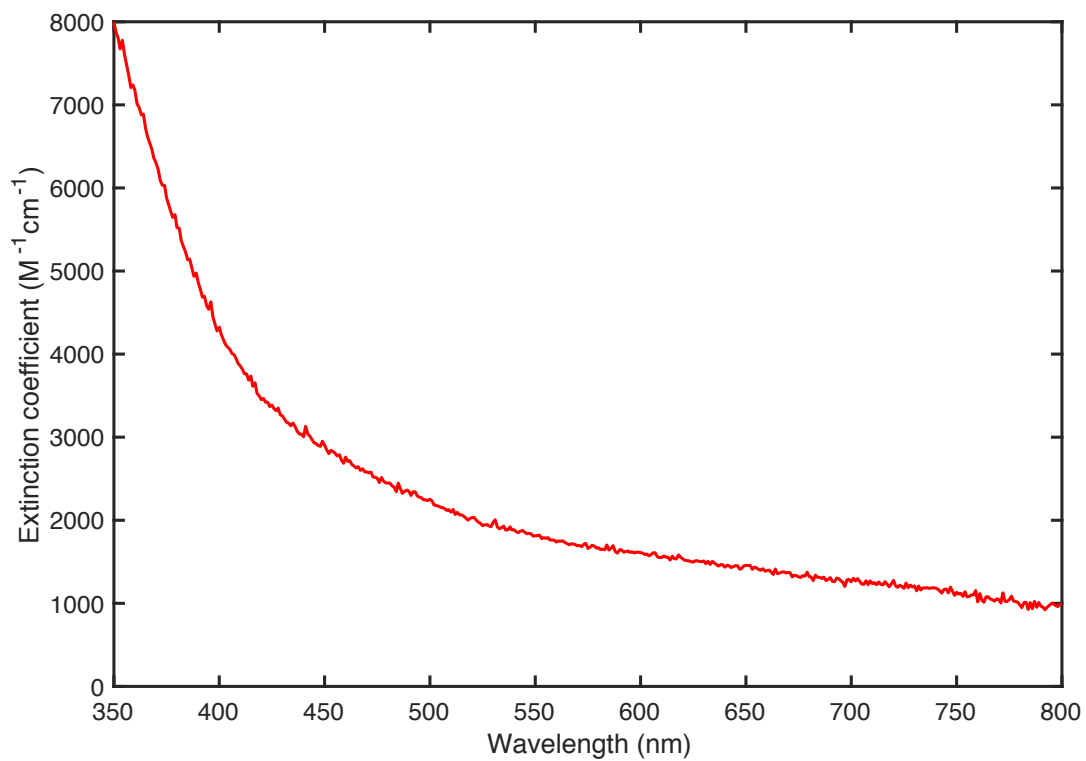


Figure S82: UV-Vis spectrum of [6]⁺ in toluene.

I. Cyclic voltammetry:

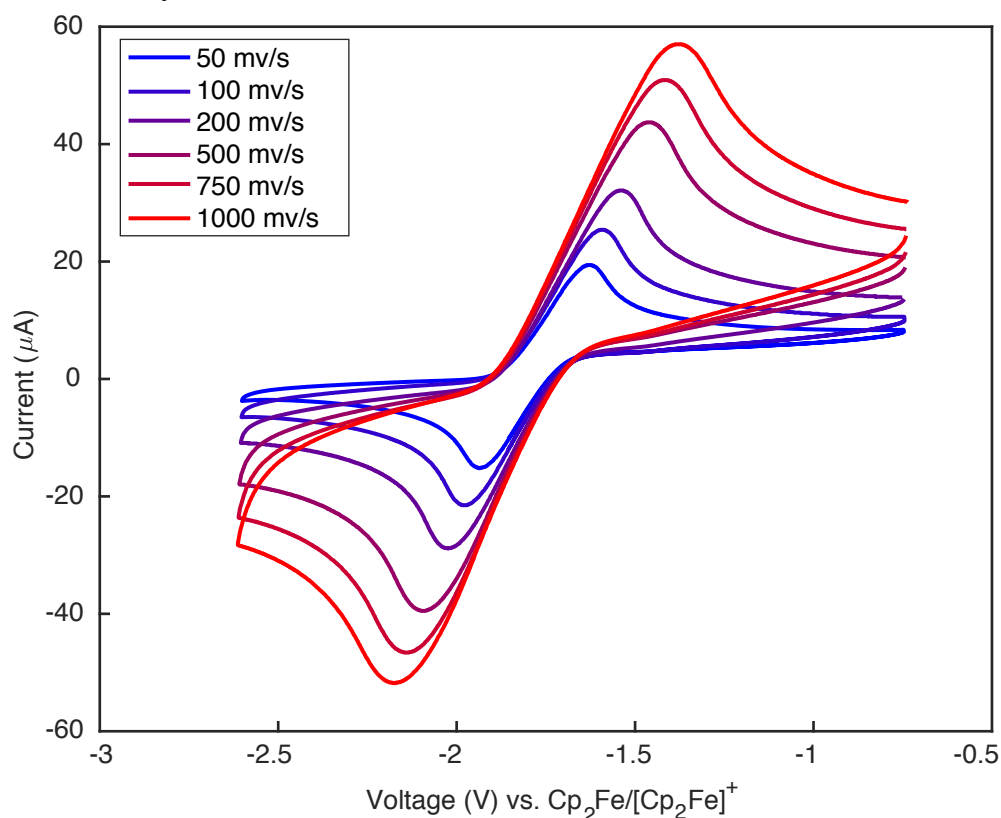


Figure S83: Cyclic voltammogram of **2** (5 mM) in PhF (0.1 M $[\text{NPr}_4][\text{BAR}^{\text{F}}_4]$) showing the $2/[2]^+$ redox couple at -1.78 V vs $\text{Cp}_2\text{Fe}/[\text{Cp}_2\text{Fe}]^+$

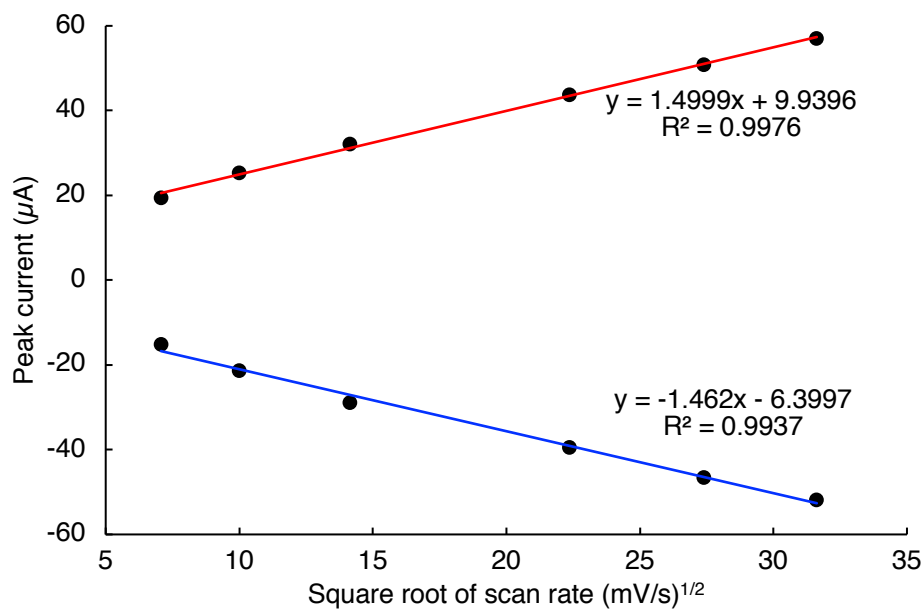


Figure S84: Plot of peak current vs. the square root of the scan rate, showing the reversibility of the $2/[2]^+$ redox couple.

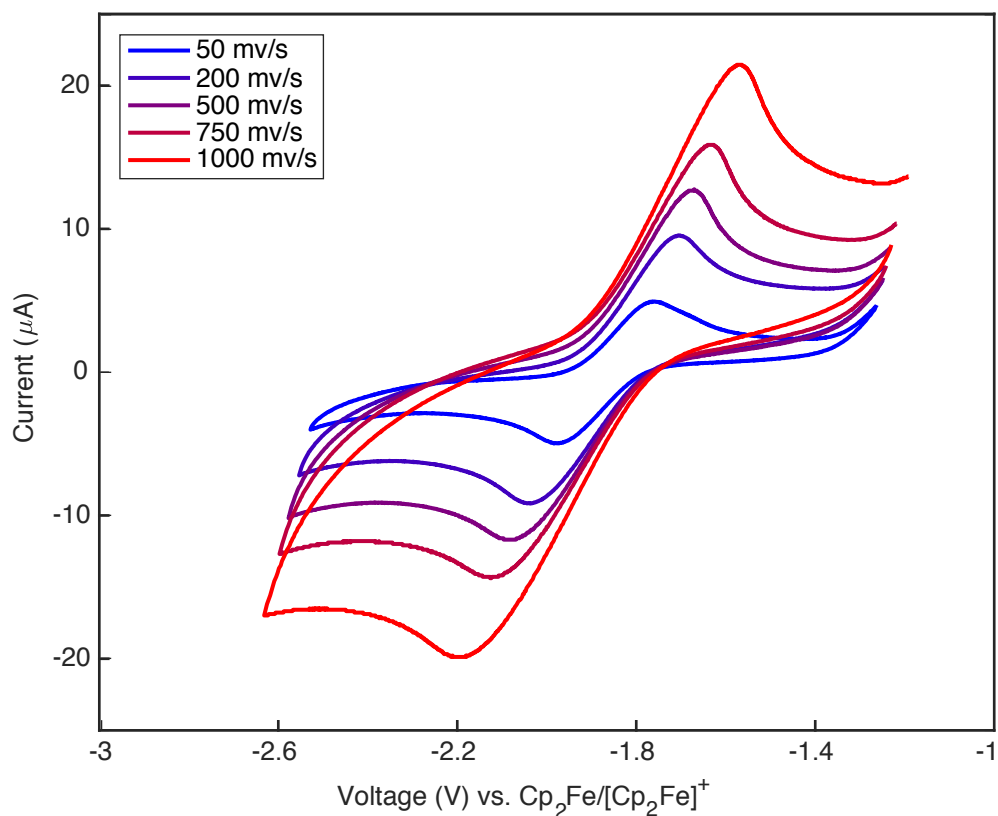


Figure S85: Cyclic voltammogram of **3** (5 mM) in PhF (0.1 M [NPr₄][BAr^F₄]) showing the **3**/**[3]**⁺ redox couple at -1.88 V vs Cp₂Fe/[Cp₂Fe]⁺

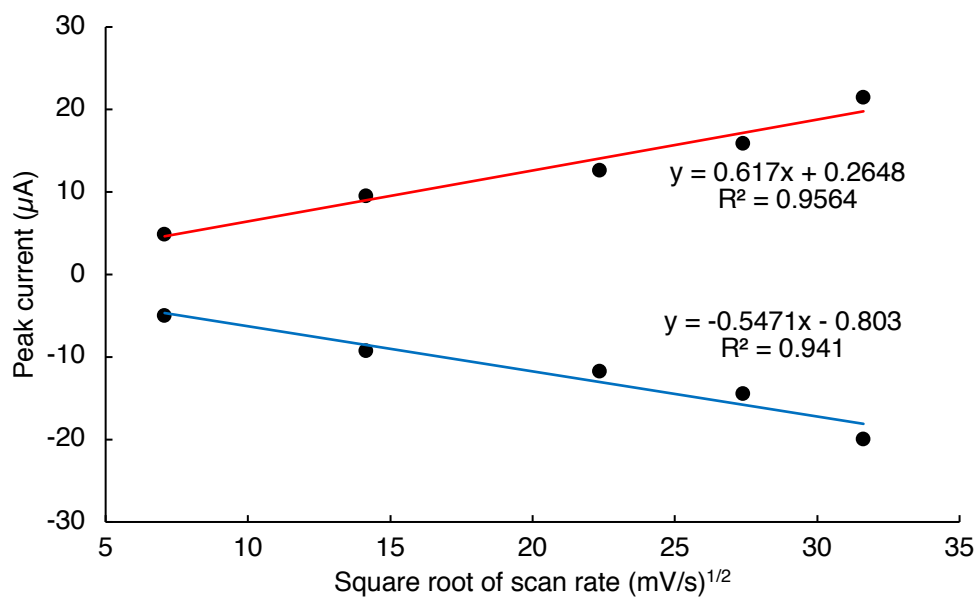


Figure S86: Plot of peak current vs. the square root of the scan rate, showing the reversibility of the **3**/**[3]**⁺ redox couple.

J. Crystallographic Details

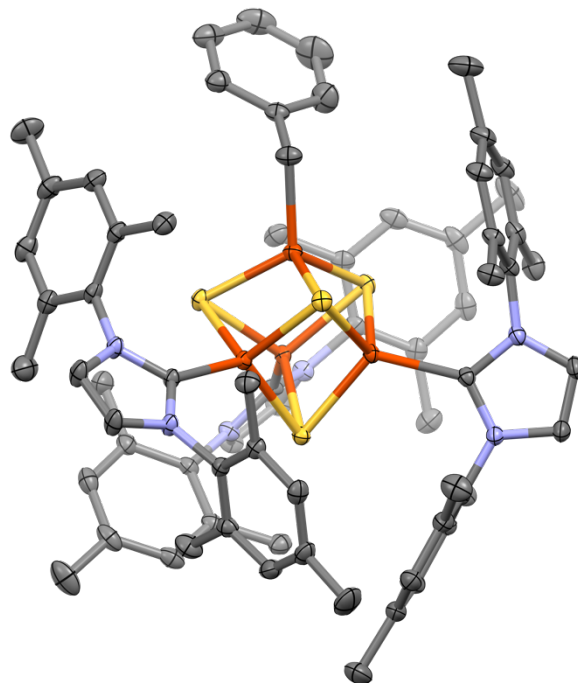


Figure S87: Thermal ellipsoid (50%) plot of **2**. Hydrogen atoms omitted for clarity

[2]⁺: Disorder was present in the benzyl group and in THF and pentane in the lattice. The disordered atoms were refined with appropriate distance and angle restraints and rigid bond restraints.

[4]⁺: Crystallized on a 3-fold symmetric axis. The triflate anion was disordered with THF over the 3-fold axis; the occupancy of the triflate was fixed at 0.333 for charge balance. The S and IMes atoms were modelled as disordered over two positions, in a 2:1 ratio. The disordered atoms were refined with appropriate distance and angle restraints and rigid bond restraints. Modeling the S atoms over two positions generates several potential cluster geometries. The atomic positions we displayed were chosen such that the cluster metrics were consistent with other $[\text{Fe}_4\text{S}_4]^+$ clusters (i.e., Fe–S distances between 2.20 and 2.35 Å, L–Fe–S angles > 90 °). The atomic positions for the NHCs were chosen so that the Fe atoms bonded to equivalent sulfurs had equivalent IMes ligands.

K. References

- (1) Brown, A. C.; Suess, D. L. M. Controlling Substrate Binding to Fe₄S₄ Clusters through Remote Steric Effects. *Inorg. Chem.* **2019**, *58* (8), 5273–5280.
- (2) Samsel, E. G.; Kochi, J. K. Oxidative Alkylation of Cobalt Complexes with Hydrazines. *Inorg. Chem.* **1986**, *25* (14), 2450–2457.
- (3) Yakelis, N. A.; Bergman, R. G. Safe Preparation and Purification of Sodium Tetrakis[(3,5-Trifluoromethyl) Phenyl]Borate (NaBArF₂₄): Reliable and Sensitive Analysis of Water in Solutions of Fluorinated Tetraarylborates. *Organometallics* **2005**, *24* (14), 3579–3581.
- (4) Chávez, I.; Alvarez-Carena, A.; Molins, E.; Roig, A.; Maniukiewicz, W.; Arancibia, A.; Arancibia, V.; Brand, H.; Manuel Manríquez, J. Selective Oxidants for Organometallic Compounds Containing a Stabilising Anion of Highly Reactive Cations: (3,5(CF₃)₂C₆H₃)₄B⁻)Cp₂Fe⁺ and (3,5(CF₃)₂C₆H₃)₄B⁻)Cp*₂Fe⁺. *J. Organomet. Chem.* **2000**, *601* (1), 126–132.
- (5) Stoll, S.; Schweiger, A. EasySpin, a Comprehensive Software Package for Spectral Simulation and Analysis in EPR. *J. Magn. Reson.* **2006**, *178* (1), 42–55.
- (6) Hübschle, C. B.; Sheldrick, G. M.; Dittrich, B. ShelXle: A Qt Graphical User Interface for SHELXL. *J. Appl. Crystallogr.* **2011**, *44* (6), 1281–1284.
- (7) Gibian, M. J.; Corley, R. C. Organic Radical-Radical Reactions. Disproportionation vs. Combination. *Chem. Rev.* **1973**, *73* (5), 441–464.
- (8) Halpern, J. Determination of Transition Metal-Alkyl Bond Dissociation Energies from Kinetic Measurements. *Polyhedron* **1988**, *7* (16–17), 1483–1490.
- (9) Halpern, J. Determination and Significance of Transition Metal-Alkyl Bond Dissociation Energies. *Acc. Chem. Res.* **1982**, *15* (8), 238–244.
- (10) Horitani, M.; Shisler, K.; Broderick, W. E.; Hutcheson, R. U.; Duschene, K. S.; Marts, A. R.; Hoffman, B. M.; Broderick, J. B. Radical SAM Catalysis via an Organometallic Intermediate with an Fe-[5'-C]-Deoxyadenosyl Bond. *Science* **2016**, *352* (6287), 822–825.
- (11) Kandt, C.; Monticelli, L. Membrane Protein Dynamics from Femtoseconds to Seconds. *Methods Mol. Biol.* **2010**, *654*, 423–440.
- (12) Ben-Nissan, G.; Sharon, M. Capturing Protein Structural Kinetics by Mass Spectrometry. *Chem. Soc. Rev.* **2011**, *40* (7), 3627–3637.